4-14-2016 12:00 AM

Angiogenic Therapy in a Fibrotic Murine Model of Duchenne Muscular Dystrophy

Kelly M. Gutpell
The University of Western Ontario

Supervisor
Dr. Lisa M. Hoffman
The University of Western Ontario

Graduate Program in Anatomy and Cell Biology
A thesis submitted in partial fulfillment of the requirements for the degree in Doctor of Philosophy
© Kelly M. Gutpell 2016

Abstract

Duchenne muscular dystrophy (DMD) is a devastating neuromuscular disorder that affects approximately 1 in 5000 males. Vascular-targeted therapy has been proposed as a treatment for DMD to reduce ischemia and enhance endogenous repair. Additionally, a more vascularized environment may enhance regenerative approaches currently under investigation. Vascular endothelial growth factor (VEGF) and angiopoietin-1 (ANG1) are two of the most studied pro-angiogenic factors for this approach. To date, little is known regarding the effect of these pro-angiogenic factors on muscle function and whether they may exacerbate fibrosis in a relevant murine model of DMD. The first aim of this thesis was to determine the murine model that is best suited for assessing vascular therapy. We demonstrate the dystrophin null, utrophin heterozygous mouse (*mdx/utrn+/-*) develops more collagen deposition at an earlier age than the commonly used *mdx* mouse and is therefore a superior choice for assessing therapeutic effects on fibrosis. Next, we investigated the effect of exogenous VEGF treatment on fibroblasts derived from severely affected diaphragm and mildly affected gastrocnemius muscles of *mdx/utrn+/-* mice. VEGF treatment induced differentiation into myofibroblasts in both cell types, suggesting induction of a fibrotic response. The final aim of the thesis was to assess the effect of VEGF alone or in combination with ANG1 on functional perfusion as assessed non-invasively using dynamic contrast-enhanced computed tomography. A combination of VEGF and ANG1, but not VEGF alone, slowed progression of ischemia in the *mdx/utrn+/-* hind limb. Increased vessel maturation, as assessed histologically, validated the imaging findings. The combination treatment also decreased fibrosis and leukocyte infiltration, consistent with decreased vascular permeability following ANG1 treatment. Overall, the research in this thesis highlights the drawbacks to use of VEGF as a treatment for ischemia associated with DMD and reveals considerations for future use of vascular therapy in murine models of the disease.

Keywords

Co-Authorship Statement

Chapter 1 entitled "Introduction," includes a portion of content that was adapted from Gutpell & Hoffman, 2013. *OA Musculoskelet Med*. 1(4):33. K.M. Gutpell wrote the manuscript with suggestions from Dr. L.M. Hoffman.

Chapter 2 entitled "Fibrosis in the *mdx*/*utrn*+/- mouse validates its use as a fibrotic model of muscular dystrophy," was adapted from Gutpell et al., 2015. *PLoS One*. 10(1):e0117306, and reproduced here from PLoS ONE under the Creative Commons Attribution license, which grants reuse of the article without the requirement of further permission. K.M. Gutpell wrote the manuscript with suggestions from Dr. L.M. Hoffman. K.M. Gutpell carried out all experiments in Dr. L.M. Hoffman's laboratory. W.T. Hrinivich wrote the Matlab™ ™ code to analyze Masson's Trichrome images.

Chapter 3 entitled "VEGF induces stress fiber formation in fibroblasts derived from a murine model of muscular dystrophy" was adapted from Gutpell et al., 2015 and reproduced here with permission from Springer. K.M. Gutpell wrote the manuscript with suggestions from Dr. L.M. Hoffman. K.M. Gutpell carried out all experiments in Dr. L.M. Hoffman's laboratory.

Chapter 4 entitled "Vascular therapy reduces ischemia and fibrosis in the *mdx*/*utrn*+/- mouse," was adapted from Gutpell et al., 2016 (in preparation). K.M. Gutpell carried out the experimental work, analyzed the data, and wrote the manuscript with suggestions from Dr. L.M. Hoffman. W.T. Hrinivich wrote the Matlab™ code for analyzing Masson's Trichrome and immunofluorescence images. N. Tasevski and B. Wong performed Masson's Trichrome and immunofluorescence microscopy, respectively. J. Hadway and L. Desjardins performed tail vein catheterizations and assisted with CT scanning procedures. F. Su stitched the heart and hind limb scans together. Dr. T-Y. Lee provided perfusion expertise.

Acknowledgments

I would like to thank my friends Laura, Spencer, Scott, Jen, and Evan for always providing an ear to listen, and a reason to laugh. To Tom: In addition to your dear friendship, I am forever indebted to you for all of your help with this project.

To all the past and present members of the Hoffman lab, including Boaz, Nik, David, Linshan, and Carl, among others: thank you for the integral role each of you played in the past 5 years. To Andrew and Becky: Thank you for going above and beyond to help me over the years, you two have helped me in more ways than you know.

I would like to thank my grandparents for their support and always showing sincere interest in my research, giving me the opportunity to talk about such an important aspect of my life whenever we speak. Thank you to my great grandmother and all my aunts and uncles for your words of encouragement, they have always motivated me.

To my "little" siblings Kristen, Derek, Leah, and Beck: thank you for being rays of sunshine when I needed to smile and for using your wit and sarcasm to make me laugh. To my brother-in-law Jeff: thank you for your constant support and reminding me to enjoy the finer things in life (i.e. the Blue Jays and Guinness). To my best friend, Jenn: thank you for believing in me, lifting me up, and making me feel as though I can do anything.

I am so grateful to have received endless love and encouragement from all my parents. To Isabel: Thank you for being my second mom and genuinely caring for my wellbeing. To Joe: Thank you for your constant advice and "stimulating" conversations. To Steve: Thank you for your constant support and always making me feel like my work is important to you. To my dad: Thank you for instilling in me the importance of hard work and always encouraging me not to sweat the small stuff. To my mom: Thank you for being my role model. I will always strive to emulate you in everything I do.

To my partner in life: I will never forget the thousands of research-related conversations you have not only put up with, but also genuinely engaged me in. You have been my soundboard through it all and to say I will be forever grateful would fall far short. Your intellect drives me to be a better scientist, and your kindness inspires me to be a better person. This accomplishment would not have been possible without you, Nate.

Project Proposal Summary

BACKGROUND: The most commonly diagnosed fatal childhood disorder is Duchenne muscular dystrophy (DMD), a neuromuscular disease that is invariably fatal by the age of 30. Regenerative therapy research has been ongoing for decades with little or no significant efficacy reported in pre-clinical trials. A major contributor to this inefficacy is the ischemia, inflammation, and fibrosis that progressively dominate the degenerating muscle tissue, creating a hostile environment for cell transplantation. Studies have proposed the use of angiogenic factors to alleviate the ischemia inherent to DMD pathology, creating a more optimal environment for regeneration. Vascular endothelial growth factor (VEGF) is a known potent inducer of angiogenesis and is of particular interest in the field given that preliminary. Recent studies have also proposed a combinatorial approach, using VEGF to induce angiogenesis and angiopoietin-1 (ANG1) to mature vessels, since VEGF alone is known to produce leaky vasculature. No studies to date have investigated whether these factors, either alone or in combination, affect perfusion longitudinally in a relevant animal model of DMD. There is also very little known regarding the effect, if any, these angiogenic factors may have on inflammation and fibrosis. Finally, much of what is currently known about vascular therapies is derived from invasive muscle biopsies that may contribute to disease progression and are limited in that they provide a small perspective of a very heterogeneous disease.

HYPOTHESES: A combination of VEGF and ANG1, but not VEGF alone, will reduce disease progression in a murine model of muscular dystrophy and this effect can be measured non-invasively using dynamic contrast-enhanced computed tomography.

SPECIFIC AIMS:

i) Investigate histopathological features in the *mdx*, *mdx*/*utrn*+/- and dko mice to determine the suitability of each as a model of Duchene muscular dystrophy. Hallmark features that will be assessed include percentage of centrally nucleated myofibers and extent of fibrosis as indicated by Masson's Trichrome staining.

ii)   Determine whether VEGF elicits a pro-fibrotic response in fibroblasts derived from a murine model of DMD. Fibroblasts isolated from gastrocnemius and diaphragm muscles of 10 week-old mice will be treated with $VEGF_{164}$. qPCR will be employed to measure changes in mRNA levels of fibrotic genes including *Col1A*, *Ccn2/Ctgf, Acta2 and Fn1.*

iii)   Assess the ability of VEGF alone or in combination with ANG1 to enhance the microenvironment in dystrophic murine skeletal muscle. *Ex vivo* analyses including immunohistochemistry and western blot will be used to measure changes in expression of: alpha smooth muscle actin (marker of mature blood vessels), CD45 (leukocyte marker), and collagen (fibrotic marker).

iv)   Use dynamic contrast-enhanced computed tomography (DCE-CT) to determine if *ex vivo* changes in angiogenic, inflammatory, and fibrotic markers observed in aim 3 correlate with functional changes in skeletal muscle perfusion.

SIGNIFICANCE: Addressing the hostile regenerative environment in dystrophic muscle may address the lack of efficacy observed with current therapeutic approaches in DMD patients. The proposed research will further investigate the role of vascular-targeted therapy *in vivo* in a relevant animal model that more accurately reflects the pathophysiology of DMD in patients. The majority of current research utilizes histological and post-mortem means of assessing the effect of VEGF treatment, impeding accurate interpretation of the effect of treatment on muscle function. The proposed research is novel in that it will correlate CT findings with traditional histological analyses following treatment with pro-angiogenic agents to better elucidate the potential for its use in the clinical arena.

Table of Contents

List of Tables

List of Figures

List of Appendices

List of Abbreviations

αSMA   Alpha smooth muscle actin

°C   degrees Celsius

ΔΔCT   Delta-delta threshold cycle

Acta2   Alpha smooth muscle actin

ANG1   Angiopoeitin-1

ANOVA   Analysis of variance

BF   Blood flow

BSA   Bovine serum albumin

BV   Blood volume

Ca^{2+} Calcium ion

cGMP   Cyclic guanosine monophosphate

CK   Creatine kinase

CNF   Centrally-nucleated fiber

CO_2 Carbon dioxide

Col1a1   Alpha strand of type 1 collagen

Ctgf/ccn2   Connective tissue growth factor

DAPI   4,6-diamidino-2-phenylindole

DCE-CT   Dynamic contrast-enhanced computed tomography

DGC	Dystrophin glycoprotein complex
dko	Dystrophin-null, utrophin-null double knockout mouse
DMD	Duchenne muscular dystrophy
DMEM	Dulbecco's Modified Eagle's Medium
EC	Endothelial cell
ECM	Extracellular matrix
ELISA	Enzyme-linked immunosorbent assay
FBS	Fetal bovine serum
FDG	Fluorodeoxyglucose
Fn1	Fibronectin-1
GE	General Electric
GM	Gastrocnemius
H&E	Hematoxylin and Eosin
HBSS	Hanks buffered saline solution
HRP	Horse radish peroxidase
IgG	Immunoglobulin G
kDa	Kilodaltons
LDI	Laser Doppler imaging
MDSC	Muscle-derived stem cells
mdx	Dystrophin-null

mdx/utrn+/-	Dystrophin-null, utrophin hemi/heterozygous mouse
MRI	Magnetic resonance imaging
mRNA	Messenger ribonucleic acid
nNOS	Neuronal nitric oxide synthase
NO	Nitric oxide
PBS	Phosphate-buffered saline
PET	Positron emission tomography
PVDF	Polyvinylidene fluoride
RNA	Ribonucleic acid
Rpm	Rotations per minute
SC	Satellite cells
SD	Standard deviation
SDS-PAGE	Sodium dodecyl sulfate poly-acrylamide gel electrophoresis
SJHC	St. Joseph's Health Care
TA	Tibialis anterior
TBS-T	Tris-buffered saline with 0.05% tween-20
TGFβ	Transforming growth factor beta
utrn	Utrophin
VEGF	Vascular endothelial growth factor

Chapter 1

Introduction[1]

---

1 Introduction

1.1 Chapter Summary

Duchenne muscular dystrophy (DMD) is the most severe form of muscular dystrophy. It is also the most fatal genetic disorder diagnosed in children (Emery 2002). DMD is caused by a mutation, or mutations, in the gene encoding dystrophin, a large cytoskeletal protein that confers membrane integrity in muscle cells. Since dystrophin was discovered in 1987, many research groups have attempted to restore its expression in patients and animal models of the disease. Although promising results have surfaced in recent years, 100% dystrophin expression has not yet been achieved, and thus muscle degeneration and accompanying fibrosis still occurs. As such, it is well accepted that any real cure to DMD will involve a multifaceted approach including methods to both restore dystrophin and alleviate the hostile muscular environment already present at the time of diagnosis.

This chapter provides background on the underlying pathophysiology of DMD, therapeutic approaches under investigation to treat the disease, and some of the main limitations to current research. Important considerations in conducting DMD research are also discussed, including animal models of the disease and techniques for assessing functional efficacy of therapies. The aim of this chapter is to provide the overarching rationale for the research presented in this thesis.

1.2   Duchenne muscular dystrophy

1.2.1   Living with DMD

A DMD diagnosis is typically given within the first three to five years of life. The most common sign observed by parents is the onset of the "Gower's maneuver," whereby a child cannot use his leg muscles alone to stand up. Instead, he must use his arms to "walk" up his legs to reach a standing position. The first step in diagnosing DMD is testing levels of creatine kinase (CK), a metabolite of muscle breakdown (Van Ruetin et al. 2014). If CK levels are elevated, physicians will often order genetic testing on blood samples to determine if a mutation in the dystrophin gene is present. In some, but not all cases, a biopsy will be ordered to confirm a lack of dystrophin protein in the patient's skeletal muscle.

Once a diagnosis occurs, the life path that each child takes is unique, with some responding positively to treatments and living well into their thirties, and others succumbing to the disease by their late teenage years. Due to vast improvements in healthcare - particularly in the fields of cardiology and pulmonology - the former case is becoming increasingly common, with some DMD patients going to college, attaining a career and, in some cases, having children (Eagle et al. 2002). Nevertheless, DMD patients are limited to wheelchair mobility by approximately age 12 and the care they receive is purely palliative, with no current treatments offering an actual cure to date (Landfeldt et al. 2015). Eventually, patients succumb to the disease, typically due to respiratory complications (Cruz Guzmán et al. 2012, Wei et al. 2016).

1.2.2   Murine models of DMD

The most widely studied murine model of DMD is the *mdx* mouse, a dystrophin-null mouse that genotypically mimics the human form of the disease (Sicinski et al. 1989; Partridge et al. 2013). While this model exhibits classic histological features of muscle pathology such as centrally nucleated myofibers and inflammatory infiltrate, it is generally healthy until 10 months of age and nearly indistinguishable from a wild-type mouse (Stedman et al. 1991, Desguerre et al. 2012). Perhaps most importantly, the

disease does not manifest in the same manner as it does in patients, with very little skeletal muscle fibrosis observable at any point in the progression of the disease. The *mdx* diaphragm does develop increased fibrotic marker expression, but the extent of fibrosis is non-life threatening. Fibrosis and muscle degeneration of the diaphragm muscle is a major cause of death in DMD patients and is therefore an important feature in an accurate animal model. Further, fibrosis is nearly absent in the hind limb skeletal muscles, even at an advanced age. Considering that a large portion of tissue regeneration research in this field injects into this area, the lack of fibrosis in the *mdx* mouse may present a potential source of misinterpreted results. A double knockout mouse lacking dystrophin and its analogue, utrophin (*utrn*), more closely phenocopies DMD (Grady et al. 1997). This double knockout mouse (dko) develops observable muscular dystrophy by 4 weeks of age that rapidly progresses until death, which is typically around 16-22 weeks of age. Importantly, the dko mouse also develops fibrosis, which is a major contributor to the severity of DMD in patients (Isaac et al. 2013). Although this double knockout model is preferred over the mildly affected *mdx* mouse, it is difficult to keep this mouse alive through the course of a longitudinal study. Additionally, in our laboratory, we observe that disease severity ranges in this dko mouse, with some animals gaining very little weight, only up to 10g, and barely surviving to 8 weeks of age. On the other hand, we have a number of dko mice that grow up to 20-25g and survive with minimal intervention up to 20 weeks of age. This disparity we observe in our dko mice introduces a great deal of variability in our studies and makes interpretation of results difficult. Regardless, any therapy should exhibit efficacy in the dko mouse if it holds any real promise of affecting patients. Given these considerable issues with the *mdx* and dko models, the heterozygous mouse (*mdx/utrn*+/-) has received attention in recent years for its potential to act as an intermediate model, but the research findings to validate this model as superior to the *mdx* mouse are still lacking.

1.2.3   DMD pathophysiology

DMD is caused by an absence of dystrophin, due to one or more mutations in the gene that encodes the protein (Emery et al. 2002). Since the dystrophin gene is located on the

X Chromosome, a mutation almost exclusively affects males, with female carriers of the mutation rarely exhibiting a phenotype typical of DMD (Hoffman et al. 1987, Song et al. 2011). In very rare cases, females may carry mutations on both X Chromosomes and therefore exhibit the full phenotype observed in male patients. The gene that encodes dystrophin is composed of 79 exons. One or more of these exons can be mutated, with exons 45-55 accounting for the most common sites of mutation (Blake et al. 2002). Although DMD is an inherited genetic disorder, the mutation may also arise spontaneously, accounting for 30-40% of DMD cases. Typically, these mutations result in a truncated protein due to the premature addition of a stop codon. In some cases, this truncation produces a protein that has reduced, but not completely absent, function (Laing et al. 2011). In these cases the disease phenotype is less severe and the patient would be diagnosed with Becker's muscular dystrophy (Hoffman et al. 1989, Hoogerwaard et al. 1999). When the mutation results in a truncated, non-functional protein, or no protein at all, patients are severely affected by the disease and are diagnosed with Duchenne's muscular dystrophy.

Dystrophin is a 427 kDa cytoplasmic protein. It is expressed in a variety of cell types, including, but not limited to, cardiac, skeletal, and smooth muscle cells. Dystrophin acts to link cytoskeletal actin filaments, the contractile units of myofibers, to extracellular matrix proteins, such as laminin (Figure 1.1). Dystrophin is a component of the dystroglycan complex, along with sarcoglycan and dystroglycan transmembrane proteins. This link provides a scaffold against which cells may contract and confers overall membrane integrity to myofibers (Rybakova et al. 2000). Disruption of this connection through loss of dystrophin leads to an increased susceptibility to injury due to mechanical stress. This lack of sarcolemma (muscle cell membrane) integrity leads to an increase in intracellular free calcium, which has been directly linked to an increase in proteolysis, leading to eventual cell death (Hopf et al. 1996). Rapid inflammation responds to this muscle necrosis. The infiltrating inflammatory cells are not only responsible for clearing away the necrotic muscle cells, but they are a major source of pro-fibrotic signalling molecules. Of particular importance is transforming growth factor beta (TGFβ), expressed by macrophages and other inflammatory cells, which act on resident fibroblasts

to induce differentiation into myofibroblasts. Myofibroblasts are largely responsible for laying down the collagen matrix that contributes to tissue rigidity and fibrosis (Desguerre et al. 2009, Klinger et al. 2012). This cascade of events continues throughout the life of the patient, with fibrotic and adipose tissue progressively dominating what was once functional skeletal muscle (Figure 1.2).
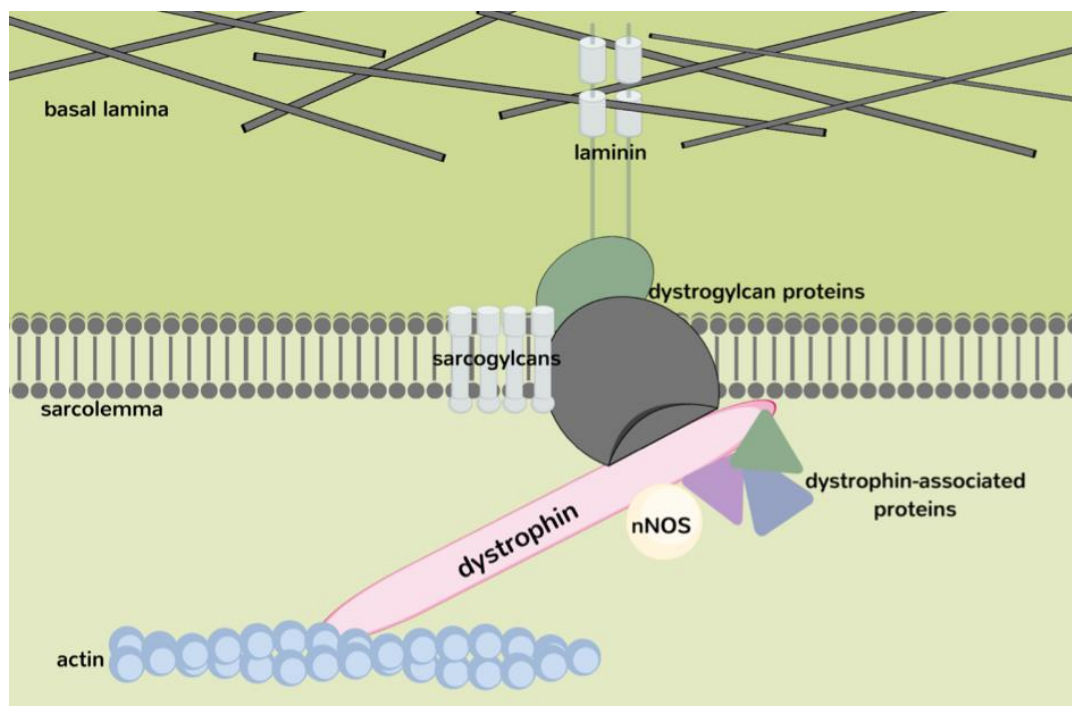
Figure 1.1: Dystrophin is an integral part of a protein complex that links the cytoskeletal elements in muscle cells to the extracellular matrix.

As part of the dystrophin glycoprotein complex, dystrophin confers overall membrane strength to myofibers. The N-terminal domain of dystrophin interacts with actin and the C-terminal domain interacts with the dystrophin-associated glycoprotein (DAG) complex, composed of sarcoglycans and dystroglycans. The DAG complex binds to extracellular proteins in the basal lamina, such as laminin. Additionally, neuronal nitric oxide synthase (nNOS) interacts with dystrophin between exons 42-45 at the sarcolemma, an interaction that confers enzymatic activity to the protein.
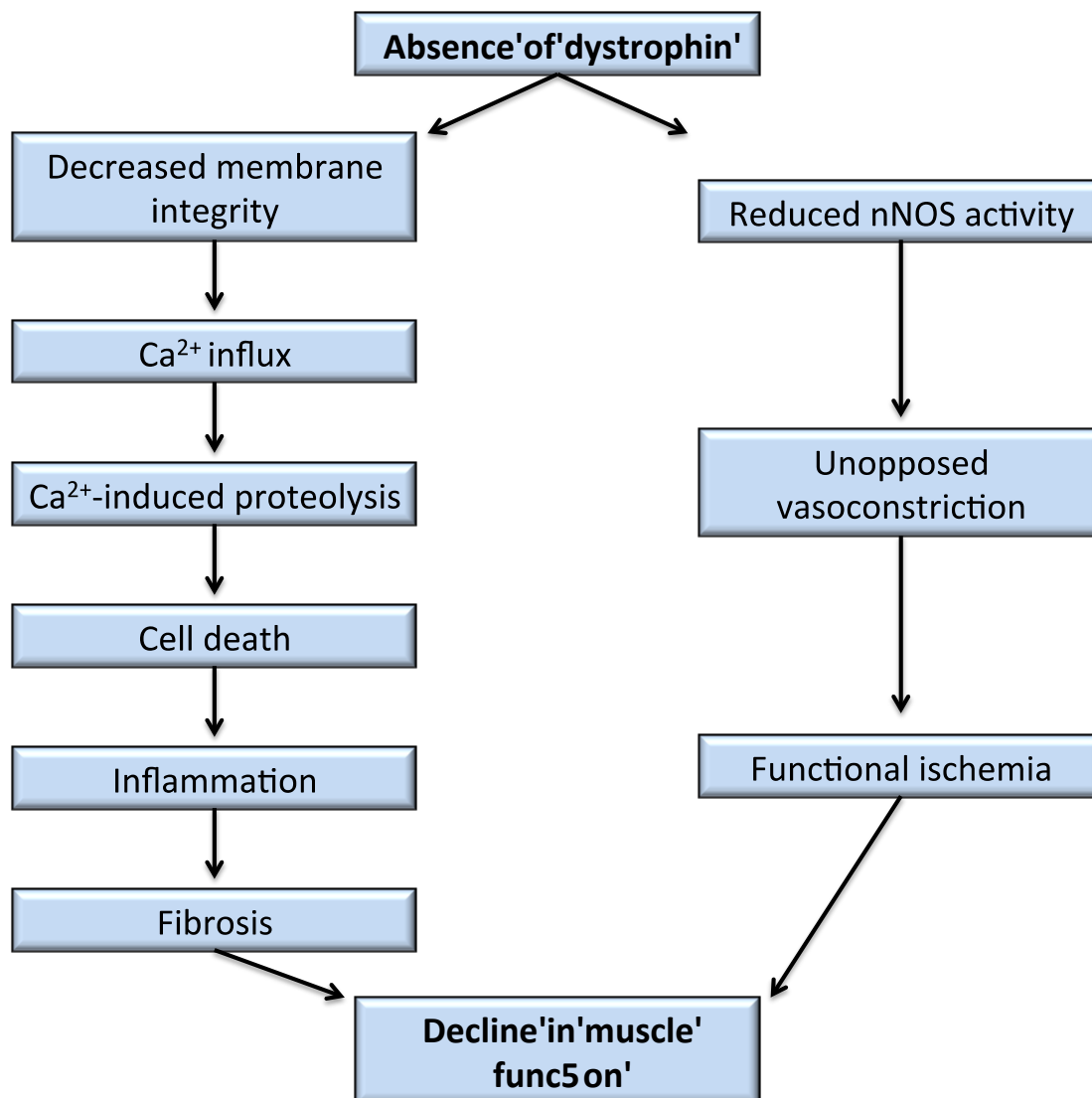
Figure 1.2: An X-linked mutation in the dystrophin gene leads to rapid decline in muscle function.

A two-hit hypothesis is used to describe the pathways by which DMD progresses. Reduced sarcolemma integrity results in an increased susceptibility to contraction-induced cellular damage. Damaged muscle tissue is continually replaced by fibrotic and adipose tissue. At the same time, reduced nNOS activity leads to impaired vasodilation, resulting in ischemia. Many therapeutic approaches aim to restore dystrophin in muscle tissue.

1.2.4   Muscle ischemia due to loss of dystrophin

Accompanying muscle degeneration is a progression of muscle ischemia in both DMD patients and animal models of the disease (Sander et al. 2000). While the primary function of dystrophin is to anchor the sarcolemma to the extracellular matrix for structural stability, its presence is also important for a number of other functions in skeletal and smooth muscle cells. Dystrophin functions as a signal transducer for the catalytic activity of neuronal nitric oxide synthase (nNOS). Through a physical interaction with dystrophin, nNOS catalyzes the production of nitric oxide (NO) in skeletal muscle (van den Bergen et al. 2015, Shiao et al. 2004). NO plays a key role in a variety of skeletal muscle cell functions including force production, regulation of blood flow, and glucose metabolism (Sander et al. 2000). Thus, with reduced nNOS activity, many normal functions of muscle may be impaired. Additionally, loss of dystrophin in smooth muscle cells leads to an inability to produce vasodilation when an increased metabolic load is placed on skeletal muscle tissue (Ito et al. 2006). As a result, there is an unopposed sympathetic vasoconstriction leading to decreased muscle perfusion in patients with DMD. Work by others has shown there is an increase in vasoconstriction in DMD patients as indicated by a 16% decrease in blood flow compared to healthy forearm muscle. Blood oxygenation is also 7% lower in DMD muscle (Sander et al. 2000). Muscle biopsies from these patients confirm this difference in blood flow corresponds to decreased nNOS protein levels in DMD patients. Immunohistological analysis of nNOS shows almost no expression of the protein at the sarcolemma. The importance of dystrophin in regulating nNOS activity is further demonstrated in transgenic *mdx* mice expressing smooth muscle-specific dystrophin whereby they exhibit improved vasoregulation compared to normal *mdx* mice. While vasodilation is not increased to that of a wild type mouse in the transgenic mice, blood flow is significantly increased compared to *mdx* mice lacking dystrophin in smooth muscle cells (Kobayashi et al. 2008). Overall, the deleterious effect of nNOS inactivity in DMD patients highlights a severe need for improved vasorelaxation in DMD patients.

In addition to reduced nNOS activity in dystrophic muscle cells, there is increasing evidence to suggest that the vascular network in dystrophic tissue is also compromised. A

decrease in vascular density has been demonstrated in the *mdx* mouse (Loufrani et al. 2004 & Asai et al. 2007). Microfilm perfusion has been used to visualize the total vasculature in the tibialis anterior muscle of the *mdx* mouse to demonstrate a reduced vascular network in the *mdx* mouse compared to healthy controls (Matsakas et al. 2013). Standard immunohistochemical techniques also indicate reduced arteriole density in *mdx* mice. It has not been reported whether a decrease in vascular density exists in DMD patients, but it is well known that fibrotic and fatty deposits progressively dominate muscle tissue in DMD patients. The dense, fibrotic connective tissue that displaces muscle is not well vascularized and therefore may impede blood delivery to the tissue. Without proper blood flow, muscle regeneration, by endogenous repair mechanisms or exogenous dystrophin delivery, may not occur. Enhancing the vascular environment by increased vascular density may confer some of the function that is aberrant due to a lack of dystrophin.

Dystrophin absence in endothelial cells (ECs) has also been linked to impaired angiogenesis in *mdx* mice (Palladino et al. 2013). Although dystrophin was classically considered to be a muscle-specific protein, this study demonstrates the importance of its expression in ECs as well. As with muscle cells, the loss of nNOS activity at the EC membrane leads to a cGMP deficiency that affects not only blood blow, as previously discussed, but also impairs the ability of ECs to migrate, proliferate, and form tubules in *in vitro* culture assays. Interestingly, a low dose of aspirin aided in EC production of NO and cGMP, leading to an increase in microvascular density post-treatment. These findings shed a new light on the use of pro-angiogenic growth factors for enhancing the microvasculature in *mdx* mice and DMD patients. Prior to this study, little attention has been given to the possibility that, regardless of growth factor treatment, there may be an inherent impairment in EC ability to form new vessels in muscular dystrophy. Thus, the results of this study may help explain differences in angiogenesis following treatment in dystrophic compared to healthy muscle.

There is evidence of decreased vasodilation, vascular density, and angiogenic capability in dystrophin-related myopathy. Taken together, studies relating to ischemia in DMD

highlight the need to not only address ways to regenerate muscle cells, but also address the vascular problems inherent in this pathology. Without proper vasculature, regenerative techniques to restore dystrophin may be rendered futile.

1.3   Strategies to restore dystrophin

Given the importance of dystrophin in nNOS activity and conferring sarcolemma integrity, a number of groups are attempting to restore dystrophin expression in animal models of DMD. Some of the most promising approaches to restoring dystrophin include exon skipping, genome editing using the Crispr/Cas9 system, and stem cell therapy.

1.3.1   Exon skipping

When a genetic mutation disrupts the reading frame of nucleotide triplets, or codons, the result may be a truncated protein. This is the case in DMD whereby a mutation in one or more exons leads to a premature stop codon, resulting in a truncated, non-functional form of the dystrophin protein. In most cases, this truncated version of the protein is not even detectable as dystrophin. Fortunately, cells have an inherent ability to excise, or "splice", introns, which are portions of a pre-mRNA strand that do not contribute to the amino acid sequence of a peptide. Researchers have exploited this innate machinery in cells to splice out the mutated exons in the dystrophin gene (Hoffman et al. 2014). The result is an imperfect, but largely functional, dystrophin protein. Eteplirsen, developed by Sarepta Therapeutics, has been used in Phase III clinical trials to treat patients with a mutation in exon 51, one of the more commonly mutated sites in DMD. The United States Food and Drug Administration is reviewing Sarepta's New Drug Application for Eteplirsen in February 2016. Although only 13% of DMD patients may be amenable to exon 51 skipping, this technology could significantly improve quality of life for that patient population (Mendell et al. 2016). It is important to note, though, the dystrophin expressed in these cases often lacks its full function and only improves the disease phenotype to a less severe form, one similar to that observed in Becker's muscular dystrophy.

1.3.2   Genome editing

In contrast to exon skipping, whereby the mutation is left intact and a downstream target (RNA) is manipulated, genome editing involves correcting the mutation that is embedded in the genetic code. A powerful new genome editing tool known as clustered regularly interspaced short palindromic repeat/Cas9 (CRISPR/Cas9) has emerged as one of the most promising tools of the 21st century. This system involves the use of RNA to guide a nuclease (Cas9) to a specified site in the genome to induce a double-stranded break. An exogenous template is then used to modify the mutated site, thereby correcting the original defect in the gene. Various groups have used CRISPR/Cas9 to introduce dystrophin expression *in vitro* to immortalized DMD-derived myoblasts and *in vivo* to the *mdx* mouse, the most commonly used model of DMD (Iyombe-Engembe et al., 2016, Long et al. 2014, 2016, Nelson et al., 2016 Tabebordbar et al., 2016). An important aspect of the CRISPR system that renders it perhaps more useful than current exon skipping practices is the ability to excise a large fragment of DNA, spanning a number of exons. By covering the mutations in exons 45-55, CRISPR/Cas9 offers the potential to address over 60% of DMD cases.

1.3.3   Cell therapy

The chief self-renewing muscle progenitor cell is the satellite cell (SC), named for its location under the basal lamina. SCs are the primary physiologically relevant stem cell population contributing significantly to muscle regeneration (Murphy et al., 2011, Chang et al. 2014). When satellite cells are activated, they undergo myogenesis, differentiating into myoblasts that fuse with each other to form multinucleated myotubes (Figure 1.3). Given the ability of SCs and other muscle progenitor cells to undergo myogenesis, various groups are looking at these populations as ways to introduce dystrophin-expressing stem cells into dystrophic muscle (Mendell et al. 1995, Skuk et al. 2006, 2007). Stem cell therapy has been one of the most widely studied- and perhaps most hotly contested- approaches to treating DMD. Clinical trials involving muscle-specific stem cells have been ongoing since the 1990's. There is evidence of donor cells present in recipient tissue up to 13 years post implant, suggesting the possibility for using cell therapy in the future (Gussoni et al. 2002, Skuk & Tremblay 2016). Although these initial

studies have furthered our knowledge regarding the role of various cell populations in regenerating lost muscle, there have been no widespread reports of any cell therapy having significant effects on muscle function following treatment. There are a number of ongoing clinical trials with estimated completion dates in 2016-2018 using various populations of stem cells including umbilical cord-derived mesenchymal stem cells and bone marrow-derived stem cells. Rita Perlingeiro's group is currently investigating the efficiency of induced pluripotent stem cells to regenerate muscle in *mdx* mice (Filareto et al. 2012). This approach involves isolating skin fibroblasts from *mdx* mice/DMD patients, reprogramming them back to a pluripotent stem cell state, correcting the dystrophin mutation, and implanting them back into the host. This approach is attractive in that it uses an autologous transplant, which largely mitigates the chances of stem cell rejection post-implant.

While cell therapy research may be promising for the future, this and other regenerative approaches face a significant hurdle in that they attempt to introduce dystrophin into a hostile, fibrotic environment that is not conducive to regeneration (Klinger et al. 2012). The "seed and soil" hypothesis, often referred to in cancer research, is also applicable to regenerative therapy for DMD. Regardless of the regenerative capacity of any specific cell population, its potential for reconstituting muscle is dependent on the transplantation environment. Given the inflammation and fibrosis that is so prominent in muscular dystrophy, it is not surprising that cells do not survive after transplantation. Since parents are often unaware their child is affected until 1-6 years of age, this pathogenesis has already been initiated and any therapeutic approaches would involve the presence of inflammation and potentially fibrosis. Thus, in addition to researching methods for introducing dystrophin into muscle, there is also a need to find ways to improve the hostile environment that will receive cell transplantation.
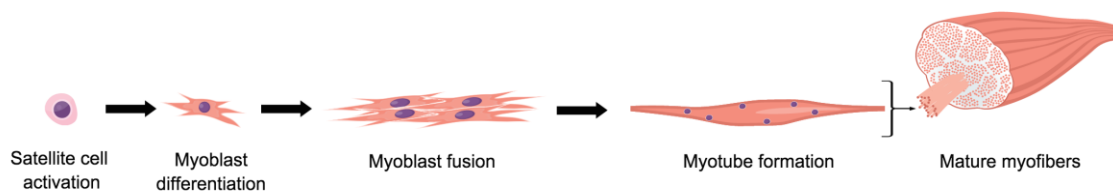
Figure 1.3: Muscle-specific stem cells known as satellite cells undergo myogenesis to form muscle tissue.

Satellite cells, while present in DMD patients, are quickly exhausted and the process of myogenesis is insufficient to meet the demands of reconstituting muscle in patients.
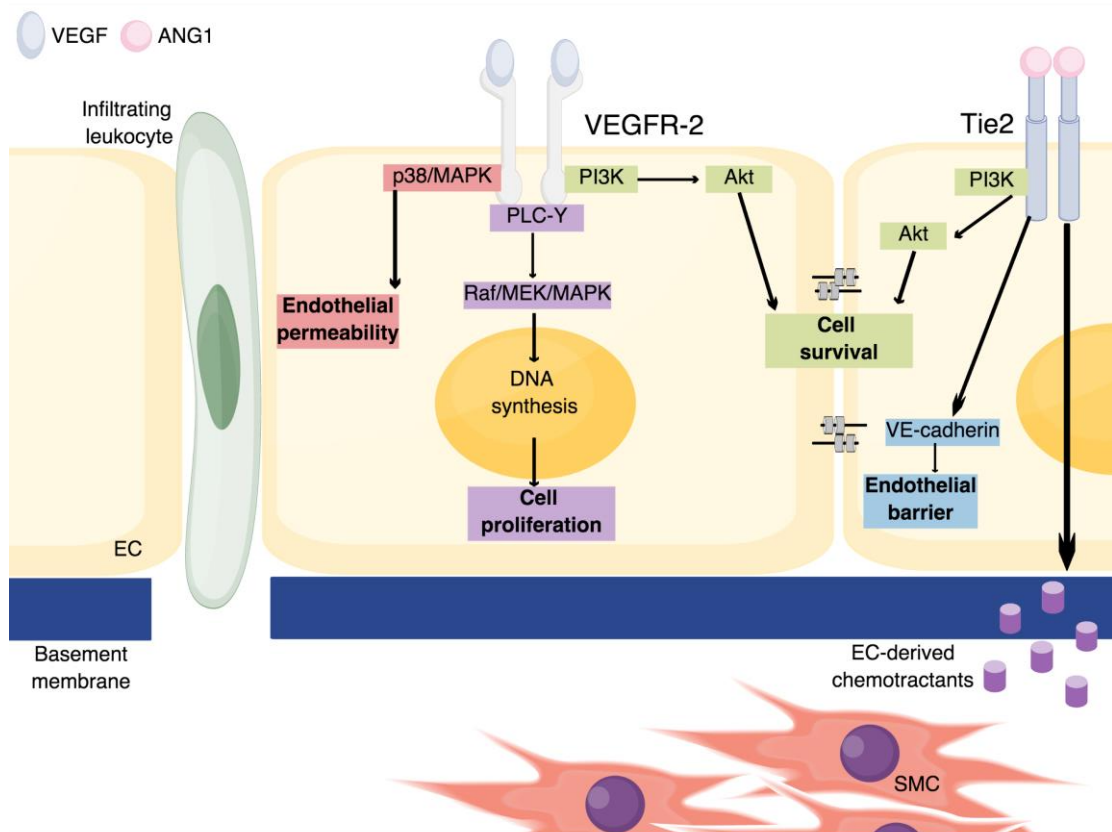
Figure 1.4: VEGF and ANG1 play a role in angiogenesis by eliciting different responses upon binding to their receptors on endothelial cells.

Upon binding to its type-2 receptor (VEGFR-2), VEGF increases endothelial pores through p38/MAPK signaling, allowing for extravasation of leukocytes from the blood into tissue. Upon activation of phospholipase C-gamma (PLC-ϒ), signaling through the Raf/MEK/MAPK pathway results in DNA synthesis and cell proliferation. Upon ANG1 binding to the Tie2 receptor, vascular-endothelial (VE) cadherin increases cell-cell interaction for increased barrier function. ANG1 also increases vascular smooth muscle cell (SMC) recruitment indirectly by increasing expression of endothelial cell (EC)-derived chemoattractants, such as platelet-derived growth factor, hepatocyte growth factor, and heparin-binding epidermal growth factor. Binding of both VEGF and ANG1 to VEGFR-2 and Tie2, respectively, lead to increased cell survival through phosphoinositide 3-kinase (PI3K) activation. Portions of the figure adapted from

Ilvanainen et al. 2003; Kobayashi et al. 2006, Shibaya & Claesson-Welsh 2006, Olsson et al. 2006; Li et al. 2015).

1.4   Vascular targeted therapy for DMD

Vascular therapy has been identified as a potential treatment for DMD (Ennen et al. 2013). Since vascular endothelial growth factor (VEGF) has long been accepted as a master regulator of vessel development, groups are attempting to increase its function- through receptor modulation or administration of the growth factor itself- to enhance the vasculature in animal models of DMD. VEGF exerts its effect by binding to its type II receptor, VEGFR2, inducing receptor dimerization, leading to phosphorylation of intracellular tyrosine residues (Ruch et al. 2007). Activation of VEGFR2 can lead to increased signalling through a variety of pathways, but the most relevant to the angiogenic response in endothelial cells is the RAS/RAF/MEK/MAPK pathway, although the details have not been fully elucidated (Meadows et al. 2001). Ras activation in ECs has been shown to play a role in proliferation, migration, and branching cues. Importantly, VEGF binding to VEGFR2 also increases vascular permeability through formation of endothelial pores (Garrido-Urbani et al. 2008). Although VEGF induces an angiogenic response, the newly formed vessels are "leaky", lacking functional maturity, which may impede any enhancements to the blood flow. As such, it is hypothesized that use of VEGF in combination with other factors may be necessary to attain fully functional vessels. One factor in particular is the secreted glycoprotein angiopoietin-1 (ANG1), a member of the angiopoietin family of growth factors. By binding to the Tie2 receptor, ANG1 plays a vital role in endothelial remodelling (Baffert et al. 2004 & Thurston et al. 2005), vascular reinforcement (Gamble et al. 2000), and vessel survival (Cho et al. 2004). ANG1 is therefore under investigation for a range of diseases including sepsis and stroke (Sato et al. 2005). Given its role in promoting vascular maturity during both development and in adult tissue, ANG1 is a prime candidate to exert synergistic effects along with VEGF in dystrophic, ischemic muscle.

Another reason angiogenic growth factor supplementation may be beneficial to DMD patients is the fact that current gold standard medications may interfere with endogenous VEGF action. Glucocorticoids (Prednisone, Deflazacort), are the cornerstone therapy currently offered to DMD patients, with therapy beginning around five years of age. Randomized controlled trials that originated in the late 1980's revealed a short-term benefit to patients receiving glucocorticoids, evidenced by improved muscle function for six months to two years, but long term benefits were not apparent (Mendell et al. 1989). Although this study occurred decades ago, glucocorticoid treatment is still prescribed based on these findings. One potential explanation for this lack of long-term efficacy may reside in the fact that glucocorticoids inhibit VEGF and MMP-2 (Ishiguro et al. 2014). Matrix metalloproteinase-2 (MMP-2) is a promising candidate for enhancing VEGF-induced angiogenesis since it increases the ability of endothelial cells to degrade ECM components and invade through the matrix. Thus, while glucocorticoids may reduce inflammation, they may also be acting to reduce angiogenesis and perhaps contribute to the long-term progression of disease. It is possible that increasing circulating VEGF levels through treatment may alleviate this undesired effect of glucocorticoids and increase their efficacy as well.

1.4.1   Vascular therapy to reduce muscle ischemia

Proper blood delivery is vital to maintenance of healthy organs. In a highly metabolic tissue such as skeletal muscle, proper blood flow is crucial for delivering oxygen and nutrients that are in high demand, particularly during exercise and contractions required from day-to-day movements. The vascular response is crucial in mediating changes in blood flow, inducing vasodilation when there is an increased metabolic demand. Thus, in DMD patients in whom vasodilation is impaired, oxygen and nutrient delivery is reduced (Nelson et al. 2014). Although muscle ischemia is not the primary culprit responsible for the DMD pathology, it certainly perpetrates myonecrosis, adding to overall disease progression. Specifically, functional ischemia plays an integral, although not exclusive, role in contraction-induced muscle damage (Asai 2007). Increasing vasodilation via phosphodiesterase-5 (PDE-5) inhibitor, tadalafil, has been shown to lessen the extent of

myofiber damage in the *mdx* mouse (Adamo et al. 2010 Percival et al. 2012). In DMD patients, sildenafil, another PDE-5 inhibitor, rescues exercise-induced hyperaemia (Nelson et al. 2014). These findings highlight the value of increasing blood flow in the poorly perfused dystrophic skeletal muscle. An important question that is still unanswered is whether restoring blood flow actually slows disease progression in dystrophic muscle.

1.4.2   Vascular therapy to enhance endogenous repair

One of the main goals of vascular therapy is to introduce a factor, or factors, that act on vascular cells (endothelial cells, smooth muscle cells), to increase their function in the vascular network. An added benefit of vascular therapy that has been elucidated since the early 2000's is its effect on endogenous repair mechanisms. A number of studies have eloquently demonstrated that endogenous repair mechanisms are insufficient in DMD and animal models of the disease (Sacco et al. 2010, Dumont et al. 2015). In healthy individuals, muscle-specific stem cells, known as satellite cells, are largely responsible for this repair mechanism by regenerating new myofibers. A 2010 study by Sacco et al. demonstrated a reduced regenerative capacity of SCs derived from dystrophic muscle. Due to shortened telomere length and decreased telomerase activity, SCs in dystrophic skeletal muscle are unable to keep up with the self-renewal required to regenerate lost tissue. A 2015 study by Dumont et al. has received a great deal of attention for uncovering another deficient mechanism in *mdx* SCs. For decades, researchers have shown that myoblasts in culture do not express dystrophin, but this study showed, for the first time, that SCs do express the protein and that it is necessary for proper cell polarity. This polarity gives SCs important cues regarding needs for replication, activation, and differentiation. Thus dystrophin-deficient SCs do not receive proper environmental cues and therefore lack their full function. This study has paved the way for DMD to now be classified not only as a muscle-wasting disease, but also as a stem cell disease. Taken together, these studies have highlighted the need to improve endogenous repair mechanisms in a system where this process is quickly exhausted.

Viral delivery of VEGF has demonstrated its ability to improve endogenous repair in skeletal muscle. Following injection of recombinant adeno-associated VEGF (rAA VEGF), histological findings show an increase in myogenin-positive SCs. Myogenin is expressed early in myogenesis and is therefore a good indicator of regeneration. This study also demonstrated a significant increase in the number of regenerating myofibers compared to *mdx* mice receiving a control injection (Messina et al. 2007). Similar results were observed in a hind limb ischemia model and the glycerol and cardiotoxin models of muscle injury (Arsic et al. 2004). It is now well accepted that SCs express both VEGF as well as its receptor, VEGFR-2, and in fact, in healthy skeletal muscle, SCs account for the majority of VEGF and VEGFR-2 expression.

1.4.3   Vascular therapy to enhance cell therapy

In regards to using vascular therapy as an adjunct to other therapeutic approaches, there is a growing body of evidence to suggest that it may enhance the engraftment and function of transplanted cells. A major hurdle of current cell therapy approaches is the lack of survival, migration, proliferation, and function of transplanted cells. In 1977, Schmalbruch et al. discovered that SCs reside in close proximity to microvasculature, suggesting a possible role for blood vessels in directing the movement of stem cells. Indeed, a 1984 study by Venkatasubramanian and Solursh demonstrated that embryonic skeletal muscle cells migrate toward a gradient of growth factors whereas other mesenchymal cell types present in the limb bud do not exhibit this chemotactic behaviour. The finding that myoblasts migrate towards areas of existing vasculature, due to secretion of pro-angiogenic growth factors, has prompted researchers to investigate the ability of angiogenesis to aid in the migration of transplanted myoblasts. Thus, in 2001, Corti et al. tested the ability of various growth factors to enhance migration of C2C12 myoblasts across an endothelial layer. Various growth factors, in particular hepatocyte growth factor as well as platelet-derived growth factors A and B significantly increased migration of myoblasts. VEGF has also been shown to increase migration of C2C12 myoblasts and SCs in the Boyden chamber assay, an *in vitro* experiment used to measure

cell migration (Germani et al. 2003). The hypothesis that VEGF may in fact enhance cell transplants was put to the test in a study assessing the effects of the growth factor on muscle derived stem cell transplants into the *mdx* mouse (Deasy et al. 2009). VEGF was shown to increase proliferation and differentiation of the stem cells *in vitro*, lending further evidence that VEGF does not act solely on endothelial cells in the context of DMD treatment. Although this group reported an increase in endogenous repair, decrease in fibrosis, and increase in microvasculature following transplantation of VEGF-expressing muscle stem cells, VEGF expression did not result in an increase in dystrophin-positive myofibers, which would be expected if these cells had indeed contributed to the new muscle. The authors do postulate, however, the lack of dystrophin-positive fibers could be due to the pro-proliferative effect of VEGF on MDSCs, resulting in increased proliferation of these transplanted cells, but not necessarily increased differentiation. Interestingly, a more recent study from the same group demonstrated the regenerative capacity of MDSCs is reduced when VEGF signalling is inhibited (Beckman et al. 2013). This study and others have highlighted the beneficial effect of VEGF on cell transplants, but have proposed that it may be through mechanisms other than enhancing the engraftment of these cell populations contribute to the reconstitution of the muscle (Distefano et al. 2013). VEGF as a proliferative stimulus may increase the survival of transplanted cells, thereby allowing them to exert a paracrine effect for a larger amount of time, contributing to further endogenous repair in the muscle. Overall, based on the chemotactic effect of pro-angiogenic factors such as VEGF, future studies using angiogenesis as a pre-treatment for cell transplants may augment the effect of these cells following treatment.

1.4.4   Limitations to current vascular therapy

Given the potential of angiogenesis to enhance both endogenous repair and cell therapy for treating DMD, methods for increasing VEGF, a potent inducer of angiogenesis, are attractive. Although an impressive body of research supports the potential efficacy of

VEGF as a DMD drug, the majority of studies have used viral methods to deliver the growth factor. Although adeno-associated viruses have been used in a number of clinical trials and appear to be relatively safe, it is not yet clear whether the actual dose of VEGF expressed in the tissue could be predicted in a consistent manner. This concern is of special importance considering the findings that describe formation of hemangiomas following long-term exposure to VEGF treatment at high doses (Springer et al. 1998, Lee et al. 2000). Thus, it would be of particular value to deliver the growth factor at a low dose in a more controlled manner.

The standard method for determining the effect of vascular therapy on angiogenesis is *ex vivo* histology. Elevation in expression of CD31, a marker of endothelial cells, is the most commonly used measurement of angiogenesis. Since CD31 is also a marker of macrophages and neutrophils, extreme care must be taken to ensure that measurement of this marker excludes any type of inflammatory cells present in dystrophic muscle. Further, CD31 marks the endothelial layer, but it does not mark functionally mature vessels. Thus, in addition to CD31, assessing alpha-smooth muscle actin expression in vascular smooth muscle cells may demarcate vessels that confer functional benefit to the muscle. Much like CD31 staining, though, extreme care must be taken to ensure distinction is made between αSMA that marks blood vessels compared to that which marks myofibroblasts. Previous studies that have reported changes in either CD31 or αSMA do not elaborate on the methods used to quantify expression of these markers histologically. Even taking these limitations into account, very few studies go beyond histological findings to assess the functional efficacy of vascular-targeted therapy. Thus, there is little evidence, to date, that VEGF, with or without ANG1, actually affects functional perfusion. Therefore, it is absolutely critical to determine whether or not these factors may affect perfusion and correlate those findings to conventional histological data.

Transplant studies using cells expressing VEGF have demonstrated a decrease in fibrosis following treatment. While these findings may suggest an anti-fibrotic role of VEGF in dystrophic muscle, this is an important assumption that has not yet been rigorously tested.

The importance of fibrosis in DMD has gained more attention in recent years and any therapeutic approach under investigation should specifically assess its effect on fibrosis in this disease. To do so, an appropriate animal model, one that develops significant fibrosis, must be used. There is currently a lack of data to support the anti-fibrotic role of VEGF in DMD. Given that VEGF has been shown to exacerbate extracellular matrix (ECM) deposition in other fibrotic diseases such as scleroderma and idiopathic pulmonary fibrosis (Maurer et al. 2014 & Hostettler et al. 2014), it is plausible that VEGF may also exert a pro-fibrotic response in DMD. Testing the effect of VEGF at an appropriate stage of disease progression and in a relevant model should be done prior to moving to larger animal models and, certainly, prior to clinical studies.

1.5 Functional assessment of therapeutic efficacy

While vascular-targeted therapy offers significant potential for the treatment of DMD, current research is hindered by an important limitation. The standard method for assessing the effect of vascular therapy is through invasive muscle biopsies that may themselves contribute to further disease progression (Forbes et al. 2013; Triplett et al. 2014). In addition to the invasive nature of muscle biopsies, information gleaned from this tissue is limited to histological (H&E, Masson's Trichrome stains), biochemical, and molecular (western blotting, gene expression) analyses that preclude any sort of longitudinal, functional assessment. DMD manifests as a very heterogeneous disease affecting certain muscle groups differently (Forbes et al. 2013; Triplett et al. 2013). In fact, some muscle groups appear nearly unaffected in DMD. Depending on the tissue region selected for biopsy, this sample may drastically over or underestimate the true extent of therapeutic efficacy in the patient. Thus, there is a critical need for ways to noninvasively assess disease progression and subsequent efficacy of therapeutic interventions.

1.5.1 Laser Doppler Imaging

Laser Doppler imaging (LDI) utilizes infrared light to monitor the movement of blood cells in the microvasculature. Since it is an optical technique, it is primarily used to

monitor blood flow in superficial tissues, such as in skin, to assess burns and the extent of fibrosis in systemic scleroderma, as well as intraoperatively during brain surgery. Researchers have used it to assess blood flow in a rodent hind limb ischemia model in rodents. In this model, an incision is made in one hind limb and the femoral artery is occluded, inducing ischemia in that limb. LDI is then used to monitor re-perfusion of that muscle over time. In recent years, groups have used the hind limb ischemia model to assess angiogenic capabilities in *mdx* mice (Palladino et al. 2013) and the effect of cell therapy on blood flow (Brenes et al. 2012). While these studies have tremendous value in demonstrating functional changes in the disease with and without a therapeutic intervention, there are inherent limitations to the use of LDI to assess therapy in DMD research. Depth of penetration is minimal, with the average depth capable of imaging via laser Doppler being 1mm (Rajan et al. 2008), although this value is strongly dependent on wavelength. This limited penetration makes LDI suitable for skin and superficial imaging, but not suitable for deeper tissues without invasive surgery. The degree of ligation is also a source of variability in inducing ischemia, opening up a potential source of misinterpreted results. Lastly, and perhaps most importantly, the hind limb ischemia model is an acute, invasive technique, suitable for animal research only. Although LDI studies provide valuable insights into functional effects of therapeutic intervention, a number of modifications would be required to use LDI to assess vascular therapy in patients. It would be invaluable to use a functional imaging tool that could be performed in both preclinical animal models as well as patients to better elucidate what differences may exist in treatment responses. Further, in a disease characterized by inflammation and constant muscle degeneration, studying therapeutic efficacy following an additional surgical injury may introduce a source of confounding results.

1.5.2 Non-invasive imaging

While the use of LDI in the hind limb ischemia model offers a number of advantages for basic researchers, it is not a practicable option for patient studies. The potential benefits that non-invasive imaging offers for both monitoring disease status and therapeutic outcome are numerous and may change our understanding of DMD progression and treatment. From the perspective of a patient, non-invasive imaging would eliminate the

need for painful muscle biopsies, which are the typical method of assessing muscle damage. The biopsy process itself may also induce further damage to already injured muscle. From the perspective of a researcher, non-invasive imaging allows for a more global analysis of what is happening *in vivo*, an advantage not offered by *ex vivo* histological analyses. It has also been suggested that changes observed non-invasively may precede changes in physiological outcome, i.e. muscle contractile strength and endurance (Ahmad et al. 2010), which is important when considering the timing of therapeutic intervention. It should be noted, however, that non-invasive imaging is not yet able to definitively diagnose DMD in patients (Grounds et al. 2008 Kuru et al. 2013). While new blood tests for detecting specific mutations in the dystrophin gene are being developed (Kim et al. 2010), it would be advantageous to investigate the use of non-invasive imaging for diagnostic purposes as well. Regardless, computed tomography (CT), magnetic resonance imaging (MRI), and positron emission tomography (PET) may be viable options to non-invasively assess disease progression and therapeutic efficacy.

1.5.2.1   DCE-CT

X-ray computed tomography (CT) technology utilizes computed-processed X-rays to produce a three-dimensional image of the internal structures of an object. Dense tissues such as bones will attenuate an X-ray more than tissues that are composed largely of water or air. CT resolutions between tissue densities allow researchers to distinguish between tissues that vary by only 1% in their densities, making it an ideal tool to image fat and muscle tissue (Gellerich et al. 1990; Goodpaster et al. 2000).   Given these characteristics, CT has been in use since the 1980's to monitor structural changes in dystrophic skeletal muscle, becoming a gold standard in assessing muscle degeneration.

While dynamic contrast enhanced CT (DCE-CT) has not been widely used in the DMD research field, it has made significant contributions to the diagnosis and treatment strategies of other diseases. DCE-CT has significantly improved outcomes for stroke patients by helping to distinguish stroke sub-types, which has enhanced patient quality of life and lessened the economic burden associated with poorly managed stroke treatment. There are some important limitations to using CT to assess muscle involvement in DMD

patients, which may explain the lack of routine clinical use. First, there are concerns with x-ray exposure to humans; repeated scans during a longitudinal study may be particularly unsafe for pediatric patients (Brenner et al. 2001). Current research is attempting to implement dose reduction methods using various software and hardware techniques that may reduce radiation dose by 2–3 fold, making it more suitable for use in young patients (Lee et al. 2010). Additionally, most CT methods are unable to distinguish between connective tissue and muscle, which makes it difficult to assess extent of fibrosis, another hallmark of DMD (Liu et al. 1993; Nakayama et al. 2013). Dynamic contrast-enhanced CT (DCE-CT) may address this issue by providing measurements of perfusion in skeletal muscle. Since fibrotic tissue is largely under perfused, blood flow to those areas is limited and thus may be detected via DCE-CT. The use of a radiopaque contrast agent, such as iodine with a high atomic number, is also ideally suited to monitor changes in muscle ischemia that are inherent to disease progression in DMD. DCE-CT has been used to assess changes in blood flow in the *mdx* mouse following exercise and to monitor disease progression in a severely affected model of DMD (Ahmed et al. 2011). While these results point to the usability of DCE-CT in murine models of DMD, no study to date has used this tool to assess therapeutic intervention.

1.5.2.2   MRI and PET

Magnetic resonance imaging (MRI) is an ideal imaging modality for visualizing the anatomy of soft tissue within the body, thus offering many potential benefits for use in assessing muscle pathogenesis in both animal models of DMD, DMD patients and other patients suffering from a broad spectrum of myopathies (Lamminen et al. 1990, a,b; Liu et al. 1993). Magnetic resonance imaging (MRI) involves placing a subject in a strong magnetic field, which results in the alignment of hydrogen nuclei that are part of water molecules. When an external radio wave is applied to the subject in the magnetic field, some of the nuclei are excited. After relaxing from this excited state, the released energy produces small radio signals, or pulses, that are detected by the scanner, in both time and space. The time it takes for the longitudinal or transverse excitations to relax are referred to as T1- and T2-relaxation times, respectively. Imaging techniques focused on transverse relaxation times produce images with areas of high water content appearing dark (weak

signal strength), and areas of higher fat content appearing bright (strong signal strength). To this end, MRI has been utilized to distinguish healthy versus dystrophic muscle in the *mdx* mouse (McIntosh et al. 1998). Specifically, T2-weighted images illustrate that degenerating muscle in *mdx* mouse hind limbs appear more heterogeneous on an MR image compared to hind limb musculature of a wild-type mouse, which appears largely homogeneous; higher T2 values were attained in control muscles and these regions of interest appeared "lighter" than in the degenerating muscle in *mdx* mice. Histologically, the "dark" areas on a T2 map were found to correspond to areas of inflammation and macrophage infiltration in dystrophic muscle lesions, as validated histologically. Additionally, some areas on a T2 map of dystrophic hind limbs exhibited an intense signal, indicating the presence of fatty infiltrate in the *mdx* mouse that was not present in healthy wild-type hind limb musculature (Dunn et al. 1999). Recent work by Vandenbourne and colleagues, confirms the use of T2 mapping to assess changes in skeletal muscle of the lower extremities in DMD patients aged 5–15. Specifically, this group confirmed that T2 values are elevated in lower limb muscles of DMD patients versus healthy, age-matched control subjects, including younger subjects between the ages of 5 and 8. Interestingly, these differences in T2 values correlated well with functional tests of muscle contractile strength tests in these individuals. Another recent study from 2010 reported the use of T2 mapping to examine the effect of corticosteroid treatment—the current gold standard therapy to inhibit/reduce inflammation—in DMD patients relative to both untreated and healthy patients. While patient compliance is always a potential issue given the age of DMD patients, MRI may be safely repeated and confers no pain to the individual. Furthermore, MRI does not involve ionizing radiation, making it an attractive tool for pediatric patient use. Taken together, these studies provide compelling evidence that MRI may be a valuable tool for providing information on global changes in muscle composition as disease progresses, with or without the use of therapeutic interventions.

While MRI and CT are useful for their detailed anatomical data and high resolution, PET imaging may offer more information in regards to muscle function in animal models and in DMD patients. PET involves the use of a radiolabeled substance that will emit positrons after injection into the body. When a positron collides with a nearby electron,

two 511 keV photon are created. Detectors in the PET scanner capture this coincidence event allowing for localization of the collision. Thus, depending on the radiolabeled substance, various types of cells and tissues can be imaged. The most widely used substance in patients today, mainly as a standard diagnostic imaging tool for cancer is fluorine[18]-labeled fluorodeoxyglucose (^{18}F-FDG), a glucose analog. Cells that express the GLUT-1 glucose transporter, mainly metabolically active cells, take up ^{18}F-FDG. While some studies have used FDG-PET for assessing muscular dystrophy-related cardiomyopathy in patients (Quinlivan et al. 1996), it has yet to be assessed in significant studies of skeletal muscle metabolism in DMD patients. There is strong evidence that FDG-PET will be a useful tool for monitoring inflammation in myopathies as indicated by a progressive increase in FDG uptake compared to wild-type controls (Tateyama et al. 2015, Al Nahhas et al. 2011).

While PET imaging may be a promising avenue for longitudinally assessing muscle degeneration and therapeutic interventions, there are a few limitations that must also be considered. First, more work needs to be conducted to determine the utility of FDG as a radiolabel for inflammatory cells. Although inflammatory cells express the GLUT-1 receptor, muscle cells, which are highly metabolic, express this receptor as well. As such, changes in FDG uptake could be due to changes in inflammation or due to changes in muscle metabolism. Thus, more proof-of-principle studies will be required prior to using FDG in the context of DMD. Similarly, although MRI offers considerable advantages for imaging skeletal muscle, there are still drawbacks to using this modality. Hence CT is most optimal for preclinical studies in DMD research. Imaging time is significantly longer for MRI compared to CT, which is a drawback for both pediatric patients as well as preclinical studies in mice whereby a mouse would need to be anesthetised for hours compared to just minutes for CT. In terms of feasibility, the cost of an MRI scan is much higher than for a CT scan and, for clinical studies, claustrophobia and patient compliance would be a more significant issue using MRI.

1.6   Thesis hypotheses and specific objectives

1.6.1   Hypotheses

A combination of VEGF and ANG1, but not VEGF alone, will enhance skeletal muscle perfusion in a murine model of muscular dystrophy and this effect can be measured non-invasively using dynamic contrast-enhanced computed tomography.

1.6.2   Specific objectives

Chapter 2

i)   Investigate histopathological features in the *mdx*, *mdx*/*utrn*+/- and dko mice and compare those findings to C57BL/10 mice to determine the suitability of each as a model of Duchene muscular dystrophy.

Chapter 3

ii)   Determine whether VEGF elicits a pro-fibrotic response in fibroblasts derived from a murine model of DMD.

Chapter 4

iii) Assess the effect of VEGF alone or in combination with ANG1 on the microenvironment (i.e. vasculature, collagen deposition, and inflammatory infiltration) in dystrophic murine skeletal muscle.

iv)   Employ dynamic contrast-enhanced computed tomography (DCE-CT) to determine if *ex vivo* changes in angiogenic, inflammatory, and fibrotic markers observed in aim 3 correlate with functional changes in skeletal muscle perfusion.

1.7 References

Abreu JG, Ketpura NI, Reversade B, De Robertis EM. Connective-tissue growth factor (CTGF) modulates cell signaling by BMP and TGF-beta. *Nat Cell Biol* 2002;4(8):599-604. 22.

Ahmad N, et al. Use of imaging biomarkers to assess perfusion and glucose metabolism in the skeletal muscle of dystrophic mice. *BMC Musculoskelet Disord*. 2011;12:127.

Amthor H, Egelhof T, McKinnell I, Ladd ME, Janssen I, Weber J. Albumin targeting of damaged muscle fibres in the *mdx* mouse can be monitored by MRI. *Neuromuscul Disord*. 2004;14(12):791-6.

Arpan I, Forbes SC, Lott DJ, Senesac CR, Daniels MJ, Triplett WT. T2 mapping provides multiple approaches for the characterization of muscle involvement in neuromuscular diseases: a cross-sectional study of lower leg muscles in 5–15-year-old boys with Duchenne muscular dystrophy. *NMR Biomed*. 2013;26(3):320-8.

Asai A, Sahani N, Kaneki M, Ouchi Y, Martyn JA, Yasuhara SE. Primary role of functional ischemia, quantitative evidence for the two-hit mechanism, and phosphodiesterase-5 inhibitor therapy in mouse muscular dystrophy. *PLoS One*. 2007;2:e806.

Baffert F, Thurston G, Rochon-Duck M, Le T, Brekken R, McDonald DM. Age-related changes in vascular endothelial growth factor dependency and angiopoietin-1-induced plasticity of adult blood vessels. *Circ Res*. 2004;94: 984–992.

Best TM, Gharaibeh B, Huard J. Stem cells, angiogenesis and muscle healing: A potential role in massage therapies? *Postgrad Med J*. 2013; 89(1057):666-70.

Biernacka A, Dobaczewski M, Frangogiannis NG. TGF-beta signaling in fibrosis. *Growth Factors*. 2011;29(5):196-202.

Blake DJ, Weir A, Newey SE, Davies KE. Function and genetics of dystrophin and dystrophin-related proteins in muscle. *Physiol Rev.*2002; 82(2):291-329.

Brandan E, Cabello-Verrugio C, Vial C. Novel regulatory mechanisms for the proteoglycans decorin and biglycan during muscle formation and muscular dystrophy. *Matrix Biol*. 2008;27(8):700-8. 21.

Brenner D, Elliston C, Hall E, Berdon W. Estimated risks of radiation-induced fatal cancer from pediatric CT. *AJR Am J Roentgenol*. 2001;176(2):289-96.

Cabello-Verrugio C, Brandan E. A novel modulatory mechanism of transforming growth factor-beta signaling through decorin and LRP-1. *J Biol Chem* 2007;282(26):18842-50.

Cho CH, et al. Designed angiopoietin-1 variant, COMP-ANG1, protects against radiation-induced endothelial cell apoptosis. *Proc Natl Acad Sci U S A*. 2004;101: 5553–5558

Cirak S, et al. Restoration of the dystrophin-associated glycoprotein complex after exon skipping therapy in Duchenne muscular dystrophy. *Mol Ther*. 2012;20(2):462-7.

Corti S, et al.. Chemotactic factors enhance myogenic cell migration across an endothelial monolayer. *Exp Cell Res.* 2001;268(1):36-44.

Cruz Guzmán Odel R, Chávez García AL, Rodríguez-Cruz M. Muscular Dystrophies at Different Ages: Metabolic and Endocrine Alterations. *Int J Endocrinol*. 2012; 2012:485376.

Deasy BM, Feduska JM, Payne TR, Li Y, Ambrosio F, Huard J. Effect of VEGF on the regenerative capacity of muscle stem cells in dystrophic skeletal muscle. *Mol Ther.* 2009;17(10):1788-98.

Desguerre I, Arnold L, Vignaud A, Cuvellier S, Yacoub-Youssef H, Gherardi RK, et al. A new model of experimental fibrosis in hindlimb skeletal muscle of adult mdx mouse mimicking muscular dystrophy. *Muscle Nerve*. 2012;45(6):803-14.

Dunn JF, Zaim-Wadghiri Y. Quantitative magnetic resonance imaging of the *mdx* mouse model of Duchenne muscular dystrophy. *Muscle Nerve*. 1999;22(10):1367-71.

Eagle M, et al. Survival in duchenne muscular dystrophy: Improvements in life expectancy since 1967 and the impact of home nocturnal ventilation. *Neuromuscul Disord.* 2002;12(10):926-9.

Emery AE. Population frequencies of inherited neuromuscular diseases--a world survey. *Neuromuscul Disord.* 1991;1(1):19-29.

Emery AE. The muscular dystrophies. *Lancet* 2002;359(9307):687-95.

Emery AE. The muscular dystrophies. *Lancet*. 2002;359 (9307): 687–695

Ennen JP, Verma M, Asakura A. Vascular-targeted therapies for duchenne muscular dystrophy. *Skelet Muscle.* 2013;3(1):9,5040-3-9.

Fakhfakh R, Lee S-J, Tremblay JP. Administration of a soluble activin type iib receptor promotes the transplantation of human myoblasts in dystrophic mice. *Cell transplantation*. 2012;21(7):1419-1430.

Filareto A, Parker S, Darabi R, Borges L, Iacovino M, Schaafet T, et al. An ex vivo Gene Therapy Approach to Treat Muscular Dystrophy Using inducible Pluripotent Stem Cells. *Nature communications*. 2013;4:1549.

Flanigan KM, von Niederhausern A, Dunn DM, Alder J, Mendell J, Weiss RB. Rapid Direct Sequence Analysis of the Dystrophin Gene. *Am J Hum Genet.* 2003; 72(4):931-9.

Forbes SC, Walter GA, Rooney WD, Wang DJ, DeVos S, Pollaro J. Skeletal muscles of ambulant children with Duchenne muscular dystrophy: validation of multicentre study of evaluation with MR imaging and MR spectroscopy. *Radiology*. 2013;269(1):198-207.

Fujimoto T, Itoh M, Tashiro M, Yamaguchi K, Kubota K, Ohmori H. Glucose uptake by individual skeletal muscles during running using whole-body positron emission tomography. *Eur J Appl Physiol*. 2000;83(4–5):297-302.

Gamble JR, et al. Angiopoietin-1 is an antipermeability and anti-inflammatory agent in vitro and targets cell junctions. *Circ Res*. 2000;87: 603–607

Garrido-Urbani S, Bradfield PF, Lee BP, Imhof BA. Vascular and epithelial junctions: a barrier for leucocyte migration. *Biochem Soc Trans*. 2008;36(Pt 2):203-11.

Gellerich I, Koch RD. Computerized tomography findings in malignant progressive Duchenne muscular dystrophy. *Psychiatr Neurol Med Psychol (Leipz)* 1990;42(5): 282-90.

Goodpaster BH, Kelley DE, Thaete FL, He J, Ross R. Skeletal muscle attenuation determined by computed tomography is associated with skeletal muscle lipid content. *J Appl Physiol*. 2000;89(1):104-10.

Grounds MD, Radley HG, Lynch GS, Nagaraju K, De Luca A. Towards developing standard operating procedures for pre-clinical testing in the *mdx* mouse model of duchenne muscular dystrophy. *Neurobiol Dis.* 2008;31(1):1-19.

Hoffman EP, Brown RH,Jr, Kunkel LM. Dystrophin: The protein product of the duchenne muscular dystrophy locus. *Cell.* 1987;51(6):919-28.

Hogrel JY, et al.. Assessment of a symptomatic duchenne muscular dystrophy carrier 20 years after myoblast transplantation from her asymptomatic identical twin sister. *Neuromuscul Disord.* 2013;23(7):575-9.

Iivanainen E, et al. Angiopoietin-regulated recruitment of vascular smooth muscle cells by endothelial-derived heparin binding EGF-like growth factor. *FASEB J.* 2003;17(12):1609-21.

Ito K, et al. Smooth muscle-specific dystrophin expression improves aberrant vasoregulation in *mdx* mice. *Hum Mol Genet.* 2006;15:2266-2275.

Iyombe-Engembe JP, Ouellet DL, Barbeau X, Rousseau J, Chapdelaine P, Lagüe P, Tremblay JP Efficient Restoration of the Dystrophin Gene Reading Frame and Protein

Structure in DMD Myoblasts Using the CinDel Method. *Mol Ther Nucleic Acids.* 2016;5:e283.

Jackson RS, Schlarkman TC, Hubble WL, Osman MM. Prevalence and patterns of physiologic muscle uptake detected with whole-body 18F-FDG PET. *J Nucl Med Technol.* 2006;34(1):29-33.

Kim HK, Laor T, Horn PS, Wong B. Quantitative assessment of the T2 relaxation time of the gluteus muscles in children with Duchenne muscular dystrophy: a comparative study before and after steroid treatment. *Korean J Radiol.* 2010;11(3):304-1.

Kinahan PE, Hasegawa BH, Beyer T. X-ray-based attenuation correction for positron emission tomography/computed tomography scanners. *Semin Nucl Med.* 2003;33(3):166-79.

Klingler W, Jurkat-Rott K, Lehmann-Horn F, Schleip R. The role of fibrosis in duchenne muscular dystrophy. *Acta Myol.* 2012;31(3):184-95.

Kobayashi H, DeBusk LM, Babichev YO, Dumont DJ, Lin PC. Hepatocyte growth factor mediates angiopoietin-induced smooth muscle cell recruitment. *Blood.* 2006;108(4), 1260–1266.

Kobayashi YM, et al. Sarcolemma-localized nNOS is required to maintain activity after mild exercise. *Nature.* 2008;27;456(7221):511-5.

Koch S, Claesson-Welsh L. (2012). Signal Transduction by Vascular Endothelial Growth Factor Receptors. *Cold Spring Harb Perspect Med.* 2012;2(7):a006502.

Kuru S, Satai M, Tanaka N, Konagaya M, Nakayam T, Kawai M. Natural course of muscular involvement assessed by computed tomography method in Duchenne muscular dystrophy. *Neurol Clin Neurosci.* 2013;1(2):63-8.

Laing NG, Davis MR, Bayley K, Fletcher S. Wilton SD. Molecular Diagnosis of Duchenne Muscular Dystrophy: Past, Present and Future in Relation to Implementing Therapies. *Clin Biochem Rev.* 2011;32(3), 129–134.

Lamminen AE, Tanttu JI, Sepponen RE, Suramo IJ, Pihko H. Magnetic resonance of diseased skeletal muscle: combined T1 measurement and chemical shift imaging. *Br J Radiol*. 1990a;63(752):591-6.

Lamminen AE. Magnetic resonance imaging of primary skeletal muscle diseases: patterns of distribution and severity of involvement. *Br J Radiol.* 1990b;63946-50.

Landfeldt E, et al. Compliance to Care Guidelines for Duchenne Muscular Dystrophy. *J Neuromuscul Dis.* 2015; 2(1), 63–72.

Leask A, Abraham DJ. All in the CCN family: Essential matricellular signaling modulators emerge from the bunker. *J Cell Sci.* 2006;119:4803-10.

Leask A. TGFbeta, cardiac fibroblasts, and the fibrotic response. *Cardiovasc Res* 2007;74(2):207-12.

Lee TY, Chhem RK. Impact of new technologies on dose reduction in CT. *Eur J Radiol.* 2010;76(1):28-35.

Lemieux C, Maliba R, Favier J, Theoret J-F, Merhi Y, Sirois MG. Angiopoietins can directly activate endothelial cells and neutrophils to promote proinflammatory responses. *Blood.* 2005;105:1523–1530

Li L, et al. P38/MAPK contributes to endothelial barrier dysfunction via MAP4 phosphorylation-dependent microtubule disassembly in inflammation-induced acute lung injury. *Sci Rep.* 2015;5:8895. doi: 10.1038/srep08895.

Liu GC, Jong YJ, Chiang CH, Jaw TS. Duchenne muscular dystrophy: MR grading system with functional correlation. *Radiology.* 1993;186(2):475-80.

Liu M, Chino N, Ishihara T. Muscle damage progression in Duchenne muscular dystrophy evaluated by a new quantitative computed tomography method. *Arch Phys Med Rehabil.* 1993;74(5): 507-14.

Long C, Amoasii L, Mireault AA, McAnally JR, Li H, Sanchez-Ortiz E, et al. Postnatal genome editing partially restores dystrophin expression in a mouse model of muscular dystrophy. *Science*. 2016;351(6271):400-403.

Long C, McAnally JR, Shelton JM, Mireault AA, Bassel-Duby R, Olson EN. Prevention of muscular dystrophy in mice by CRISPR/Cas9–mediated editing of germline DNA. *Science*. 2014;345(6201):1184-1188.

Loufrani L, Matrougui K, Gorny D, et al. Flow (shear stress)-induced endothelium-dependent dilation is altered in mice lacking the gene encoding for dystrophin. *Circulation.* 2001;103(6):864–870.

Lynn S, et al. Measuring clinical effectiveness of medicinal products for the treatment of Duchenne muscular dystrophy. *Neuromuscul Disord.* 2015;25(1):96-105.

Matsakas A, Yadav V, Lorca S, Narkar V. Muscle ERRgamma mitigates Duchenne muscular dystrophy via metabolic and angiogenic reprogramming. *FASEB J.* 2013;27(10):4004-16.

McIntosh LM, Baker RE, Anderson JE. Magnetic resonance imaging of regenerating and dystrophic mouse muscle. *Biochem Cell Biol.* 1998;76532-41.

Mendell JR, et al. Myoblast transfer in the treatment of Duchenne's muscular dystrophy. *N Engl J Med.* 1995;333:832–838.

Mendell JR, et al. Randomized, double-blind six-month trial of prednisone in Duchenne's muscular dystrophy. *N Engl J Med.* 1989;320(24):1592-7.

Miyazaki D, et al. Matrix metalloproteinase-2 ablation in dystrophin-deficient *mdx* muscles reduces angiogenesis resulting in impaired growth of regenerated muscle fibers. *Hum Mol Genet.* 2011;20(9):1787-99.

Nakayama T, Kuru S, Okura M, Motoyoshi Y, Kawai M. Estimation of net muscle volume in patients with muscular dystrophy using muscle CT for prospective muscle volume analysis: an observational study. *BMJ Open.* 2013;3(10):e003603.

Nelson CE, Hakim CH, Ousterout DG, Thakore PI, Moreb EA, Castellanos Rivera RM, et al. In vivo genome editing improves muscle function in a mouse model of Duchenne muscular dystrophy. *Science*. 2016;351(6271):403-7.

Oi N, Iwaya T, Itoh M, Yamaguchi K, Tobimatsu Y, Fujimoto T. FDG-PET imaging of lower extremity muscular activity during level walking. *J Orthop Sci.* 2003;8(1):55-61.

Olsson AK, Dimberg A, Kreuger J, Claesson-Welsh L. VEGF receptor signalling - in control of vascular function. *Nat Rev Mol Cell Biol.* 2006;7(5):359-71.

Palladino M, et al. Angiogenic impairment of the vascular endothelium: A novel mechanism and potential therapeutic target in muscular dystrophy. *Arterioscler Thromb Vasc Biol.* 2013;33(12):2867-76.

Pappas GP, Olcott EW, Drace JE. Imaging of skeletal muscle function using (18) FDG PET: force production, activation and metabolism. *J Appl Physiol.* 2001;90(1):329-37.

Quinlivan RM, Lewis P, Marsden P, Dundas R, Robb SA, Baker E. Cardiac function, metabolism and perfusion in Duchenne and Becker muscular dystrophy. *Neuromuscul Disord.* 1996;6(4):237-46.

Rodino-Klapac LR, Mendell JR, Sahenk Z. Update on the treatment of duchenne muscular dystrophy. *Curr Neurol Neurosci Rep.* 2013;13(3):332,012-0332-1.

Ruch C, Skiniotis G, Steinmetz MO, Walz T, Ballmer-Hofer K. Structure of a VEGF-VEGF receptor complex determined by electron microscopy. *Nat Struct Mol Biol*. 2007; 14(3):249-50.

Rybakova IN, Patel JR, Ervasti JM. The dystrophin complex forms a mechanically strong link between the sarcolemma and costameric actin. *J Cell Biol.* 2000;150(5):1209-14.

Sampaolesi M, et al. Mesoangioblast stem cells ameliorate muscle function in dystrophic dogs. *Nature.* 2006;444(7119):574-9.

Sander M, et al. Functional muscle ischemia in neuronal nitric oxide synthase-deficient skeletal muscle of children with duchenne muscular dystrophy. *Proc Natl Acad Sci.* 2000;5;97(25):13818-23.

Sato T, et al. Distinct roles of the receptor tyrosine kinases Tie-1 and Tie-2 in blood vessel formation. *Nature.* 1995;376: 70–74

Seto JT, Bengtsson NE, Chamberlain JS. Therapy of genetic disorders-novel therapies for duchenne muscular dystrophy. *Curr Pediatr Rep.* 2014; 2(2):102-12.

Shiao T, et al. Defects in neuromuscular junction structure in dystrophic muscle are corrected by expression of a NOS transgene in dystrophin-deficient muscles, but not in muscles lacking alpha- and beta1-syntrophins. *Hum Mol Genet.* 2004;13(17):1873-84.

Shibuya M, Claesson-Welsh L. Signal transduction by VEGF receptors in regulation of angiogenesis and lymphangiogenesis. *Exp Cell Res.* 2006;312(5):549-60.

Skuk D, et al. Dystrophin expression in muscles of Duchenne muscular dystrophy patients after high-density injections of normal myogenic cells. *J Neuropathol Exp Neurol.* 2006;65: 371–386

Skuk D, et al. Dystrophin expression in myofibers of Duchenne muscular dystrophy patients following intramuscular injections of normal myogenic cells. *Mol Ther.* 2004;9: 475–482.

Skuk D, et al. First test of a "high-density injection" protocol for myogenic cell transplantation throughout large volumes of muscles in a Duchenne muscular dystrophy patient: eighteen months follow-up. *Neuromuscul Disord.* 2007;17: 38–46

Skuk D, Tremblay JP. Confirmation of donor-derived dystrophin in a Duchenne muscular dystrophy patient allotransplanted with normal myoblasts. *Muscle Nerve*. 2016. doi: 10.1002/mus.25129. [Epub ahead of print]

Song T-J, Lee K-A, Kang S-W, Cho H, Choi Y-C. Three Cases of Manifesting Female Carriers in Patients with Duchenne Muscular Dystrophy. *Yonsei Med J.* 2011;52(1), 192–195.

Straub V, Donahue KM, Allamand V, Davisson RL, Kim YR, Campbell KP. Contrast agent-enhanced magnetic resonance imaging of skeletal muscle damage in animal models of muscular dystrophy. *Magn Reson Med*. 2000;44655-5.

Sun G, et al. Connective tissue growth factor is overexpressed in muscles of human muscular dystrophy. *J Neurol Sci.* 2008;267(1-2):48-56.

Suri C, et al. Requisite role of angiopoietin-1, a ligand for the TIE2 receptor, during embryonic angiogenesis. *Cell.* 1996;87(7):1171-80.

Tabebordbar M, Zhu K, Cheng JK, Chew WL, Widrick JJ, Yan WX, et al. In vivo gene editing in dystrophic mouse muscle and muscle stem cells. *Science.* 2016;351(6271):407-11.

Thurston G, et al. Angiopoietin 1 causes vessel enlargement, without angiogenic sprouting, during a critical developmental period. *Development.* 2005;132: 3317–3326.

Triplett WT, et al.. Chemical shift-based MRI to measure fat fractions in dystrophic skeletal muscle. *Magn Reson Med.* 2014;72(1):8-19

van den Bergen JC, Wokke BH, Hulsker MA, Verschuuren JJ, Aartsma-Rus AM. Studying the role of dystrophin-associated proteins in influencing becker muscular dystrophy disease severity. *Neuromuscul Disord*. 2015;25(3):231-7.

Van Ruiten, H. J. A., Straub, V., Bushby, K., & Guglieri, M. Improving recognition of Duchenne muscular dystrophy: a retrospective case note review. *Arch Dis Child.* 2014;99(12), 1074–1077.

Venkatasubramanian K, Solursh M. Chemotactic behavior of myoblasts. *Dev Biol.* 1984;104(2):428-33.

Verrecchia F, Mauviel A. Transforming growth factor-beta and fibrosis. *World J Gastroenterol.* 2007;13(22):3056-62.

Wei Y, Speechley KN, Zou G, Campbell C. Factors Associated With Health-Related Quality of Life in Children With Duchenne Muscular Dystrophy. J Child Neurol. 2016; pii: 0883073815627879. [Epub ahead of print]

White JA, Rajchl M, Butler J, Thompson RT, Prato FS, Wisenberg G. Active cardiac sarcoidosis: first clinical experience of simultaneous positron emission tomography—magnetic resonance imaging for the diagnosis of cardiac disease. *Circulation.* 2013;127(22):e639-41.

Xie T, Bolch WE, Lee C, Zaidi H. Pediatric radiation dosimetry for positron-emitting radionuclides using anthropomorphic phantoms. *Med Phys.* 2013;40(10):e102502.

Yeung HD, Grewal RK, Gonen M, Schoder H, Larson SM. Patterns of F-FDG uptake in adipose tissue and muscle: a potential source of false-positives for PET. *J Nucl Med* 2003;441789-9.

Yokoyama I, Inoue Y, Moritan T, Ohtomo K, Nagai R. Simple quantification of skeletal muscle glucose utilisation by static 18F-FDG PET. *J Nucl Med.* 2003;44(10):1592-8.

Chapter 2

Skeletal Muscle Fibrosis in the *mdx*/*utrn*+/- Mouse Validates Its Suitability as a Murine Model of Duchenne Muscular Dystrophy [2]

---

2 Skeletal muscle fibrosis in the *mdx/utrn+/-* mouse validates its suitability as a murine model of DMD

2.1 Chapter Summary

The *mdx* mouse and X-linked canine muscular dystrophy are the two most widely used animal models of DMD. Given the ethical concerns regarding the use of canine models for basic research, the *mdx* mouse is by far the most commonly cited model in preclinical studies. Although the dystrophin-null *mdx* mouse genotypically mimics the human disease, recent focus on the importance of fibrosis in DMD highlights the importance of this aspect be represented in any suitable model. Since our research focus on the use of angiogenic factors as a treatment for DMD and other studies have suggested the ability of some angiogenic growth factors to induce fibrosis, using a model that is more prone to fibrosis is absolutely critical in the accurate assessment of therapeutic side effects. The presence of utrophin, a dystrophin analogue, inversely correlates with disease progression. Therefore, the *mdx* (utrophin +/+), heterozygous (*mdx/utrn+/*), and double knockout (*mdx/utrn-/-*) mice all represent varying degrees of disease severity. In the present study, we compare disease pathology in the *mdx* mouse with the other two models. Importantly, we also compare disease pathology to the C57BL/6 wild type mouse to provide an accurate margin for classifying fibrotic from non-fibrotic muscle tissue. Using extent of collagen deposition and number of centrally nucleated myofibers as indicators of disease severity, we show that the heterozygous *mdx/utrn+/-* mouse is a superior model to the *mdx* mouse since extent of collagen deposition is greater by 7-8 weeks of age compared to the wild-type or *mdx* models. This study established the best model and age to incorporate in the subsequent studies described in this thesis.

2.2   Introduction

Treatment strategies for Duchenne muscular dystrophy (DMD), a severe neuromuscular degenerative disorder, have been ongoing for decades with little significant long-term efficacy reported (Pichavant et al. 2011). While scientific and technological advancements have enhanced patient quality of life, the disease remains invariably fatal. The majority of current research into treating DMD involves the restoration of the protein dystrophin, which is absent or non-functional in these patients. Of these, a number of studies in DMD patients have used cell therapy to replace dystrophin, reporting an increase in dystrophin-positive myofibers (Mendel et al. 1995; Skuk et al. 2004, 2006, 2007; Rodino-Klapac et al. 2013; Cirak et al. 2012; Seto et al. 2014). While these studies have successfully reintroduced the protein to dystrophic skeletal muscle, improvements in function have been limited. A recent study by Hogrel et al. reported a potential long-term effect of a myoblast transplant into an affected female carrier of the dystrophin mutation. Although long-term functional effects could not be definitively concluded from this study, the results suggest beneficial effects of cell therapy (Hogrel et al. 2013). To date, the most commonly used murine model to test cell replacement and other strategies in a pre-clinical setting has been the *mdx* mouse, which lacks dystrophin due to an X-linked mutation in its gene (Partridge et al. 1989; Hindi et al. 2013). Although the *mdx* mouse is a genetic homolog of the human disease, it has been shown that this model does not mimic the pathology observed in patients because up-regulation of utrophin, a dystrophin analogue, partially compensates for the absence of the cytoplasmic protein (Grady et al. 1997). Additionally, the longer telomere length present in inbred laboratory mice confer a greater regenerative capacity of muscle progenitor cells in these animals compared to human skeletal muscle (Sacco et al. 2010). As a result of these differences, the disease does not manifest severely in *mdx* mice. Specifically, fibrosis, a hallmark feature of DMD in patients, is not overt in *mdx* mice (Desguerre et al. 2014). A lack of dystrophin in skeletal muscle leads to decreased sarcolemma integrity, which causes an increase in cell membrane permeability. As a result, an influx of calcium ions causes increased protein degradation that eventually leads to muscle cell death. Inflammatory cells that infiltrate the site of necrosis are a rich source of transforming growth factor beta (TGFβ). TGFβ then exerts its pro-fibrotic effect on fibroblasts, which then increase

production of extracellular matrix (ECM) proteins. An excessive amount of ECM production leads to the eventual onset of fibrosis (Desguerre et al. 2009). The fact that DMD patients develop severe fibrosis whereas *mdx* mice do not may, in part, explain why treatments performed in murine studies have been ineffective in human trials. Fibrosis limits the amount of available muscle tissue to target with stem cell, gene or drug therapy (Bernasconi et al. 1999). Thus, use of an appropriate model that more accurately reflects the histopathology of DMD fibrosis may better direct current research. Recent advances in exon-skipping have highlighted the importance of a suitable murine model in pre-clinical studies. In 2010, Goyenvalle demonstrated an increase in dystrophin expression in severely affected mice lacking both utrophin and dystrophin following multiple injections with a morpholino oligomer targeted to exon 23 of the dystrophin gene (Goyenvalle et al. 2010). Two years later, the same group modified their protocol to use an adeno-associated virus vector containing a small nuclear RNA specific to exon 23. A single treatment was sufficient to restore dystrophin in all muscles examined, including heart tissue, and dramatically increased life expectancy from 10 to 50 weeks of age (Goyenvalle et al. 2012). These studies have been crucial in highlighting the need for inclusion of a more accurate DMD mouse model with which to assess the efficacy of therapeutic strategies.

Although utrophin-dystrophin-deficient (dko) mice were generated in 1997, they are scarcely used in current studies, perhaps in part due to their severe disease phenotype, which makes them difficult to include in longitudinal studies. While a select number of research groups have used this severely affected mouse model, the predominant model used in today's research lab is still the *mdx* mouse. A few studies have suggested that haploinsufficiency of the utrophin gene (*mdx*/*utrn*+/-) may provide a more appropriate murine model of DMD (Huang et al. 2011). For example, it has been shown that diaphragm and quadriceps muscles of *mdx*/*utrn*+/- mice become fibrotic as early as 3 and 6 months of age, respectively (Zhou et al. 2008). Many studies involving murine models of DMD have used mice younger than 6 months of age, thus the purpose of this study was to investigate extent of fibrosis in the *mdx*/*utrn*+/- mouse at an earlier age to determine its suitability as a more accurate representation of the human pathology. Additionally, since quadriceps and diaphragm muscles were the only groups examined in

the aforementioned study, we focused our study on the gastrocnemius muscle as it has often been used as a site of cell implant (Beckman et al. 2013). In the present study, we examine extent of fibrosis and muscle regeneration in 8 week-old mice as well as aged 10 month-old mice and provide a comprehensive analysis of these parameters in various skeletal muscles that are used in DMD research.

2.3   Materials and Methods

2.3.1   Animal Care and Ethics Statement

Experiments were performed at The Lawson Health Research Institute at St. Joseph's Health Care (SJHC) in London, Ontario. Female C57BL/6 mice (5-7 weeks old upon arrival) were purchased from Charles Rivers and *mdx/utrn+/-* mice, originally generated by Dr.'s Mark Grady and Josh Sanes (Washington University, St. Louis) (Grady et al. 1997), were generously provided to us by Dr. Robert Grange (Virginia Polytechnic and State University) and maintained in the Animal Care Facility at SJHC. Colonies were maintained under controlled conditions (19-23˚C, 12 hour light/dark cycles) and allowed water and food *ad libitum*. 7 to 8 week-old and 10 month-old male and female C57BL/6, *mdx* and *mdx/utrn+/-* mice were used in this study. Only 7-8 week-old dko mice were used since these mice do not tend to live past 20 weeks of age. For comparison of various skeletal muscles, twelve week-old *mdx/utrn+/-* male and female mice were used. All procedures involving animal experiments were carried out in strict accordance with the Canadian Council on Animal Care (CCAC) and were approved by the Animal Use Subcommittee at Western University.

2.3.2   Genotyping

Genomic DNA from tail snips or ear notch tissue was used for genotyping. Briefly, ear notch tissue was lysed in a proteinase K solution at 50° C overnight. DNA was diluted appropriately and polymerase chain reaction was used to amplify the utrophin gene using Platinum *Taq* polymerase. Presence of the utrophin gene was detected using the following set of primers (Sigma): 5'-TGCAGTGTCTCCAATAAGGTATGAAC-3', 5'-

TGCCAAGTTCTAATTCCATCAGAAGCTG -3' (forward primers) and 5'-CTGAGTCAAACAGCTTGGAAGCCTCC-3' (reverse primer).

2.3.3   Tissue Preparation and Histology

For tissue collection, mice were sacrificed via gas euthanasia. Diaphragm and gastrocnemius (GM) muscles from 8 week-old and 10 month-old mice were dissected and immediately fixed in formalin for 24-48h and embedded in paraffin. For a more comprehensive analysis of disease manifestation in *mdx*/*utrn*+/- mice, diaphragm, quadriceps, soleus, tibialis anterior (TA) and gastrocnemius (GM) muscles were similarly isolated from 12 week-old *mdx*/*utrn*+/- mice. Extreme care was taken to ensure muscles were embedded in the same orientation across each muscle group. Tissue blocks were sectioned at 5um thickness and dried in an oven at 37°C overnight. To achieve representative sections from the whole muscle tissue, serial sections were taken every 20 slices, except for the diaphragm muscle where serial sections were taken every 3 slices. Tissue sections were then deparaffinised and rehydrated in a series of xylene and ethanol washes to prepare them for subsequent Masson's Trichrome staining for collagen content, or haematoxylin and eosin staining to visualize regenerating myofibers. Serial sections were used for the two staining methods to ensure that analysis of both collagen content and muscle regeneration referred to the same samples. Following the staining step, slides were dehydrated, washed in xylene and mounted with Permount mounting medium.

2.3.4   Microscopy and Image Analysis

Histological images were acquired on a Zeiss Axioscope microscope under a 20x objective using Northern Eclipse software. Non-overlapping fields of view of the entire tissue were taken for each section. Five sections were imaged per tissue. For assessment of myofiber damage, percentage of centrally located nuclei was used as an indication of regeneration. All fields of view containing cross-sectional myofibers were imaged and manually analyzed. Collagen content was assessed across the entire tissue slice and automatically quantified using an in-house colour thresholding algorithm written in MATLAB 2010a (Mathworks, Natick, MA, USA). Briefly, all images were transformed into Lab colour space allowing the isolation of the colour and lightness components of

each pixel. A k-means clustering algorithm was then applied to the colour components of each individual image to partition the pixels into groups of relatively 'red' or 'blue' colour values (Appendix A). A uniform threshold was applied to all images to mask regions with high lightness (appearing as white). Finally, morphological closing operations were performed on the 'red' and 'blue' regions to fill any gaps less than 3 pixels in radius. The percent of collagen present in each image was calculated as the area of the remaining 'blue' region divided by the area of the entire image. Automatic thresholds were manually verified with labeled colour overlays on the original histology images to ensure that collagen presence was accurately identified.

2.3.5   Statistical Analysis

For quantified images, a one-way ANOVA was performed followed by Tukey's post-hoc test to determine difference between groups using GraphPad Prism. Differences between groups were considered significant at a *p*-value less than 0.05 (n=3 for wild-type and dko mice and n=5 for *mdx* and *mdx*/*utrn*+/- mice).

2.4   Results

2.4.1   Fibrosis is present at 10 months of age in *mdx*/*utrn*+/-, but not *mdx*, GM muscle

At ten months of age, *mdx* gastrocnemius (GM) muscle did not differ in collagen content compared to GM muscle of wild-type mice (Figure 2.1). In contrast, haploinsufficiency of utrophin led to significant collagen deposition in GM tissue of aged *mdx*/*utrn*+/- mice (mean±SD: 12.76%±3.06, p=0.0033). There was no significant difference in collagen deposition between *mdx* and *mdx*/*utrn*+/- GM muscle. Although GM muscles of aged *mdx* mice did not show significant fibrosis compared to healthy wild-type controls, there was a large proportion of centrally-located nuclei in the myofibers indicative of muscle regeneration in both *mdx* (70.06%±7.6) and *mdx*/*utrn*+/- (58.86%±6.7) mice, respectively (p<0.0001, Figure 1D-F).
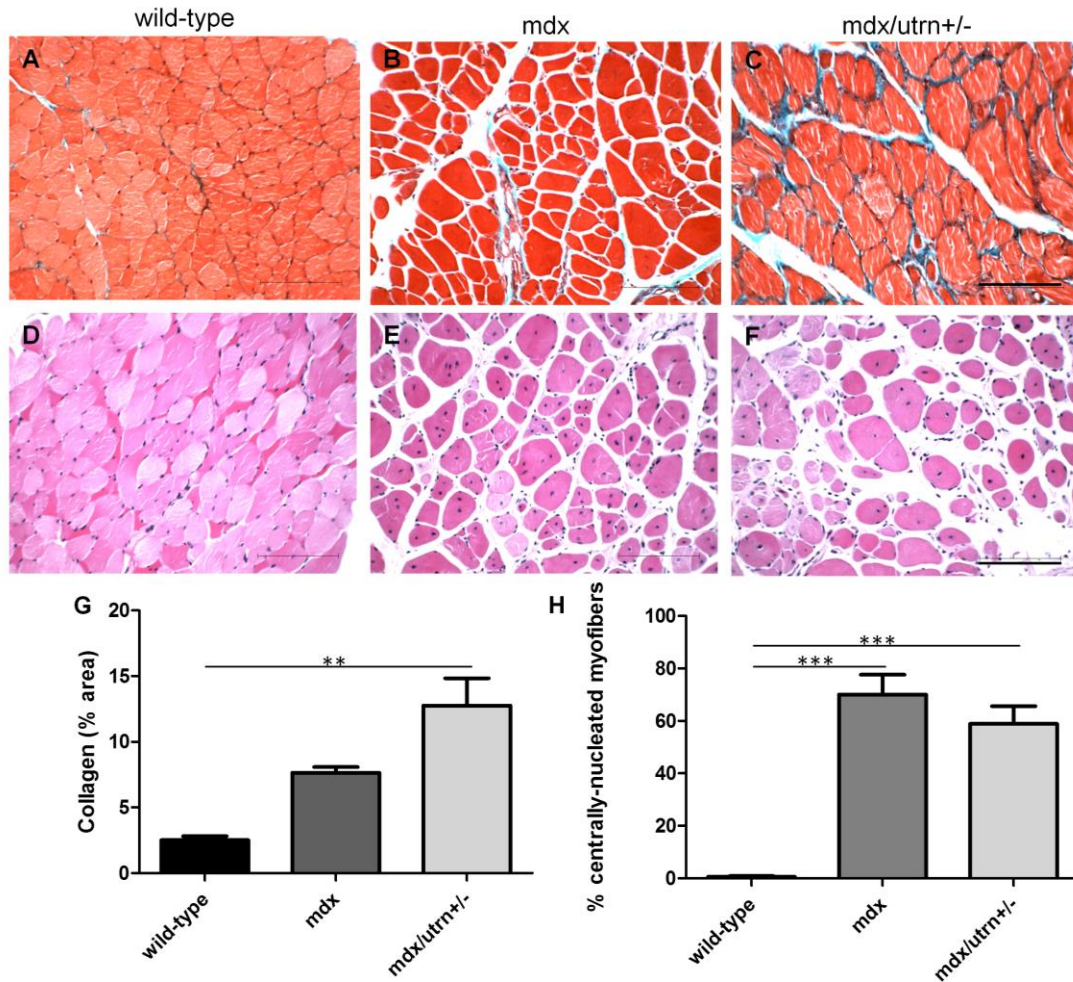
Figure 2.1: Muscle pathology in 10 month-old GM muscles of wild-type, *mdx* and *mdx/utrn+/-* mice.

Extent of total collagen staining (blue) in 10 month-old wild-type (A), *mdx* (B) and *mdx/utrn*+/- (C) GM muscle was used as a marker of fibrosis. Proportion of centrally nucleated fibers in the same tissues (D, E, and F) was measured to assess extent of regeneration. Quantification of total collagen staining (G) and proportion of centrally-nucleated myofibers (H) is represented as the mean +SD. ** represents $p<0.01$, and *** represents $p<0.001$ (scale bar=100µm).

2.4.2   DMD-associated fibrosis in present in both aged *mdx* and *mdx*/*utrn*+/- diaphragm muscle

Both *mdx* and *mdx*/*utrn*+/- diaphragm muscles were significantly fibrotic in ten month-old mice compared to age-matched wild-type controls (Figure 2A-C, p=0.026), indicated by an approximate 2.5 fold increase in collagen content. Both *mdx* and *mdx*/*utrn*+/- diaphragm muscle revealed a significantly higher percent of centrally located nuclei (34.65%±4.4 and 32.45%±5.6, respectively) compared to the age-matched wild-type mice (p<0.0001). There was no significant difference in number of centrally nucleated myofibers between *mdx* and *mdx*/*utrn*+/- mice (Figure 2.2).

2.4.3   Young *mdx*/*utrn*+/- and dko, but not *mdx*, GM muscle develops fibrosis compared to healthy GM muscle

Fibrosis was assessed in 8 week-old GM muscles of wild type, *mdx*, *mdx*/*utrn*+/- and dko mice (Figure 2.3). There was no observed fibrosis in *mdx* GM (3.38%±0.9) compared to wild-type GM (3.40 ±0.2). There was a significantly higher amount of collagen deposition in *mdx*/*utrn*+/- GM (7.28%±2.2) compared to healthy wild-type and *mdx* tissue; however this difference was not significant between GM muscles of dko mice (9.49%±1.5). Overall, quantification of collagen content indicates that fibrosis is absent in wild-type and *mdx* GM muscle, but present in *mdx*/*utrn*+/- and dko GM muscle at a young age (p=0.0003). Muscle regeneration was significantly higher in all three murine models of DMD compared to the wild-type controls (Figure 3E-H). The proportion of centrally located nuclei did not differ, however, between *mdx* (50.41%±18.2), *mdx*/*utrn*+/- (49.78%±12.0) and dko GM muscle (45.44%±4.7, p=0.0007).
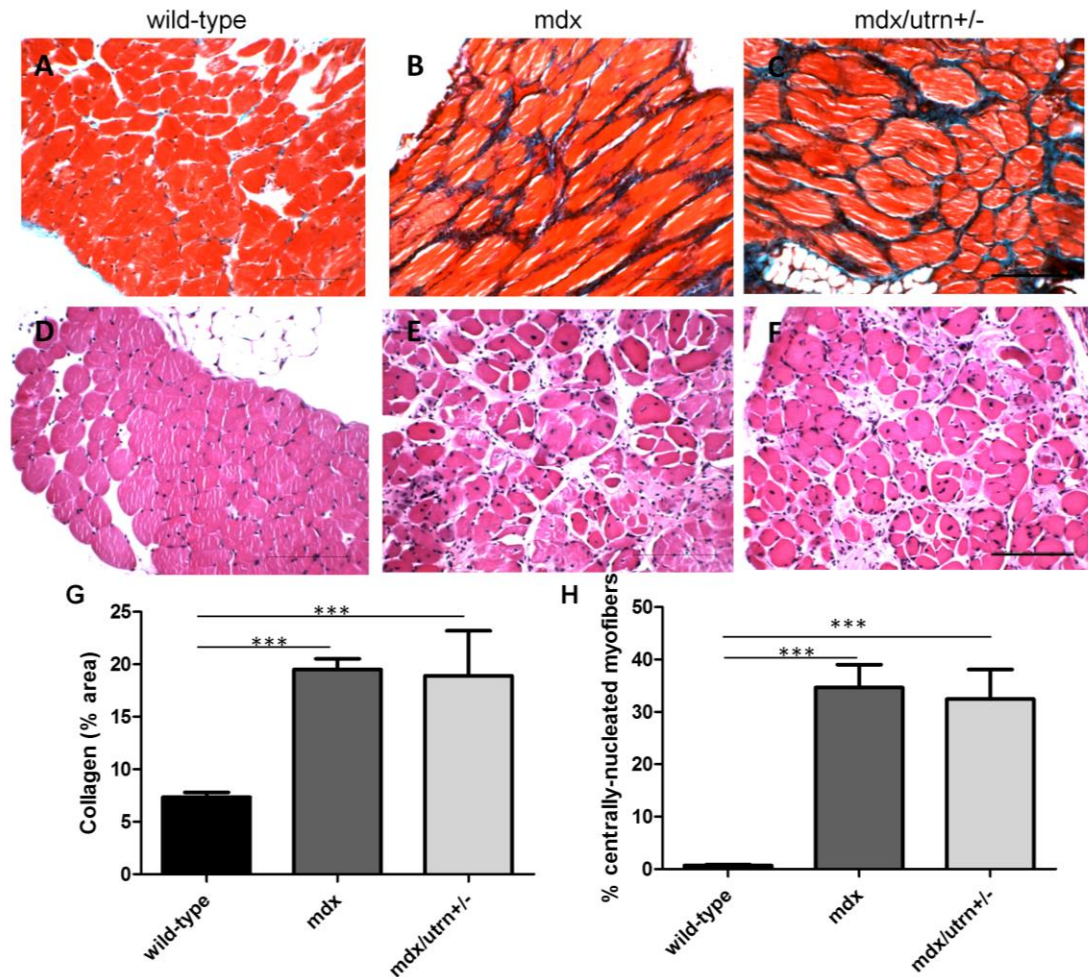
Figure 2.2: Muscle pathology in 10 month-old diaphragm muscles of wild-type, *mdx* and *mdx*/*utrn*+/- mice.

Extent of total collagen staining (blue) in 10 month-old wild-type (A), *mdx* (B) and *mdx*/*utrn*+/- (C) diaphragms was used as a marker of fibrosis. Proportion of centrally nucleated fibers in the same tissues (D, E, and F) was measured to assess extent of regeneration. Quantification of total collagen staining (G) and proportion of centrally-nucleated myofibers (H) is represented as the mean +SD. * represents $p < 0.05$ and *** represents $p < 0.001$ (scale bar=100μm).
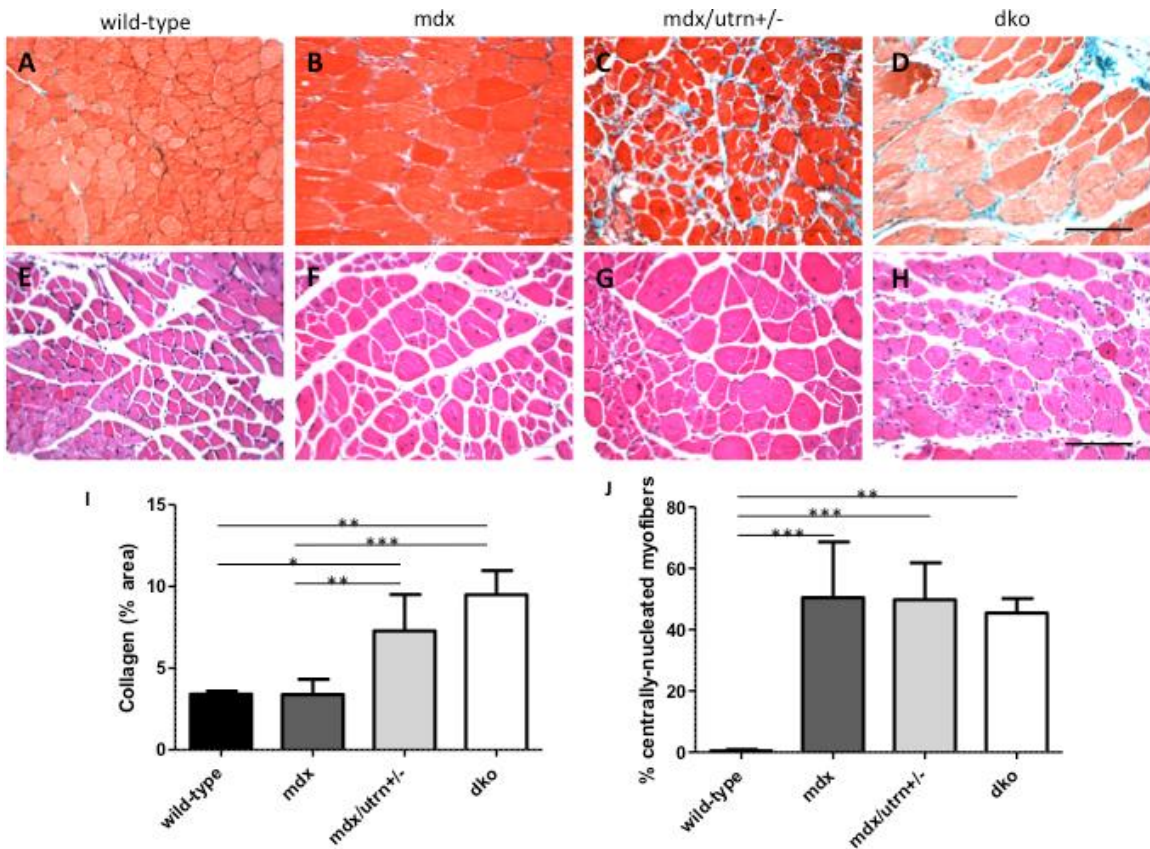
Figure 2.3: Muscle pathology in 8 week-old GM muscles of wild-type, *mdx*, *mdx/utrn+/-* and dko mice.

Extent of total collagen staining (blue) in 8 week-old wild-type (A), *mdx* (B), *mdx/utrn+/-* (C) and dko (D) GM muscles was used as a marker of fibrosis. Proportion of centrally nucleated fibers in the same tissues (E, F, G, and H) was measured to assess extent of regeneration. Quantification of total collagen staining (I) and proportion of centrally-nucleated myofibers (J) is represented as the mean +SD. * represents $p < 0.05$, ** represents $p < 0.01$, and *** represents $p < 0.001$ (scale bar=100μm).

2.4.4 Fibrosis is present in diaphragm muscle at a young age in all three murine models of DMD

Collagen content in the diaphragm muscle was not determined to be significantly different between *mdx* mice (11.04%±2.3) and the two more severely affected animal models or between healthy wild-type and *mdx* mice (Figure 4A-D). Collagen deposition was significantly higher in the diaphragm of both dko (14.17%±4.4) and *mdx/utrn+/-* (13.32%±2.5) mice at 8 weeks of age compared to age-matched wild-type diaphragm muscle (7.1%±0.3, p=0.0235). Myofiber regeneration was significantly higher in the diaphragm muscles of *mdx* (41.48%±6.6) *mdx/utrn+/-* (39.39%±10.18) and dko (30.95%±6.4) mice compared to diaphragm muscle in wild-type mice (Figure 2.4, p<0.0001).

2.4.5 Extent of fibrosis differs between muscle groups in the *mdx/utrn+/-* mouse

Diaphragm, quadriceps, soleus, tibialis anterior (TA) and gastrocnemius (GM) muscles were analyzed from 12 week-old *mdx/utrn+/-* mice (Figure 2.5). Collagen content in diaphragm muscle was significantly higher than all other muscles assessed (p<0.0001). Both the quadriceps (8.31%±0.1) and GM muscles (9.89%±2.4) were higher in collagen content than the soleus muscle (2.80%±1.0) at this age. Extent of fibrosis was not significantly different in the TA muscle (5.85%±1.1) compared to the quadriceps, GM or soleus muscles. Myofiber regeneration, indicated by centrally located nuclei, was significantly higher in all four lower limb muscles compared to myofibers in the diaphragm, which only had 35.1% of myofibers in a regenerative state (p<0.0001).
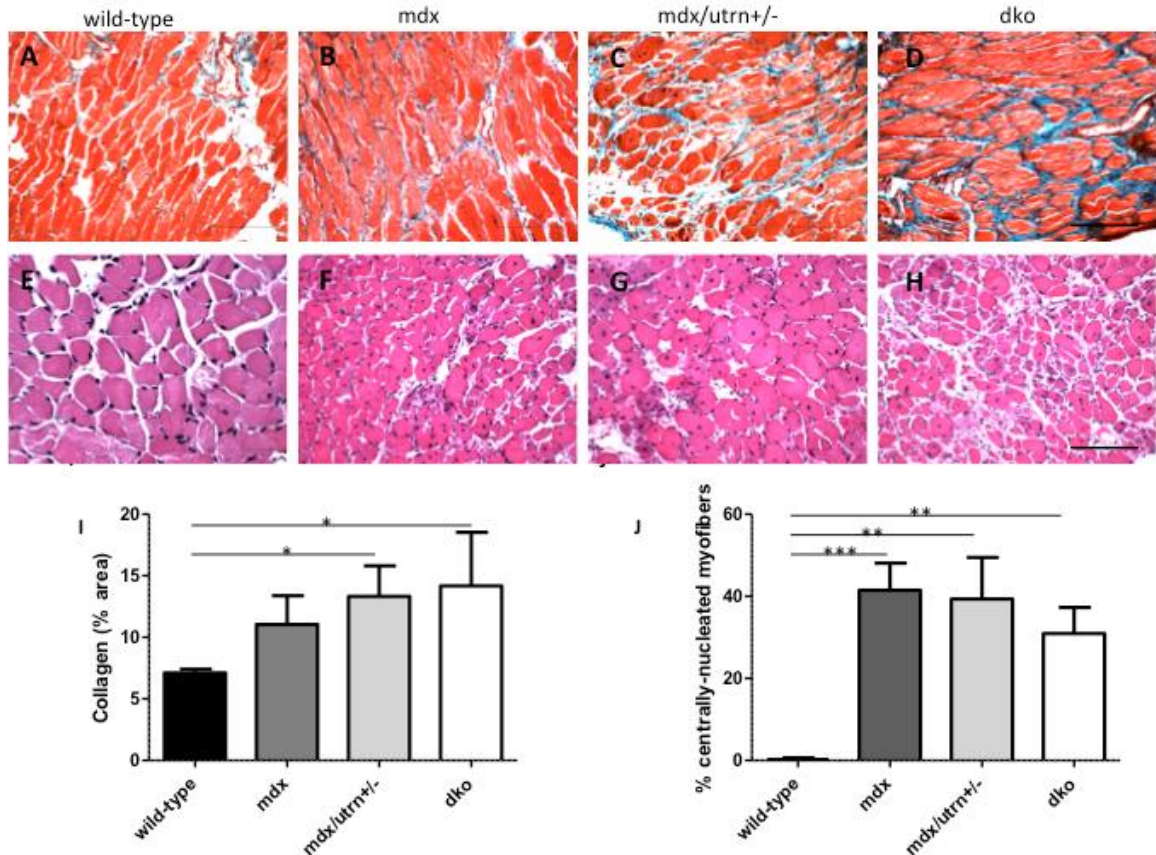
Figure 2.4: Muscle pathology in 8 week-old diaphragm muscle of wild-type, *mdx*, *mdx/utrn+/-* and dko mice.

Extent of total collagen staining (blue) in 8 week-old wild-type (A), *mdx* (B), *mdx/utrn+/-* (C) and dko (D) diaphragms was used as a marker of fibrosis. Proportion of centrally nucleated fibers in the same tissues (E, F, G, and H) was measured to assess extent of regeneration. Quantification of total collagen staining (I) and proportion of centrally-nucleated myofibers (J) is represented as the mean +SD. * represents $p<0.05$, ** represents $p<0.01$, and *** represents $p<0.001$ (scale bar=100μm)
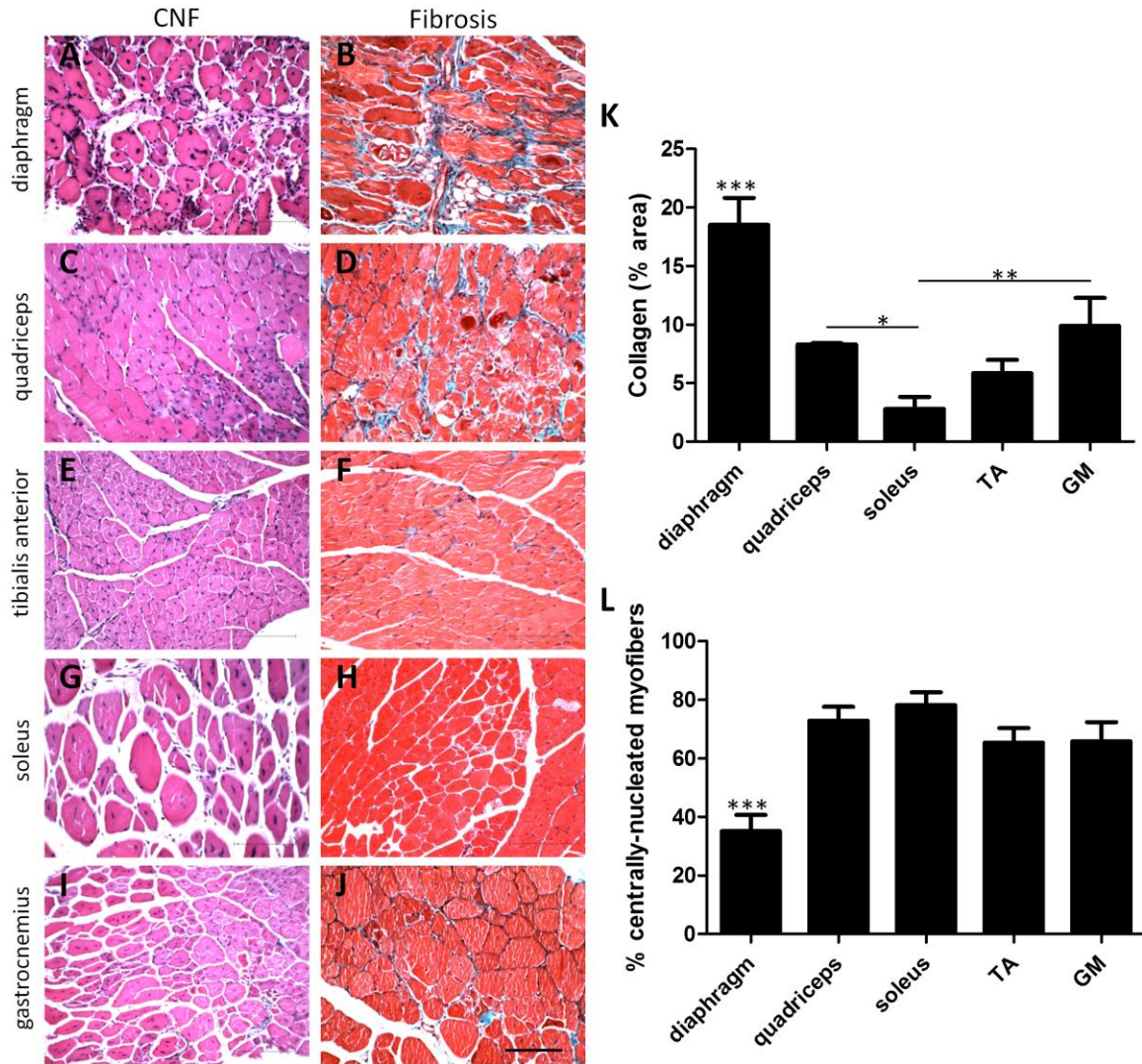
Figure 2.5: Comparison of histopathology of 12 week-old *mdx/utrn*+/- diaphragm, quadriceps, soleus, tibialis anterior and gastrocnemius muscles.

Extent of collagen staining (A,C,E,G,I) and muscle regeneration (B,D,F,H,J) in 12 week-old *mdx/utrn*+/- mice. Quantification of total collagen staining (K) and centrally-nucleated myofibers (CNF, L) is represented as the mean ±SD. * represents $p < 0.05$, ** represents $p < 0.01$, and *** represents $p < 0.001$ (scale bar=100μm). TA= tibialis anterior, GM= gastrocnemius.

2.5 Discussion

Fibrosis is a hallmark feature of Duchenne muscular dystrophy (DMD), yet the most widely- used murine model for the disease, the *mdx* mouse, does not model this aspect of DMD until an advanced age (Desguerre et al. 2002). Consistent with previous reports (Ishizaki et al. 2008), this study demonstrates that while the diaphragm muscle becomes fibrotic in aged *mdx* mice hind limb muscle does not. Many studies that investigate the potential use of stem cell or gene therapy for DMD use hind limb muscles, such as the gastrocnemius muscle (GM), for sites of injection (Qu-Petersen et al. 2002). Here, we demonstrate that neither young nor aged *mdx* mice develop a significant amount of fibrosis in the GM muscle compared to healthy wild-type controls of the same age. The fact that *mdx* mice lack this excessive deposition of extracellular matrix proteins may lead researchers to overestimate treatment efficacy in this murine model since there is a lack of environmental hostility when testing their therapeutic agents. Alternatively, the *mdx/utrn*+/- mouse exhibits hind limb fibrosis at 10 months of age. Interestingly, a large proportion of regenerating myofibers, indicative of damage, was measured in both aged animal models. Centrally located nuclei are a hallmark of muscle regeneration, and are often used as an indicator of muscle pathogenesis (Anderson et al. 1987). Indeed, while centric nuclei are prominent in the *mdx* mouse model of DMD, other aspects of the disease in humans, particularly fibrosis, are not phenocopied. This may be due, at least in part, to the up regulation of utrophin in the *mdx* mouse. As a result, overall muscle damage is significantly less in *mdx* mice than in utrophin heterozygotes and double knockout animals. Interestingly, we have further shown that in muscle tissues exhibiting higher levels of collagen (e.g. diaphragm), proportions of centric nuclei are lower. In contrast, the GM muscle in *mdx* mouse exhibits a significantly higher number of centric nuclei, but little deposition of collagen. These findings are consistent with earlier reports hypothesizing that centrally-nucleated myofibers are more resistant to mechanical stress, which may in part explain for the differences in the pathology observed in diaphragm versus hind limb skeletal muscles (Narita et al. 1999).

Since DMD manifests at a young age in humans and because most DMD research is performed in younger animals, we also investigated extent of fibrosis in eight week-old

mice. Although the GM muscles in young *mdx* mice are in a regenerative state as evidenced by the presence of centrally located nuclei, we did not measure a significant degree of fibrosis in them. In comparison, there was a higher level of collagen measured in both moderately affected *mdx/utrn*+/- and severely affected dko mice relative to their healthy counterparts, suggesting fibrotic progression in these animals. Upon validating the mdx/utrn+/- mouse as more fibrotic compared to mdx littermates, we sought to further characterize extent of fibrosis in various muscle groups isolated from the heterozygous mouse model. As expected, the diaphragm muscle was highly fibrotic compared to the quadriceps, soleus, tibialis anterior and GM muscles. In comparison, there was no detectable difference in collagen deposition between the quadriceps, TA or GM muscles; this is an important finding considering that all three muscles are used in current research and therefore should display signs of fibrosis (Fletcher et al. 2006, Church et al. 2014). Interestingly, we measured a lower amount of collagen content in the slow-twitch soleus muscle than the fast-twitch quadriceps and GM muscles. The fact that fibrotic progression is not equal between individual skeletal muscles is an important factor to consider in future studies.

Taken together, this study supports previous literature that argues for the replacement of the *mdx* mouse with more severely affected models of DMD, such as the *mdx/utrn*+/- or dko mouse (Deconinck et al. 1997a,b). Although dko mice develop debilitating fibrosis at a young age, these animals do not tend to live past twenty weeks and thus are not generally used in studies examining the long-term efficacy of a therapeutic intervention. Similarly, although the diaphragm muscle in all three murine models develops fibrosis at some point, a more accurate model of DMD should reflect disease manifestation in axial limbs as well. Nevertheless, it would be optimal for any therapeutic drug under investigation to show efficacy in the diaphragm muscle since failure of this respiratory organ is a common cause of death in DMD patients (Bushby et al. 2009, Gilgoff et al. 1989). Since the *mdx/utrn*+/- mouse develops fibrosis in both hind limb and respiratory skeletal muscles at a young age while not being so affected such that it dies prematurely, we provide further evidence here that it may be an appropriate and useful model of DMD. Furthermore, we report here that this increased disease severity in the *mdx/utrn*+/- mouse compared to its *mdx* counterpart is apparent by two months of age. The *mdx/utrn*+/-

mouse is also a suitable precursor model for scaling studies to large animal models of DMD such as the golden retriever model (GRMD), which exhibits signs of increased endomysial fibrosis as early as 15 days after birth, with severe fibrosis by 9 months of age (Passerini et al. 2002; Willmann 2009; Kornegay et al. 2012).

2.6 References

Anderson JE, Ovalle WK, Bressler BH. Electron microscopic and autoradiographic characterization of hindlimb muscle regeneration in the *mdx* mouse. *Anat Rec.* 1987;219(3)243-57.

Beckman SA, et al. Beneficial effect of mechanical stimulation on the regenerative potential of muscle-derived stem cells is lost by inhibiting vascular endothelial growth factor. *Arterioscler Thromb Vasc Biol.* 2013;33(8):2004-12.

Bernasconi P, et al. Transforming growth factor-beta1 and fibrosis in congenital muscular dystrophies. *Neuromuscul Disord.* 1999;9(1):28-33.

Bushby K, et al. Diagnosis and management of Duchenne muscular dystrophy, part 1: diagnosis, and pharmacological and psychological management. *Lancet Neurol.* 2009;9(1):77-93.

Church JE, et al. Alterations in notch signalling in skeletal muscles from *mdx* and dko dystrophic mice and patients with duchenne muscular dystrophy. 2014;99(4):675-87.

Cirak S, et al. Restoration of the dystrophin-associated glycoprotein complex after exon skipping therapy in duchenne muscular dystrophy. *Mol Ther.* 2012;20(2):462-7.

Deconinck AE, et al. Postsynaptic abnormalities at the neuromuscular junctions of utrophin-deficient mice. *J Cell Biol.* 1997a;136(4):883-94.

Deconinck AE, et al. Utrophin-dystrophin-deficient mice as a model for duchenne muscular dystrophy. *Cell.* 1997b;90(4):717-27.

Desguerre I, et al. A new model of experimental fibrosis in hindlimb skeletal muscle of adult *mdx* mouse mimicking muscular dystrophy. *Muscle Nerve.* 2012;45(6):803-14.

Desguerre I, et al. Endomysial fibrosis in Duchenne muscular dystrophy: a marker of poor outcome associated with macrophage alternative activation. *J Neuropathol Exp Neuro.* 2009; 68:762–773

Fletcher S, et al. Dystrophin expression in the *mdx* mouse after localised and systemic administration of a morpholino antisense oligonucleotide. *J Gene Med.* 2006;8(2):207-16.

Gilgoff I, Prentice W, Baydur A. Patient and family participation in the management of respiratory failure in Duchenne's muscular dystrophy. *Chest.* 1989;95(3):519-24.

Goyenvalle A, et al. Prevention of dystrophic pathology in severely affected dystrophin/utrophin-deficient mice by morpholino-oligomer-mediated exon-skipping. *Mol Ther.* 2010;18(1):198-205.

Goyenvalle A, et al. Rescue of severely affected dystrophin/utrophin-deficient mice through scAAV-U7snRNA-mediated exon skipping. *Hum Mol Genet.* 2012;21(11):2559-71.

Grady RM, et al. Skeletal and cardiac myopathies in mice lacking utrophin and dystrophin: a model for Duchenne muscular dystrophy. *Cell.* 1997;90(4): 729-38.

Hindi SM, Shin J, Ogura Y, Li H, Kumar A. Matrix metalloproteinase-9 inhibition improves proliferation and engraftment of myogenic cells in dystrophic muscle of *mdx* mice. *PLoS One.* 2013;8:(8):e72121.

Hogrel JY, et al. Assessment of a symptomatic duchenne muscular dystrophy carrier 20 years after myoblast transplantation from her asymptomatic identical twin sister. *Neuromuscul Disord.* 2013;23(7):575-9.

Huang P, et al. Impaired respiratory function in *mdx* and *mdx/utrn*(+/-) mice. *Muscle Nerve.* 2011;43(2):263-7.

Ishizaki M, et al. *Mdx* respiratory impairment following fibrosis of the diaphragm. *Neuromuscul Disord*. 2008;18(4):342-8.

Kornegay JN, et al. Canine models of duchenne muscular dystrophy and their use in therapeutic strategies. *Mamm Genome*. 2012;23(1-2):85-108.

Mendell JR, et al. Myoblast transfer in the treatment of Duchenne's muscular dystrophy. *N Engl J Med.* 1995;333:832–838.

Narita S, Yorifuji H. Centrally nucleated fibers (CNFs) compensate the fragility of myofibers in *mdx* mouse. *Neuroreport.* 1999;10(15):3233-5.

Partridge TA, Morgan JE, Coulton GR, Hoffman EP, Kunkel LM. Conversion of *mdx* myofibres from dystrophin-negative to -positive by injection of normal myoblasts. *Nature*. 1989;337(6203):176-9.

Passerini L, et al. Fibrogenic cytokines and extent of fibrosis in muscle of dogs with X-linked golden retriever muscular dystrophy. *Neuromuscul Disord*. 2002;12(9):828-35.

Pichavant C, et al. Current status of pharmaceutical and genetic therapeutic approaches to treat DMD. *Mol Ther.* 2011;19(5):830-40.

Qu-Petersen Z, et al. Identification of a novel population of muscle stem cells in mice: potential for muscle regeneration. *J Cell Biol.* 2002;157(5):851-64.

Rodino-Klapac LR, Mendell JR, Sahenk Z. Update on the treatment of duchenne muscular dystrophy. *Curr Neurol Neurosci Rep.* 2013;13(3):332,012-0332-1.

Sacco A, et al. Short telomeres and stem cell exhaustion model duchenne muscular dystrophy in *mdx*/mTR mice. *Cell.* 2010;143(7):1059-71.

Seto JT, Bengtsson NE, Chamberlain JS. Therapy of genetic disorders-novel therapies for duchenne muscular dystrophy. Curr Pediatr Rep. 2014;2(2):102-12.

Skuk D, et al. Dystrophin expression in muscles of Duchenne muscular dystrophy patients after high-density injections of normal myogenic cells. *J Neuropathol Exp Neurol.* 2006;65: 371–386

Skuk D, et al. First test of a "high-density injection" protocol for myogenic cell transplantation throughout large volumes of muscles in a Duchenne muscular dystrophy patient: eighteen months follow-up. *Neuromuscul Disord.* 2007;17: 38–46

Skuk D, et al. Dystrophin expression in myofibers of Duchenne muscular dystrophy patients following intramuscular injections of normal myogenic cells. *Mol Ther.* 2004;9: 475–482.

van Putten M, et al. Comparison of skeletal muscle pathology and motor function of dystrophin and utrophin deficient mouse strains. *Neuromuscul Disord.* 2012;22(5):406-17.

Willmann R, Possekel S, Dubach-Powell J, Meier T, Ruegg MA Mammalian animal models for duchenne muscular dystrophy. *Neuromuscul Disord.* 2009;19(4):241-9.

Zhou L, et al. Haploinsufficiency of utrophin gene worsens skeletal muscle inflammation and fibrosis in *mdx* mice. *J Neurol Sci.* 2008;264(1-2):106-11.

Chapter 3

VEGF induces stress fiber formation in fibroblasts isolated from dystrophic muscle[3]

---

[3] This chapter includes content reproduced with permission from:

Gutpell KM, Hoffman LM (2015). VEGF induces stress fiber formation in fibroblasts isolated from dystrophic muscle. J Cell Commun Signal, 9(4), 353–360. doi:10.1007/s12079-015-0300-z

3 VEGF induces stress fiber formation in fibroblasts isolated from dystrophic muscle

3.1 Chapter Summary

Although vascular endothelial growth factor (VEGF) has been widely studied as a possible therapeutic drug to treat DMD, recent work in other fibrotic disease such as idiopathic pulmonary fibrosis, has revealed a potential role for the growth factor in exacerbating fibrosis. No study to date has investigated whether VEGF elicits a fibrotic response in DMD, thus we sought to determine if such an effect might be exerted on DMD-derived fibroblasts. In this study, we isolated fibroblasts from severely affected diaphragm and moderately affected gastrocnemius muscles of *mdx*/*utrn*+/- mice. The effect of exogenous VEGF administration on expression of pro-fibrotic genes was assessed in vitro. The effect of VEGF on stress fiber formation was also assessed. We used transforming growth factor beta as a positive control in this study since it is a well-known inducer of a fibrotic response. VEGF did not increase expression of the genes for type-1 collagen or connective tissue growth factor in either GM- or diaphragm-derived fibroblasts. Administration of the growth factor did lead to an increase in gene expression of alpha-smooth muscle actin, but this effect was only observed in diaphragm-derived fibroblasts and not GM fibroblasts. We also show that VEGF treatment leads to induction of alpha-smooth muscle actin-positive stress fiber formation indicative of myofibroblast differentiation. Stress fiber formation occurred in both GM and diaphragm fibroblasts but the response was more pronounced in diaphragm fibroblasts. The findings of this study reveal a potential role of VEGF in promoting a fibrotic response in DMD.

3.2 Introduction

Angiogenic therapy has been proposed as a potential therapeutic agent for treating skeletal muscle ischemia inherent to Duchenne muscular dystrophy (DMD) (Shimizu-Motohashi et al. 2014). To this end, a number of studies have now used a potent inducer of angiogenesis, vascular endothelial growth factor (VEGF), as a therapeutic agent in the *mdx* mouse (Messina et al. 2007; Gregorevic et al. 2004; Beckman et al. 2013). Importantly, enhanced vascularization in dystrophic muscle has been shown to enhance the efficacy of regeneration through cell therapy (Bouchentouf et al. 2005). One aspect of these studies that has not been directly addressed is the effect of exogenous VEGF on skeletal muscle fibroblasts. Indeed, recent studies indicate that high doses of VEGF induce fibrosis in inflammatory and non-inflammatory stages of systemic scleroderma (SSc) (Maurer et al. 2014). Similarly, fibroblasts isolated from patients with idiopathic pulmonary fibrosis exhibit a decreased fibrotic response following treatment with a VEGF receptor blocker, nintedanib (Hostettler et al. 2014). The findings in the SSc study are particularly important because they highlight the differential effect observed with low levels of circulating VEGF versus high doses of VEGF typically associated with exogenous treatment. In contrast, studies utilizing murine models of DMD have shown that a loss of endogenous VEGF may have deleterious effects on regeneration. Additionally, results from studies that have administered VEGF to dystrophic muscle have suggested an anti-fibrotic role of the growth factor in this disease. While the latter findings highlight the immense therapeutic potential of VEGF to treat DMD, there is currently a lack of studies that directly investigate the effect of exogenous VEGF treatment on progression of fibrosis (Miyazaki et al. 2011; Rhoads et al. 2013).

Fibrosis develops in DMD patients and is largely responsible for disease fatality (Desguerre et al. 2009; Chen et al. 2005; Bernasconi et al. 1995). Since the *mdx* mouse model does not develop fibrosis to the same extent as is observed in patients, studying the effect of VEGF on the fibrotic response in this model may lead to an underestimation of its effect on fibrosis (Desguerre et al. 2012; Zhou et al. 2008). More recent studies have used a double knockout mutant that lacks both dystrophin and utrophin (dko), but this mouse is severely affected and does not live past 20 weeks of age (Deconinck et al. 1997;

Goyenvalle et al. 2010 and 2012; van Putten et al. 2012). We and others have demonstrated that the heterozygous *mdx*/*utrn+/-* mouse develops hind limb skeletal muscle fibrosis earlier in life than its *mdx* counterpart, but maintains a longer lifespan of approximately two years in laboratory conditions (Zhou et al. 2008; Gutpell et al. 2015). Isolation of primary fibroblasts from this mouse model thus provides a means to directly assess the effect of exogenous VEGF treatment on the expression of pro-fibrotic genes (Mezzano et al. 2007). Another important consideration for angiogenic therapy is the effect of treatment on different muscles affected by DMD. Indeed, all three murine models of DMD - *mdx*, *mdx*/*utrn+/-* and dko - develop fibrosis in the diaphragm muscle, and to a greater extent than what is observed in the hind limb musculature of any of these mice (Stedman et al. 1991; Huang et al. 2011). The underlying mechanism for this differential progression of fibrosis has not been thoroughly investigated. Therefore, this study also investigated whether the effect of VEGF treatment differs in diaphragm-derived fibroblasts versus gastrocnemius-derived fibroblasts.

3.3   Materials and Methods

3.3.1   Animal Care and Ethics Statement

All experiments were performed at Lawson Health Research Institute at St. Joseph's Health Care (SJHC) in London, Ontario. The *mdx*/*utrn+/-* mice, originally generated by Dr.'s Mark Grady and Josh Sanes (Washington University, St. Louis) (Grady et al. 1997), were generously provided by Dr. Robert Grange (Virginia Polytechnic and State University) and maintained in the Animal Care Facility at SJHC. Colonies were maintained under controlled conditions (19–23˚C, 12 hour light/dark cycles) and allowed water and food *ad libitum*. Only 10 week-old *mdx*/*utrn+/-* mice were used in this study. All procedures involving animal experiments were carried out in strict accordance with the Canadian Council on Animal Care (CCAC) and were approved by the Animal Use Subcommittee at Western University.

3.3.2   Genotyping

Genomic DNA from tail snips or ear notch tissue was used for genotyping. Briefly, ear notch tissue was lysed in a proteinase K solution at 50° C overnight. DNA was diluted appropriately and polymerase chain reaction was used to amplify the utrophin gene using Platinum *Taq* polymerase. Presence of the utrophin gene was detected using the following set of primers (Sigma): 5'-TGCAGTGTCTCCAATAAGGTATGAAC-3', 5'-TGCCAAGTTCTAATTCCATCAGAAGCTG -3' (forward primers) and 5'-CTGAGTCAAACAGCTTGGAAGCCTCC-3' (reverse primer).

3.3.3   Primary Fibroblast Isolation

Gastrocnemius and diaphragm tissue samples were isolated from 10-week old *mdx*/*utrn*+/- mice. The isolation protocol was adapted from a method previously described by others (Mezzano et al. 2007). Briefly, mice were sacrificed via gas euthanasia and dissected muscles were placed in sterile phosphate-buffered saline (PBS) and transferred to a cell culture hood. Tissues were minced into 1-2mm^3 pieces and placed on a gelatin-coated 10cm dish with sterile tweezers. Approximately 20-25 pieces were plated per dish. The tissue was then covered with primary fibroblast isolation medium (DMEM/F12 supplemented with 20% FBS plus penicillin and streptomycin) and incubated at 37°C. By day 4, fibroblasts began exiting the tissue explants. Fibroblast medium (DMEM/F12 supplemented with 20% FBS and penicillin and streptomycin) was changed every other day from this point. Cells were passaged at day 7 using 0.25% trypsin-EDTA. Tissue explants were removed by passing cells through a 100μm nylon filter. Only cells in passages 2-4 were used for experimental purposes. Fibroblast population was confirmed by expression of vimentin and matricellular protein CCN2 (Appendix B).

3.3.4   Growth Factor Supplementation

1 x 10^5 fibroblasts were seeded per well onto a 12-well plate and incubated overnight. The next day, cells were serum-deprived in reduced-serum fibroblast medium (DMEM/F12 5% FBS plus penicillin and streptomycin) for 6 hours. Following serum

deprivation, cells were treated with 50ng/ml recombinant mouse $VEGF_{164}$ (R&D Systems), 50ng/ml transforming growth factor–beta (TGFβ), or untreated. Growth factor doses were determined from previous pilot studies in our lab. TGFβ treatment served as a positive control for inducing a fibrotic response and the untreated fibroblasts served as a negative control. Cells were harvested 6 and 18 hours later for subsequent RNA extraction and 48 hours later for protein extraction.

3.3.5   Quantitative Real-Time Polymerase Chain Reaction

RNA was extracted using a QIAGEN RNeasy Plus Mini Kit. RNA concentration and quality was assessed using a Nanodrop Spectrophotometer ND-1000. 1-2μg of high-quality RNA was reverse-transcribed using the High-Capacity RNA-to-cDNA Kit (Life Technologies). Following primer validation, Taqman Gene Expression Assays were used to measure *Ctgf/ccn2* (Mm01192932_g1), *Col1a1* (Mm00801666_g1), *Acta2* (Mm01546133_m1) and *Fn1* (Mm01256744_m1) mRNA expression relative to *Gapdh* endogenous control (Mm99999915_g1) levels using the ΔΔCT method on a Real-Time PCR Applied Biosystems Inc. Prism 7500 under the following conditions: Initial denaturation at 95ºC for 5 min followed by 40 cycles of denaturation (95ºC for 15 sec), primer annealing (60ºC for 1 min) and transcript extension (50ºC for 2 min). All samples were run in triplicate.

3.3.6   Immunohistochemistry

Fibroblasts were processed for immunocytochemistry by fixing in 2-4% paraformaldehyde for 20 minutes. Fibroblasts were then washed three times with phosphate-buffered saline (PBS), and incubated at room temperature in blocking buffer (1% BSA, 10% goat serum in PBS) for 45 minutes. Fibroblasts were incubated with anti-α-SMA (Abcam, 1:100) primary antibody. Following thorough washing with PBS, Alexafluor 488-IgG (Life Technologies, 1:1000) secondary antibody was used to visualize the primary antibody, and ProLong Gold anti-fade with DAPI (Life Technologies) was added to visualize the nuclei and to mount the coverslips onto glass slides. Fluorescent images were acquired at a twenty times magnification on a Nikon Eclipse microscope.

3.3.7   Western Blot

Cells were collected in Phosphosafe lysis buffer containing a protease inhibitor cocktail and lysed via sonication. Cell culture supernatants were collected and lyophilized for 210 minutes at 45°C and re-suspended in PBS. Protein was quantified using the bicinchoninic acid assay (Pierce). 50μg of protein was heat denatured and loaded onto a TGX stain-free SDS gel. Protein was transferred onto a PVDF low fluorescence membrane using the Transblot Turbo machine (Bio-Rad) and total protein was visualized on the Bio-Rad Gel Doc system. Membranes were blocked with 5% bovine serum albumin in tris-buffered saline containing 0.05% tween 20 for 1 hour. Blots were then incubated with primary anti-fibronectin antibody (1:1000, Abcam) at 4°C overnight. Following thorough washing in TBS-T, blots were incubated with anti-rabbit HRP secondary antibody (1:5000) for 1 hour. Bands were visualized via chemiluminescence using ImageLab software (Bio-Rad) and normalized to total protein signal from the stain-free blots (Taylor et al. 2013). Bands from cell culture supernatants are shown for qualitative purposes only since normalization to total protein was not possible given the signal saturation from the serum.

3.3.8   Statistical Analysis

Gene expression data was analyzed using a two-way analysis of variance (ANOVA) to determine simple main effects of treatment and time point followed by individual one-way ANOVA to assess differences within the 6- and 18-hour time points. Differences between groups were determined using Tukey's post-hoc test. A p-value less than 0.05 was considered significant (n=6 and n=4 for gene expression and protein experiments, respectively).

3.4 Results

3.4.1   Effect of VEGF on Fibrotic Gene Expression

Expression of multiple genes involved in dysregulated tissue repair was measured to investigate whether VEGF induces a fibrotic response in fibroblasts derived from dystrophic muscle. Specifically, changes in mRNA levels of *Ctgf/ccn2*, *Col1a1*, *Fn1*, and

Acta2, were assessed in diaphragm and GM-derived fibroblasts. TGFβ increased expression of *Ctgf/ccn2* in both GM- and diaphragm-derived fibroblasts. Six hours following administration, a 4.6- and 14.2-fold increase in expression of the gene was measured in GM (p<0.0001) and diaphragm fibroblasts (p=0.0002), respectively (Figure 3.1). This level of *Ctgf/ccn2* expression was significantly higher than expression in either control fibroblasts or VEGF-treated fibroblasts. There was no measureable increase in *Ctgf/ccn2* transcript level following VEGF treatment in either diaphragm or GM fibroblasts. The gene that encodes the pro-alpha(I) chain of type-1 collagen, was assessed to represent changes in collagen expression (Figure 3.2). TGFβ led to significantly higher expression of *Col1a1* in GM fibroblasts compared to either control or VEGF-treated GM fibroblasts. In diaphragm fibroblasts *Col1a1* expression was higher in TGFβ-treated fibroblasts compared to controls, but not higher than in VEGF-treated fibroblasts.

GM#
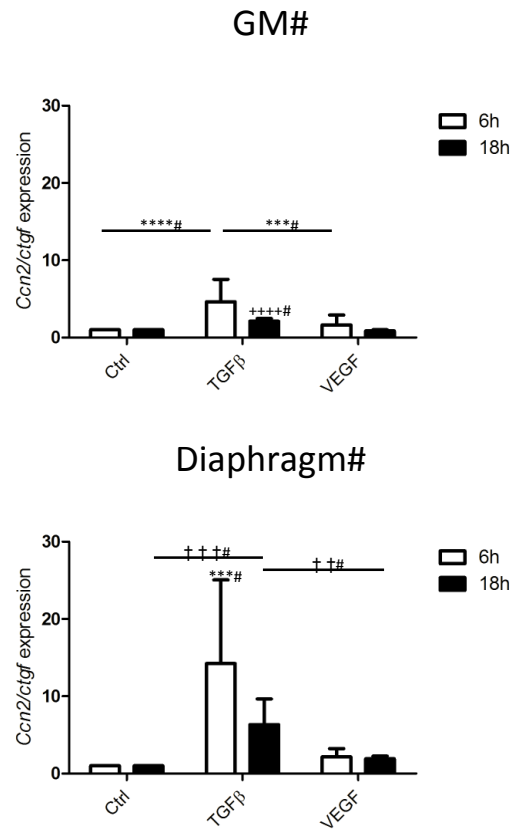
Diaphragm#

Figure 3.1: VEGF does not increase expression of *Ccn2/ctgf* in fibroblasts derived from GM or diaphragm muscle of *mdx/utrn+/-* mice.

Fibroblasts isolated from gastrocnemius (top) or diaphragm muscles (bottom) of *mdx*/*utrn*+/- mice were treated with $VEGF_{164}$ for 6 or 18 hours. Treatment with TGFβ, a known-inducer of pro-fibrotic gene expression, was used as a positive control. *Ctgf/ccn2* expression levels were measured relative to *Gapdh* (n=6). * and † denote significant difference between groups within the 6 and 18 hour time points, respectively. **p<0.01, ***p<0.001, ****p<0.0001 +SD.
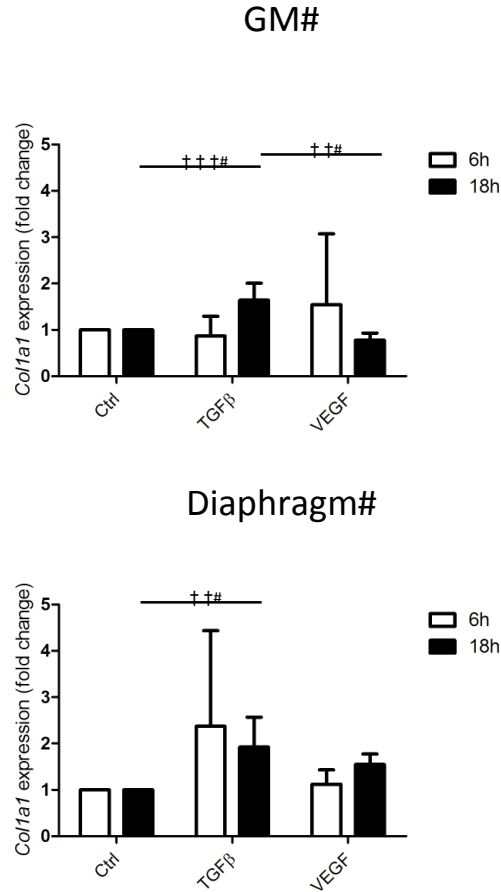
Figure 3.2: VEGF does not increase expression of *Col1a1* in fibroblasts derived from GM or diaphragm muscle of *mdx/utrn+/-* mice.

Fibroblasts isolated from gastrocnemius (top) or diaphragm muscles (bottom) of *mdx/utrn+/-* mice were treated with VEGF164 for 6 or 18 hours and expression of *Col1a1* was assessed via qPCR. Treatment with TGFβ, a known-inducer of pro-fibrotic gene expression, was used as a positive control. *Col1a1* expression levels were measured relative to *Gapdh* (n=6), * and † denote significant difference between groups within the 6 and 18 hour time points, respectively **p<0.01, ***p<0.001, +SD

3.4.2   Effect of VEGF on fibronectin expression

To determine if VEGF stimulates expression of genes that encode the extracellular matrix protein fibronectin, we assessed changes in mRNA expression of *Fn1*. Neither TGFβ nor VEGF altered expression of *Fn1* by any time points assessed in this study (Figure 3.3). Conversely, Western blot analysis of fibronectin protein (FN) confirmed that VEGF, but not TGFβ, increased expression of the protein by 1.9-fold in diaphragm fibroblasts (p=0.029) and by 1.5-fold in GM fibroblasts (p=0.001). Similar qualitative trends were observed in FN levels in the supernatant (Figure 3.4).

3.4.3   Changes in αSMA Expression Following VEGF Treatment

Acta2 expression significantly increased in GM-derived fibroblasts 1.8-fold following TGFβ treatment, but not following VEGF treatment (Figure 3.5). *Acta2* expression in diaphragm-derived fibroblasts, on the other hand, responded to both TGFβ treatment as well as VEGF treatment. TGFβ induced a 1.5-fold increase compared to control cells as early as 6 hours after administration of the growth factor. By 18 hours, *Acta2* expression was 1.9- and 1.5-fold higher in fibroblasts treated with TGFβ and VEGF, respectively (p<0.0001). Immunocytochemical analysis revealed minimal αSMA expression in both GM and diaphragm fibroblasts. While all αSMA protein expressed in untreated GM-fibroblasts was located in the cytoplasm (Figure 3.6), some untreated αSMA-positive diaphragm fibroblasts expressed the protein within stress fibers (Figure 3.7). TGFβ induced a robust response in diaphragm fibroblasts resulting in high levels of αSMA expression. Myofibroblast differentiation in these cells was evident by stress fiber formation. A similar, but less striking, response was observed in diaphragm fibroblasts treated with VEGF, as a large portion of these cells also underwent stress fiber formation. GM-derived fibroblasts appeared to respond to both TGFβ and VEGF, although the response was more subdued compared to the one observed in diaphragm fibroblasts.

GM#
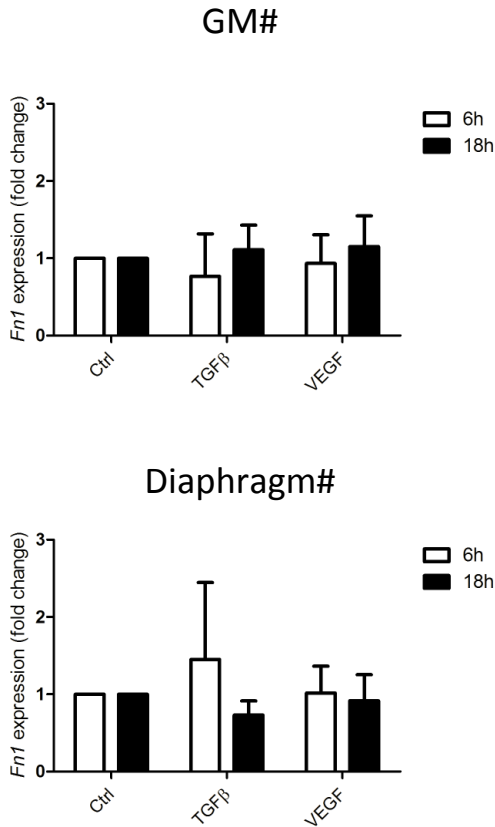
Diaphragm#

Figure 3.3: *Fn1* expression in is not altered by VEGF or TGFβ in fibroblasts isolated from either GM or diaphragm muscles of *mdx/utrn*+/- mice.

Fibroblasts isolated from gastrocnemius (top) or diaphragm muscles (bottom) of mdx/utrn+/- mice were treated with VEGF164 for 6 or 18 hours. Treatment with TGFβ, a known-inducer of pro-fibrotic gene expression, was used as a positive control. *Fn1* expression levels were measured relative to *Gapdh* (n=6), *significant difference between treatment groups within the 6 hour time point, †significant difference between groups within the 18 hour time point.
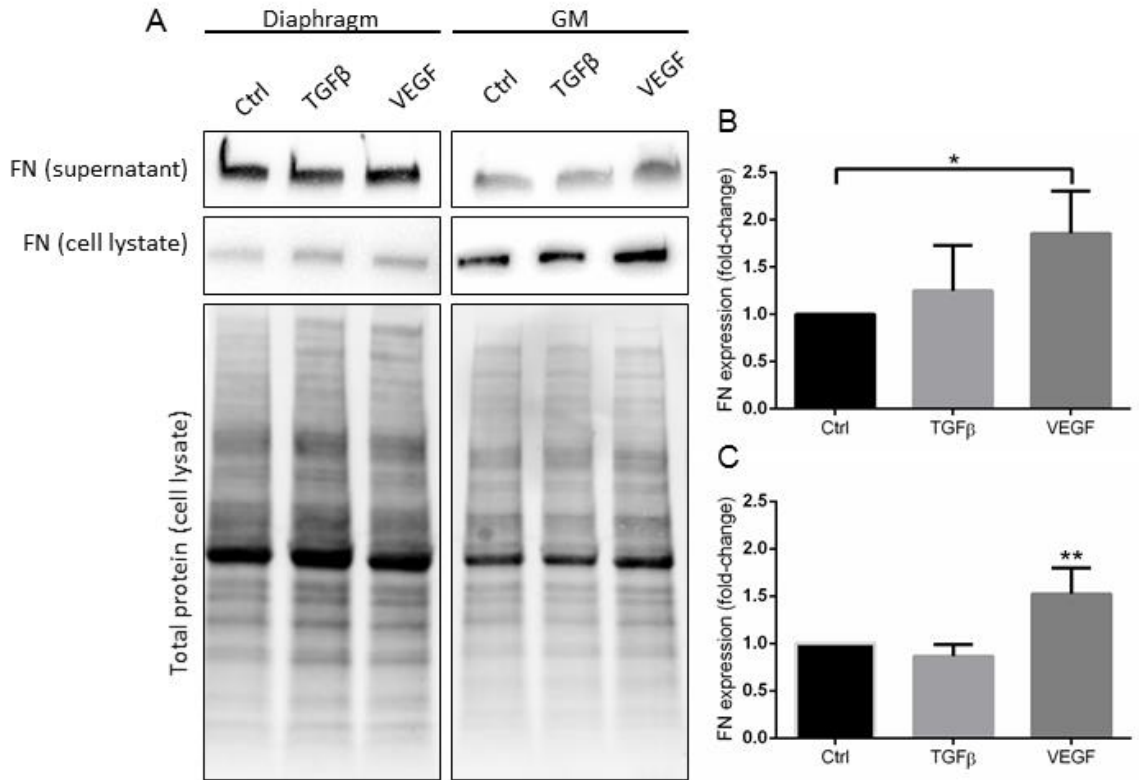
Figure 3.4: FN levels are increased following treatment of diaphragm and GM fibroblasts with VEGF.

Western blot analysis (A) reveals an increased level of intracellular FN and extracellular FN located in the cell culture supernatant following 48 hours in the presence of $VEGF_{164}$. FN levels from cell lysates of diaphragm (B) and GM (C) fibroblasts were measured relative to total protein (n=4, *$p<0.05$, **$p<0.01$).

GM#
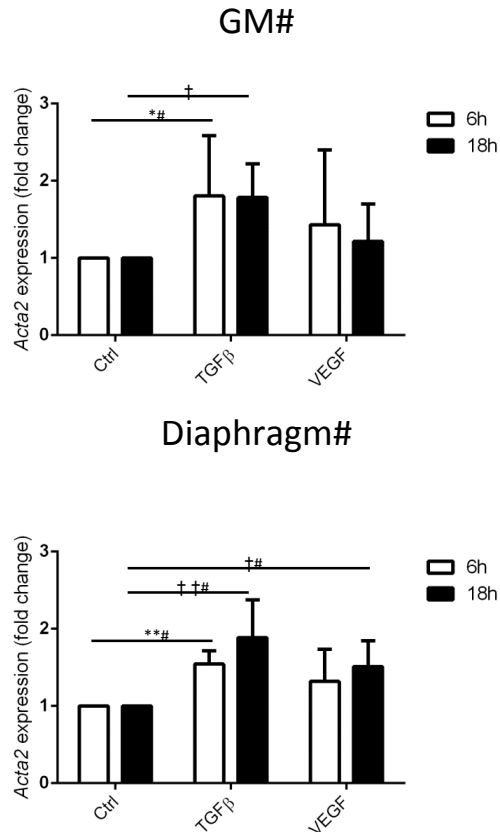
Diaphragm#

Figure 3.5: VEGF increases *Acta2* expression in diaphragm, but not in GM fibroblasts derived from *mdx/utrn+/-* mice.

Fibroblasts isolated from gastrocnemius (top) or diaphragm muscles (bottom) of mdx/utrn+/- mice were treated with VEGF$_{164}$ for 6 or 18 hours. Treatment with TGFβ, a known-inducer of pro-fibrotic gene expression, was used as a positive control. *Acta2* expression levels were measured relative to *Gapdh* (n=6), *significant difference between treatment groups within the 6 hour time point, †significant difference between groups within the 18 hour time point. *p<0.05, **p<0.01, ±SD.
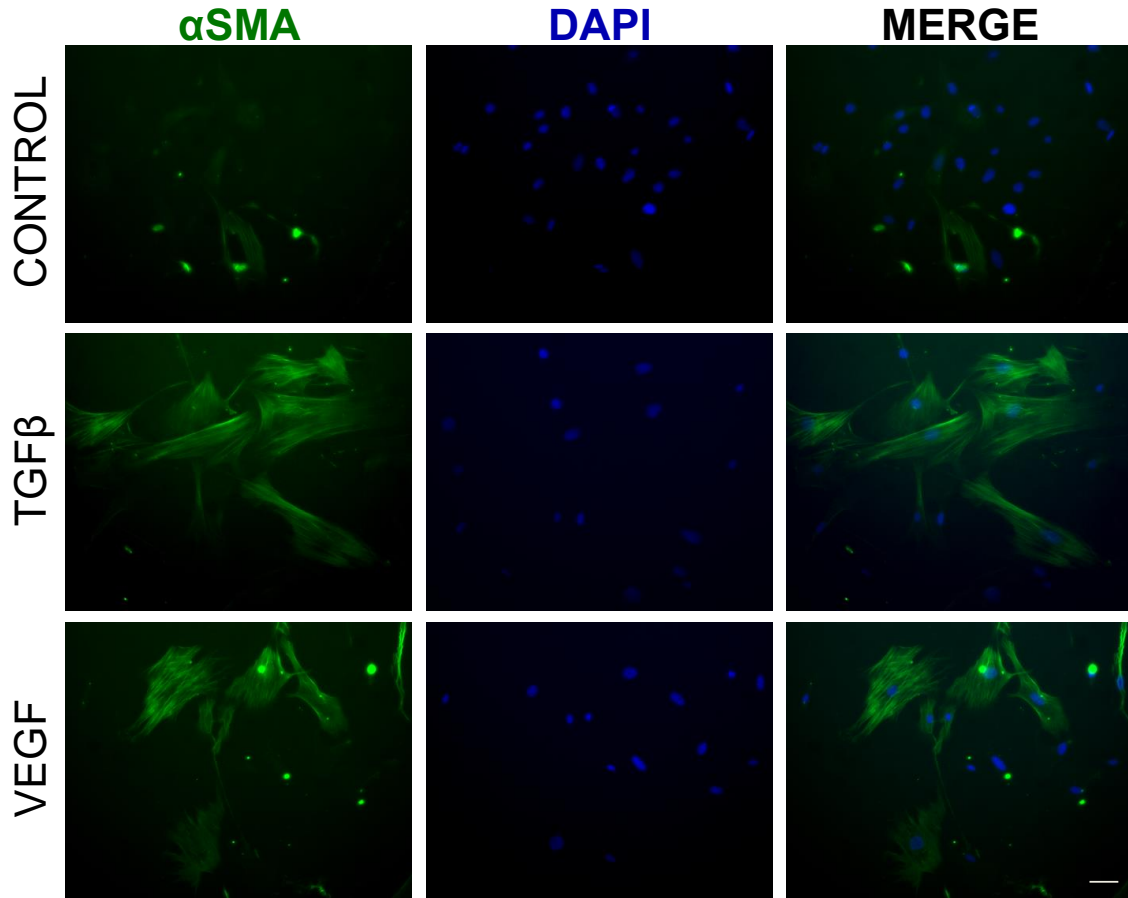
Figure 3.6: VEGF induces stress fiber formation in GM fibroblasts indicative of myofibroblast differentiation.

GM fibroblasts were treated with VEGF$_{164}$ for 48 hours. Treatment with TGFβ, a known-inducer of pro-fibrotic protein expression, was used as a positive control. Alpha-smooth muscle actin (αSMA), a marker of myofibroblasts, is shown in green. DAPI (blue) was used as a counterstain (scale bar= 50μm).
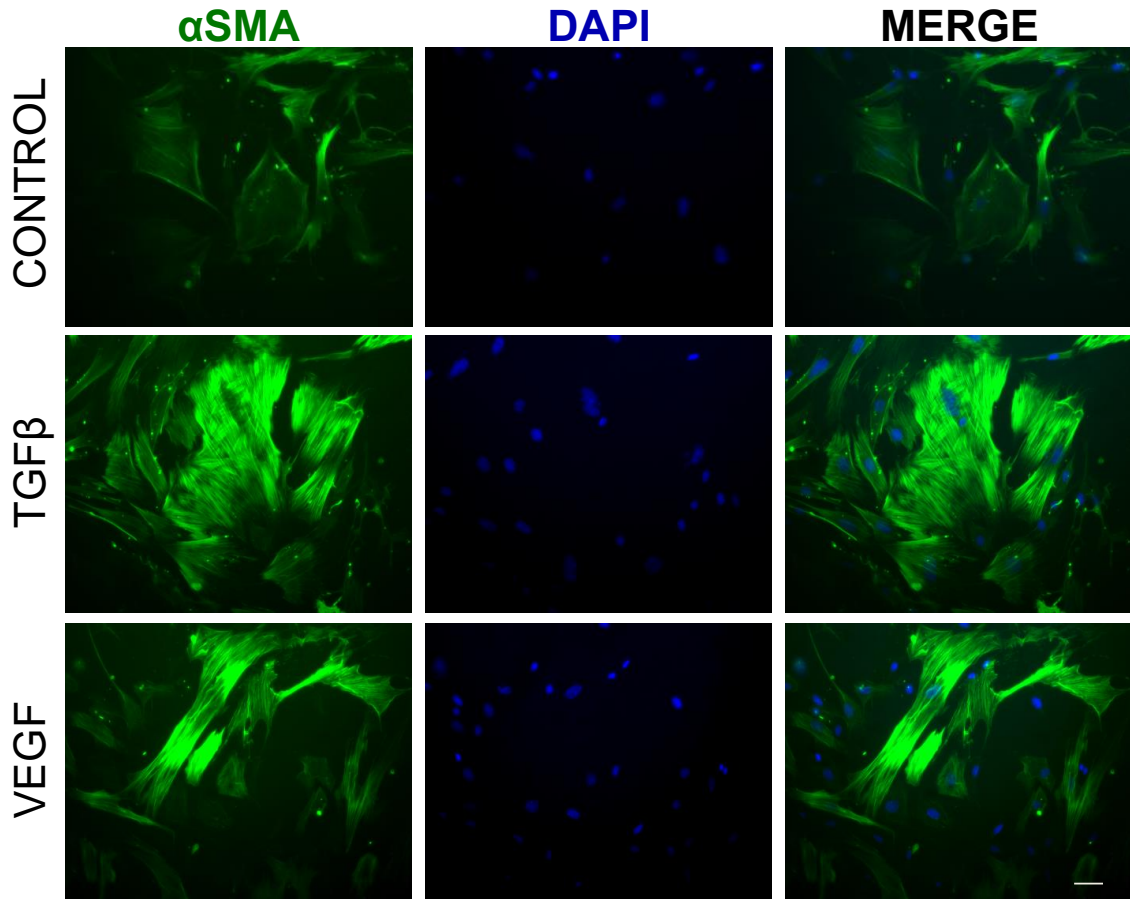
Figure 3.7: VEGF induces stress fiber formation in diaphragm fibroblasts indicative of myofibroblast differentiation.

Diaphragm fibroblasts were treated with $VEGF_{164}$ for 48 hours. Treatment with TGFβ, a known-inducer of pro-fibrotic protein expression, was used as a positive control. Alpha-smooth muscle actin (αSMA), a marker of myofibroblasts, is shown in green. DAPI (blue) was used as a counterstain (scale bar= 50μm). Although some untreated control fibroblasts are αSMA-positive, treatment with either TGFβ or VEGF led to greater expression of the protein in stress fibers.

3.5   Discussion

Therapeutic approaches to slow or attenuate the degenerative effects of DMD include attempts to restore dystrophin, the cytoskeletal protein that is missing or aberrant in DMD patients (Pessina et al. 2014). Gene and stem cell therapies are but two approaches currently under intense investigation to serve this purpose, but both of these are limited by the hostile microenvironment where regenerative therapy needs to occur. Skeletal muscle in both patients and animal models of DMD is poorly vascularized, leading to studies exploring the use of pro-angiogenic therapies to enhance the ischemic microenvironment (Arsic et al. 2004; Borselli et al. 2010). VEGF is a particularly attractive candidate for such a therapy since it is a well-known, potent inducer of angiogenesis. Although the literature currently suggests that VEGF enhances cell engraftment in the *mdx* mouse (Messina et al. 2007; Deasy et al. 2009), it remains to be determined whether VEGF induces a fibrotic response in DMD. In fact, a reduction in fibrosis following delivery of muscle-derived stem cells overexpressing VEGF has been shown in the *mdx* GM muscle (Deasy et al. 2009). The main motivation for this study was the findings from recent studies that examined the effect of VEGF in other fibrotic diseases such as SSc and idiopathic pulmonary fibrosis, whereby elevated levels of VEGF increased markers of fibrosis. In contrast, inhibition of VEGF was shown to have an anti-fibrotic effect (Maurer et al. 2014; Hostettler et al. 2014). These studies highlight the need to assess angiogenic therapy for the treatment of DMD in an animal model that develops significant fibrosis. Since the *mdx* mouse does not develop fibrosis as severely and early as DMD patients (Konieczny et al. 2013), our study focused on investigating the effect of VEGF on fibroblasts derived from a more fibrotic mouse model of DMD, the *mdx*/*utrn*+/- mouse (Zhou et al. 2008). Furthermore, since most studies to date have focused on the effect of VEGF on the hind limb muscles, our second objective was to determine whether there is a differential response to VEGF in diaphragm and gastrocnemius fibroblasts. To this end, gene expression analyses in the present study have indicated that VEGF treatment may alter expression of some genes involved in the fibrotic response, specifically *Acta2,* the gene that encodes αSMA. Expression of the genes that encode CTGF/CCN2 and collagen were not altered by VEGF, however these findings were inconclusive since we did not further investigate the levels of these two

proteins following treatment. Visualization of αSMA expression in VEGF-treated cells suggests a role for this growth factor in promoting differentiation of these fibroblasts, particularly ones derived from the diaphragm, into myofibroblasts.

Although *Fn1* levels were not affected by either treatment, protein levels of FN increased in the presence of VEGF, but not TGFβ. It is perhaps not surprising that exogenous TGFβ did not stimulate increased FN levels compared to the control treatment since all cells in this study were derived from *mdx*/*utrn*+/- mice. Previous work has demonstrated that conditioned media from *mdx* fibroblasts stimulates a fibrotic response, including increased FN, in wild-type fibroblasts (Mezzano et al. 2007). Given these findings, it may be that untreated fibroblasts in the present study also secreted pro-fibrotic factors into the culture medium, leading to an increase in FN even in the absence of exogenous TGFβ. Thus, the finding that exogenous VEGF treatment increased FN levels in our study is particularly intriguing. Since VEGF treatment resulted in increased FN protein but did not alter mRNA expression, it appears that VEGF may act translationally or post-translationally to enhance FN expression in *mdx*/*utrn*+/- fibroblast cultures. The fact that VEGF treatment led to increased FN both in cell lysates and cell culture supernatant warrants further investigation. This finding is consistent with work in other animal models of disease such as preclinical diabetic retinopathy whereby exogenous VEGF injection to a rat retina induced expression of FN as well as other fibrotic markers (Kuiper et al. 2007). That VEGF only affected protein, but not mRNA, levels in the present study also warrants further analysis. Since only two time points were assessed here, looking at FN mRNA expression over a time course may yield different results than those attained in this study. Interestingly, work over the past decade has revealed binding sites for VEGF on full length fibronectin and these studies have suggested that, in this case, the binding of these two proteins in the ECM act to increase the biological activity of VEGF (Wijelath et al. 2002, 2004; Goerges and Nugent 2004; Vempati et al. 2014). Further, it is well known that loss of FN negatively impacts vasculogenesis and angiogenesis due, in part, to the decrease in VEGF activity (Astrof and Hynes 2009). Although previous work highlights an important interaction between FN and VEGF, our results are the first to show a potential effect of VEGF on FN expression. As such, the

role of this interaction in the context of angiogenesis in dystrophic muscle also warrants further detailed investigation.

Given that diaphragm and GM muscles in *mdx/utrn+/-* mice display different abilities to develop fibrosis, we investigated whether fibroblasts from these different muscles also respond differently to VEGF treatment. Although the two cell types showed similar gene expression profiles following treatment, there were a few key differences observed here. First, untreated diaphragm fibroblasts appear to be more myofibroblast-like than GM fibroblasts, as evidenced by the presence of αSMA stress fibers, which were rare in the GM fibroblast cultures. Further, TGFβ stimulated a more drastic response in diaphragm fibroblasts compared to GM fibroblasts, evidenced by higher αSMA expressed and more prominent stress fiber formation. A similar trend was observed following VEGF treatment, although not to the same extent as observed following TGFβ administration. These findings suggest that fibroblasts from different muscles may respond in a unique way to various growth factors. As such, further work will be needed to determine whether diaphragm-derived fibroblasts indeed respond differently to VEGF treatment than do hind limb muscles. Since the pathology progression is more rapid in the diaphragm than hind limb muscles, considering the effect of treatment on both of these muscles will be crucial for future work.

3.6 References

Arsic N, et al. Vascular endothelial growth factor stimulates skeletal muscle regeneration in vivo. *Mol Ther.* 2004;10:844-854.

Astrof S, Hynes RO. Fibronectins in Vascular Morphogenesis. *Angiogenesis.* 2009;12(2):165-175.

Beckman SA, et al. Beneficial effect of mechanical stimulation on the regenerative potential of muscle-derived stem cells is lost by inhibiting vascular endothelial growth factor. *Arterioscler Thromb Vasc Biol*. 2013;33(8):2004-12.

Bernasconi P, et al. Expression of transforming growth factor-beta 1 in dystrophic patient muscles correlates with fibrosis. Pathogenetic role of a fibrogenic cytokine. *J Clin Invest.* 1995;96(2):1137-44.

Borselli C, et al. Functional muscle regeneration with combined delivery of angiogenesis and myogenesis factors. *Proc Natl Acad Sci USA.* 2010;107:3287–3292.

Bouchentouf M, et al. Vascular endothelial growth factor reduced hypoxia-induced death of human myoblasts and improved their engraftment in mouse muscles. *Gene Ther.* 2008;(6):404-14.

Chen YW, et al. Early onset of inflammation and later involvement of TGFbeta in Duchenne muscular dystrophy. *Neurology*. 2005;65(6):826-34.

Deasy BM, Feduska JM, Payne TR, Li Y, Ambrosio F, Huard J. Effect of VEGF on the regenerative capacity of muscle stem cells in dystrophic skeletal muscle. *Mol Ther.* 2009;17: 1788–1798

Deconinck AE, et al. Utrophin-dystrophin-deficient mice as a model for duchenne muscular dystrophy. *Cell.* 1997;90(4):717–27.

Desguerre I, et al. A new model of experimental fibrosis in hindlimb skeletal muscle of adult *mdx* mouse mimicking muscular dystrophy. *Muscle Nerve.* 2012;45(6):803–14.

Desguerre I, Mayer M, Leturcq F, Barbet JP, Gherardi RK, Christov C. Endomysial fibrosis in Duchenne muscular dystrophy: a marker of poor outcome associated with macrophage alternative activation. *J Neuropathol Exp Neurol.* 2009;68:762–773

Goerges AL and Nugent MA. pH Regulates Vascular Endothelial Growth Factor Binding to Fibronectin: A Mechanism for Control of Extracellular Matrix Storage and Release. *J Biol Chem.* 2004;279: 2307-2315.

Goyenvalle A, et al. Prevention of dystrophic pathology in severely affected dystrophin/utrophin-deficient mice by morpholino-oligomer-mediated exon-skipping. *Mol Ther.* 2010;18(1):198–205.

Goyenvalle A, et al. Rescue of severely affected dystrophin/utrophin-deficient mice through scAAV-U7snRNA-mediated exon skipping. *Hum Mol Genet.* 2012;21(11):2559–71.

Grady RM, Merlie JP, Sanes JR. Subtle neuromuscular defects in utrophin-deficient mice. *J Cell Biol.* 1997;136(4):871-82.

Grady RM, Teng H, Nichol MC, Cunningham JC, Wilkinson RS, Sanes JR. Skeletal and cardiac myopathies in mice lacking utrophin and dystrophin: a model for Duchenne muscular dystrophy. *Cell.* 1997;90(4): 729–38.

Gregorevic P, et al. Systemic delivery of genes to striated muscles using adeno-associated viral vectors. *Nat Med.* 2004;10(8):828-34.

Gutpell KM, Hrinivich WT, Hoffman LM. Skeletal Muscle Fibrosis in the *mdx/utrn*+/- Mouse Validates Its Suitability as a Murine Model of Duchenne Muscular Dystrophy. *PLoS ONE*. 2015;10(1): e0117306.

Hostettler KE, et al. Anti-fibrotic effects of nintedanib in lung fibroblasts derived from patients with idiopathic pulmonary fibrosis. *Respir Res*. 2014;15:157-66.

Huang P, Cheng G, Lu H, Aronica M, Ransohoff RM, Zhou L. Impaired respiratory function in *mdx* and *mdx/utrn*(+/-) mice. *Muscle Nerve.* 2011;43(2):263-7.

Konieczny P, Swiderski K, Chamberlain JS. Gene and cell-mediated therapies for muscular dystrophy. *Muscle Nerve.* 2013;47(5): 649–663.

Kuiper EJ, et al. Effect of VEGF-A on Expression of Profibrotic Growth Factor and Extracellular Matrix Genes in the Retina. *Invest Ophthalmol Vis Sci.* 2007;48(9):4267-4276.

Maurer B, et al. Vascular endothelial growth factor aggravates fibrosis and vasculopathy in experimental models of systemic sclerosis. *Ann Rheum Dis.* 2014;73(10):1880-7.

Messina S, et al. VEGF overexpression via adeno-associated virus gene transfer promotes skeletal muscle regeneration and enhances muscle function in *mdx* mice. *Faseb J.* 2007;21(13):3737-46.

Mezzano V, Cabrera D, Vial C, Brandan E. Constitutively activated dystrophic muscle fibroblasts show a paradoxical response to TGF-β and CTGF/CCN2. *J Cell Commun Signal.* 2007;1(3): 205–217.

Miyazaki D, Nakamura A, Fukushima K, Yoshida K, Takeda S, Ikeda S. Matrix metalloproteinase-2 ablation in dystrophin-deficient *mdx* muscles reduces angiogenesis resulting in impaired growth of regenerated muscle fibers. *Hum Mol Genet.* 2011;20(9):1787-99.

Pessina P, et al. Novel and optimized strategies for inducing fibrosis in vivo: focus on Duchenne Muscular Dystrophy. *Skelet Muscle*. 2014;4:7.

Rhoads RP, Flann KL, Cardinal TR, Rathbone CR, Liu X, Allen RE. Satellite cells isolated from aged or dystrophic muscle exhibit a reduced capacity to promote angiogenesis in vitro. *Biochem Biophys Res Commun*. 2013;440(3):399-404.

Shimizu-Motohashi Y, Asakura A. Angiogenesis as a novel therapeutic strategy for duchenne muscular dystrophy through decreased ischemia and increased satellite cells. *Front Physiol.* 2014;18:5:50.

Stedman HH, et al. The *mdx* mouse diaphragm reproduces the degenerative changes of duchenne muscular dystrophy. *Nature.* 1991;8: 352(6335):536-9.

Taylor SC, Berkelman T, Yadav G, Hammond M. A Defined Methodology for Reliable Quantification of Western Blot Data. *Mol Biotechnol.* 2013;55(3): 217–226.

van Putten M, et al. Comparison of skeletal muscle pathology and motor function of dystrophin and utrophin deficient mouse strains. *Neuromuscul Disord*. 2012;22(5):406–17.

Vempati P, Popel AS, Mac Gabhann F. Extracellular regulation of VEGF: isoforms, proteolysis, and vascular patterning. *Cytokine Growth Factor Rev.* 2014;25(1):1-19.

Wijelath ES, et al. Novel vascular endothelial growth factor binding domains of fibronectin enhance vascular endothelial growth factor biological activity. *Circ Res.* 2002;91:25–31.

Wijelath ES, Rahman S, Murray J, Patel Y, Savidge G, Sobel M. Fibronectin promotes VEGF-induced CD34 cell differentiation into endothelial cells. *J Vasc Surg.* 2004;39:655–660.

Zhou L, et al Haploinsufficiency of utrophin gene worsens skeletal muscle inflammation and fibrosis in *mdx* mice. *J Neurol Sci.* 2008;264(1–2):106–11.

Chapter 4

Vascular-targeted therapy attenuates ischemia and fibrosis

in DMD mice

4 Vascular-targeted therapy attenuates ischemia and fibrosis in DMD mice

4.1 Chapter Summary

A number of limitations currently surround the use of vascular-targeted therapy to treat DMD. The previous chapters describe the use of a murine model that develops more fibrosis than the *mdx* mouse. Results from chapter 2 indicate the *mdx*/*utrn*+/- mouse, a model that lacks dystrophin and is heterozygous for utrophin, exhibits more collagen deposition at an early age compared to its *mdx* counterpart. Using the *mdx*/*utrn*+/- mouse, chapter 3 demonstrated a potential role of VEGF in eliciting a fibrotic response *in vitro* in fibroblasts derived from the diaphragm and, to a lesser extent, the gastrocnemius muscles from this murine model. It is not well known whether VEGF alone induces functional changes in perfusion in a relevant murine model of DMD or if another factor, angiopoietin-1 (ANG1), is also necessary. Further, whether VEGF exerts a pro-fibrotic effect has not been confirmed *in vivo*. Using dynamic contrast-enhanced computed tomography (DCE-CT) to measure perfusion, we show that functional perfusion decreases over a two week period and that blood flow and blood volume are unaffected by localized delivery of VEGF alone compared to sham-injected controls. In contrast, mice treated with a combination of VEGF and ANG1, exhibit reduced progression of ischemia over the treatment period, evidenced by a lesser reduction in blood volume compared to either the sham- or VEGF-treated mice. These vascular differences are validated histologically by increased vessel maturation in hind limb muscles that received the combination treatment. There is also histological evidence that VEGF and ANG1 treatment resulted in reduced infiltration of leukocytes into the muscle tissue and reduced deposition of collagen in the endomysium.

4.2   Introduction

Vascular-targeted therapy to treat Duchenne muscular dystrophy (DMD) has been investigated since the early 2000's (Shimizu-Motohashi et al 2014). The proposed mechanisms by which angiogenic therapy may alleviate the pathophysiology associated with DMD are numerous. Previous work has provided evidence of compromised vasculature in the disease, including impaired angiogenesis (Palladino et al 2013) and decreased vascular density in the *mdx* mouse, the most widely used murine model of DMD (Loufrani et al 2004), as well as in the gold-retriever model of (Nguyen et al 2005). As such, many groups have attempted to increase vascular density in dystrophic muscle by treating it with vascular endothelial growth factor (VEGF), a well-known and potent inducer of angiogenesis (Messina et al. 2007; Gregorevic et al. 2004; Beckman et al. 2013). Histological markers of endothelial cells, cells that make up the luminal wall of vessels, demonstrate increased vascular density following VEGF treatment. Other studies have also shown that VEGF levels are decreased in some muscle groups in *mdx* mice as well as in patients (Abdel-Salam et al 2009). These findings are somewhat inconclusive, though, as others have shown that VEGF levels are increased in dystrophic muscle tissue. This discrepancy is likely due to a temporally dependent alteration in VEGF expression at various stages of the disease. Interestingly, hypoxia-inducible factor-1 alpha (HIF1-α) is increased in DMD patients (Abdel-Salam et al 2010) and others have shown that increases in HIF1-α in the *mdx* mouse brain correspond to elevated levels of VEGF (Nico et al 2007).

Although promising results have been shown regarding the use of VEGF to alleviate ischemia, there are a number of questions that remain unanswered. First, it has been widely proposed that VEGF, while inducing angiogenesis, creates only immature and "leaky" vessels that do not confer significant functional benefit to the muscle (Gavard et al 2008). Although histological analyses have revealed an increase in vascular density following VEGF treatment, whether these newly formed vessels are functional has not been rigorously investigated. Groups have therefore begun to use VEGF in combination with other factors, particularly angiopoietin-1 (ANG1), to induce vascular maturation (Chae et al 2000; Shyu et al 2003; Yamauchi, et al 2003 Chen et al 2007).

Binding of ANG1 to the Tie2 receptor on endothelial cells activates the receptor's tyrosine kinase activity, producing a cellular response that results in vessel survival and stabilization (Fukuhara et al 2010). Receptor activation increases phosphatidylinositol 3-kinase (PI3K) activity, leading to stimulation of AKT, a cell survival signaling molecule that inhibits transcription factors essential in vascular destabilization (Daly et al., 2004). Activation of the PI3K pathway also increases expression of survivin, an inhibitor of apoptosis in endothelial cells (Papapetropoulos et al., 2000). Upon Tie2 activation, vascular-endothelial cadherin increases adhesion between endothelial cells, lending to an increase in overall vessel stability (Gamble et al., 2000; Gavard et al 2008). Importantly, ANG1 recruits vascular smooth muscle cells by signaling through endothelial cells (Iivanainen et all 2003, Kobayashi et al 2006). This vascular smooth muscle lining ultimately confers functional maturity to newly formed vasculature (Brudno et al 2013).

Given the role of VEGF and ANG1 in angiogenesis, various groups have attempted to exploit their function as a vascular-targeted approach to treating ischemia in DMD (Mofarrahi et al 2015). Indeed, VEGF administration has been shown to increase endogenous repair and enhance the efficacy of transplanted cell populations. Still, questions remain regarding the reality of using these factors to treat DMD. Importantly, very little data exists describing the functional efficacy these factors exert in a longitudinal manner in DMD models. Position emission tomography demonstrates that blood flow is not affected by VEGF treatment alone in the rat skeletal muscle, but is significantly increased when VEGF is combined with ANG1 (Zaccigna et al 2007). Thus, the objective of the present study is to non-invasively assess the effect of VEGF treatment alone or in combination with ANG1 on functional angiogenesis in dystrophic murine hind limb skeletal muscle. Our group has previously reported the use of dynamic contrast-enhanced computed tomography (DCE-CT) to monitor disease progression in murine models of DMD (Ahmed et al 2011), but no study to date has attempted to assess therapeutic intervention in preclinical studies using this imaging modality. Further, we utilize the *mdx*/*utrn*+/- mouse, a model that lacks dystrophin and is heterozygous for utrophin, a dystrophin analogue. Previous studies have suggested the heterozygous mouse as a superior model for DMD research since this mouse develops fibrosis to a greater extent compared to the dystrophin-null *mdx* mouse (Zhou et al 2008). Using the

mdx/*utrn*+/- mouse, which is more prone to fibrosis, is of particular importance given recent findings showing a potential role of VEGF in exacerbating disease severity in other fibrotic diseases such as scleroderma and idiopathic pulmonary fibrosis (Maurer et al. 2014 & Hostettler et al. 2014). Additionally, long-term overexpression of VEGF promotes fibrosis in skeletal muscle in the ischemic hind limb rabbit model (Karvinen et al 2011).

4.3   Materials and Methods

4.3.1   Animal Care and Ethics Statement

Experiments were performed at The Lawson Health Research Institute at St. Joseph's Health Care (SJHC) in London, Ontario. Heterozygous *mdx*/*utrn*+/- mice, originally generated by Dr.'s Mark Grady and Josh Sanes (Washington University, St. Louis) [12], were generously provided to us by Dr. Robert Grange (Virginia Polytechnic and State University) and maintained in the Animal Care Facility at SJHC. Colonies were maintained under controlled conditions (19-23˚C, 12 hour light/dark cycles) and allowed water and food *ad libitum*. Nine to ten week-old male mice were used in this study. All procedures involving animal experiments were carried out in strict accordance with the Canadian Council on Animal Care (CCAC) and were approved by the Animal Use Subcommittee at Western University.

4.3.2   Genotyping

Genomic DNA from tail snips or ear notch tissue was used for genotyping. Briefly, ear notch tissue was lysed in a proteinase K solution at 50° C overnight. DNA was diluted appropriately and polymerase chain reaction was used to amplify the utrophin gene using Platinum *Taq* polymerase. Presence of the utrophin gene was detected using the following set of primers (Sigma): 5'-TGCAGTGTCTCCAATAAGGTATGAAC-3', 5'-TGCCAAGTTCTAATTCCATCAGAAGCTG -3' (forward primers) and 5'-CTGAGTCAAACAGCTTGGAAGCCTCC-3' (reverse primer).

4.3.3   Enzyme-linked immunosorbent assays

To determine endogenous levels of VEGF and ANG1, we used a Quantikine Mouse VEGF kit (R&D Systems) and a Mouse ANG1 ELISA kit (Lifespan Biosciences). 10 week-old *mdx*/*utrn*+/- mice (n=6) and C57Bl10 (n= 6) were euthanized. Dissected tissue was placed in ice cold PBS, homogenized and stored overnight at -20 ° C to ensure complete lysis of homogenates. Samples were then centrifuged at 5000xg for 5 minutes and only the supernatant assayed. Total protein was quantified using the BCA Assay (Pierce) prior to ELISA assay. All samples were run in duplicate and absorbance was measured at 450nm.

4.3.4   Local Delivery of Growth Factors

Affi-Gel Blue Beads (BioRad) were air-dried in a cell culture hood under sterile conditions overnight. The next day, beads were resuspended in 10μl of: sterile phosphate-buffered saline (PBS), 0.5μg recombinant mouse VEGF, 5μg recombinant human ANG1, or a combination of VEGF and ANG1. Beads were incubated in the growth factors overnight. The next day, beads were centrifuged for 5 minutes at 12,000rpm, the supernatant was removed and the beads were re-suspended in 10μl sterile PBS. Hind limb hair was gently plucked and the exposed skin was wiped with isopropyl alcohol to ensure sterility. The beads were implanted intramuscularly into the posterior compartment of the hind limb (lateral head of the gastrocnemius muscle) as follows: mice in the "sham" group received PBS-soaked beads in both hind limbs, "VEGF" mice received PBS-soaked beads in the right hind limb and VEGF-coated beads in the left, and the "VEGF+ANG1" group received VEGF-coated beads in the right hind limb and VEGF+ANG1-coated beads in the left. Injections took place before the anatomical axial CT scan while the mouse was anesthetized.

4.3.5   Dynamic Contrast-Enhanced Computed Tomography

Mice were scanned at baseline and 2 weeks post-injection (time point based on pilot studies previously conducted in our lab, Appendices C,D). During each imaging session, anesthesia was induced with 3% isoflurane and maintained with a 1.5% oxygen-balanced isoflurane mixture, delivered at a constant rate of 1L/min. DCE-CT protocol

was adapted from a previous study (Ahmed et al. 2011). Briefly, following an anatomical axial scan, each mouse received 200 µL of Conray 43 contrast agent (diluted 1:2 with saline) at an injection rate of 2.0 ml/min with an infusion pump (New Era Pump Systems Inc) via tail vein catheter. CT Perfusion software (GE Healthcare) was used to quantify blood flow (BF) and blood volume (BV) based on functional maps from the acquired series of CT images (Cenic A, et al., 1999). Perfusion data acquired for each mouse was normalized to baseline values to minimize biological variability between animals, thus allowing us to assess longitudinal changes between groups. Regions of interest were drawn around the whole cross-sectional slice of the hind limb, excluding the tibia and fibula, and three slices covering the leg were included in each calculation (Appendix E).

4.3.6   Tissue Preparation

At the end of the imaging study, mice were sacrificed via gas euthanasia followed by cervical dislocation. Gastrocnemius and diaphragm muscles were dissected, immediately fixed in formalin, and embedded in paraffin. Extreme care was taken to ensure muscles were embedded in the same orientation across each muscle group. Tissue blocks were sectioned at 5um thickness and dried in an oven at 37°C overnight. To achieve representative sections from the whole muscle tissue, serial sections were taken every 20 or 5 slices for the GM and diaphragm muscles, respectively. Tissue sections were then deparaffinised and rehydrated in a series of xylene and ethanol washes to prepare them for subsequent Masson's Trichrome staining for collagen content (performed at the Pathology Department at University Hospital, London, ON), or haematoxylin and eosin staining to visualize inflammation. Serial sections were used for the two staining methods to ensure that analysis of both collagen content and inflammation referred to the same samples. Following the staining step, slides were dehydrated, washed in xylene and mounted with Permount mounting medium.

4.3.7   Immunohistochemistry

Tissue sections were processed for immunocytochemistry by deparaffinising and rehydrating sections followed by heat-mediated antigen retrieval in a citrate buffer for 20 minutes. Slides were then cooled slowly to room temperature and incubated in blocking

buffer (1% BSA, 10% goat serum in PBS) for one hour. Sections were incubated with anti-αSMA (Abcam, 1:100) or anti-CD45 (Abcam, 1:50) primary antibodies at 4°C overnight. Following thorough washing with PBS, Alexa Fluor IgG (Life Technologies, 1:1000) secondary antibodies were used to visualize the primary antibodies, and ProLong Gold anti-fade with DAPI (Life Technologies) was added to visualize the nuclei and to mount the coverslips onto glass slides. Fluorescent images were acquired on a Nikon Eclipse microscope.

4.3.8 Microscopy and Image Analysis

For Masson's Trichrome sections, colour histological images were acquired on a Zeiss Axioscope microscope under 10x objective using Northern Eclipse software. Non-overlapping fields of view of the entire tissue were taken for each section. Collagen content was assessed across the entire tissue slice and automatically quantified using an in-house colour thresholding algorithm written in MATLAB 2015b (Mathworks, Natick, MA, USA) designed to separate red and blue image components as previously described (Gutpell et al. 2015). The percentage of each slide area positive for collagen presence was calculated, and automatic thresholds were manually verified with labeled colour overlays on the original histology images to ensure that collagen presence was accurately identified.

For αSMA and CD45 sections, grey scale fluorescence images were acquired on a Nikon Eclipse Microscope using NIS Elements Microscope Image Software. Non-overlapping fields of view of the entire tissue were taken for each section. A semi-automatic grey scale thresholding algorithm was implemented in MATLAB 2015a to quantify the area of each slide positive for αSMA or CD45 while mitigating variations due to image exposure and auto-fluorescence; referred to as "background" intensity variations. The three major steps of the algorithm are 1) background intensity estimation, 2) stain identification, and 3) stain area calculation. These steps are briefly described as follows. 1) The intensity gradient magnitude of each slide was calculated, and contiguous regions with a gradient magnitude less than a constant threshold were assigned as background. This background threshold was empirically selected as 40 intensity units, or roughly 8% of the maximum signal intensity gradient observed across slides. 2) All closed non-background regions

with maximum signal intensity greater than a stain threshold were assigned positive for stain presence. The stain threshold was manually selected as either 4× or 5× times the mean background signal intensity of each slide. 3) Within each closed non-background region considered positive for stain presence, the final stained area was determined by applying a threshold of 25% of the maximum intensity in that region. The percentage of total area positive for stain was calculated for each slide. Again, automatic thresholds were manually verified using labeled colour overlays on the original images, and any features incorrectly identified as positive for stain were manually edited.

4.3.9   Western Blot

Tissue was collected in Phosphosafe lysis buffer (EMD Millipore) containing a protease inhibitor cocktail (EMD Millipore) and homogenized. Protein was quantified using the bicinchoninic acid assay (Pierce). 25 μg of protein was heat denatured and loaded onto a TGX stain-free SDS gel. Protein was transferred onto a PVDF low fluorescence membrane using the Transblot Turbo machine (Bio-Rad) and total protein was visualized on the Bio-Rad Gel Doc system. Membranes were blocked with 5% bovine serum albumin in Tris-buffered saline containing 0.05% Tween 20 for 1 hour. Blots were then incubated with primary αSMA (1:1000, Abcam) or anti-CD45 (1:500, Abcam) primary antibodies at 4°C overnight.   Following thorough washing in TBS-T, blots were incubated with anti-rabbit or anti-mouse horseradish peroxidase secondary antibodies (1:5000) for 1 hour. Bands were visualized via chemiluminescence using ImageLab software (Bio-Rad) and normalized to total protein signal from the stain-free blots (Taylor et al. 2013).

4.3.10   Statistical Analysis

Data was analyzed using Student's t-test for ELISA results and an analysis of variance (ANOVA) for the perfusion and histology results. Differences between groups were determined using Tukey's post-hoc test. A p-value less than 0.05 was considered significant. Replicate values for each experiment are presented with the results.

4.4   Results

4.4.1   Endogenous levels of both VEGF and ANG1 are significantly reduced in severely fibrotic diaphragm tissue, but not weakly affected GM tissue of the *mdx/utrn+/-* mouse

Endogenous expression of VEGF and ANG1 was measured in the diaphragm and GM muscles at 9-10 weeks of age (Figure 4.1). The level of VEGF in GM muscle of *mdx/utrn+/-* mice (19.6pg/ml) was similar to that measured in wild-type mice (19.3pg/ml, p=0.93). However, compared to healthy diaphragm muscle (63.0pg/ml), the concentration of VEGF in dystrophic diaphragm muscle (39.2pg/ml) was significantly reduced (p=0.0049). A similar trend was observed for the endogenous concentration of ANG1 in healthy versus dystrophic diaphragm and GM muscles. Specifically, ANG1 expression in healthy and dystrophic GM muscles was 85.3 and 54.1 pg/ml, respectively, but these values were not determined to be significantly different from one another (p=0.09). In contrast, a marked reduction of ANG1 expression was measured in the diaphragm of dystrophic mice relative to wild-type controls (148.3 and 365.6 pg/ml, respectively; p<0.0001).
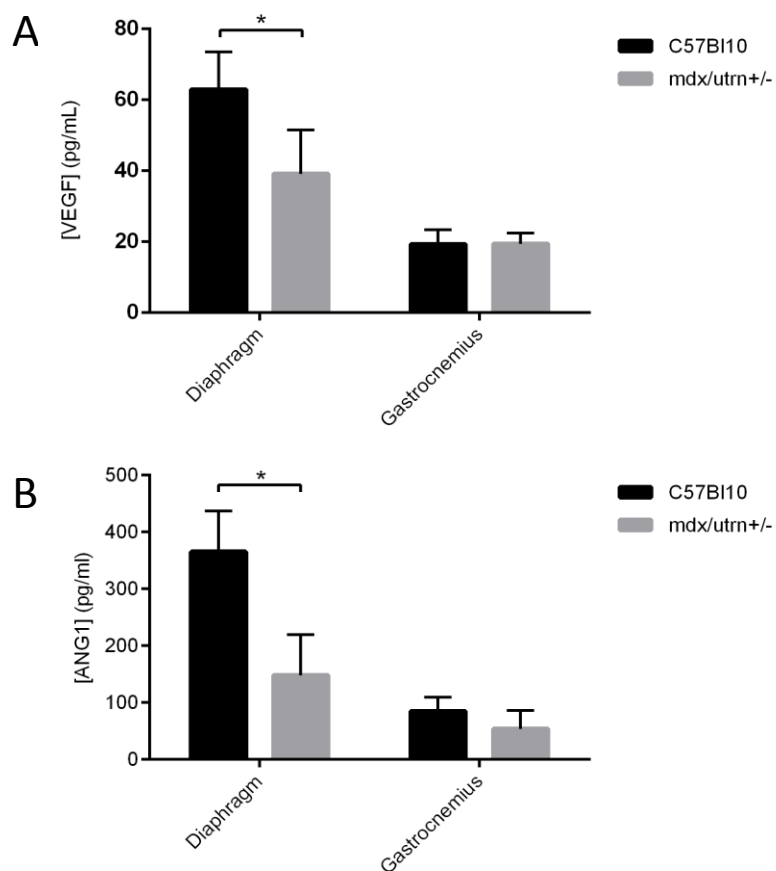
Figure 4.1: VEGF and ANG1 are decreased in dystrophic diaphragm and murine muscles.

ELISA analysis of VEGF and ANG1 in 9 to 10 week-old *mdx/utrn+/-* diaphragm and GM muscles compared to healthy wild type controls. A. VEGF was lower in *mdx/utrn+/-* diaphragm muscles compared to healthy wild-type controls. VEGF expression was not significantly different between dystrophic and healthy GM muscles. B. ANG1 was lower in *mdx/utrn+/-* diaphragm muscles compared to healthy wild-type controls. ANG1 expression was not significantly different between dystrophic and healthy GM muscles. n = 6 per group, *P < 0.05, by Student's t-test. Error bars represent SD.

4.4.2   Effect of VEGF and ANG1 on perfusion

Blood flow (BF) and blood volume (BV) were assessed as parameters of perfusion in this study. There was no significant difference measured between the two hind limbs, regardless of treatment. BF and BV are therefore presented as fold change averages between the two limbs after 16 days of growth factor treatment (Figure 4.2). Absolute values for BF and BV indicate that measurements were not significantly different among mice in different treatment groups at baseline (Table 4.1). Baseline values also indicate the degree of variability between mice. BF decreased in all mice, regardless of treatment, over the course of the study (Figure 4.3). There was no significant difference in BF fold change between sham-injected (0.417±0.26), VEGF-treated (0.408±0.17), and VEGF+ANG1-treated mice (0.979±0.64; p= 0.0614). BV also decreased over the two-week period, but the change was less marked in mice that received the combination treatment of VEGF+ANG1 (0.847±0.40) compared to either the sham-injected control (0.284±0.12) or VEGF-treated groups (0.398±0.16; p= 0.0109). No significant difference in BV fold change was measured between the sham-injected and VEGF-treated mice (Figure 4.4).

4.4.3   VEGF and ANG1 increase vessel maturation in gastrocnemius muscle of *mdx*/*utrn*+/- mice

Western blot analysis was employed to assess total alpha-smooth muscle actin (αSMA) in GM tissue homogenates following the two-week treatment period (Figure 4.5). Total αSMA expression was increased in GM muscles from VEGF+ANG1 treated mice compared to controls. Since αSMA identifies both blood vessels as well as myofibroblasts, we further employed IHC analysis to determine αSMA expression only in vessels (Appendix F). While no significant differences were measured between the sham-injected (0.18% ±0.033) and the VEGF-treated mice (0.23% ±0.066), we did measure a significant increase in αSMA-positive vessels in hind limb muscles treated with both VEGF and ANG1 (0.36% ±0.054) relative to either sham or VEGF-treated mice (p<0.0001). Many newly formed αSMA-positive vessels were detected at the injection area in VEGF+ANG1-treated hind limbs. Very few mature vessels were observed at the injection site of VEGF-treated hind limbs.
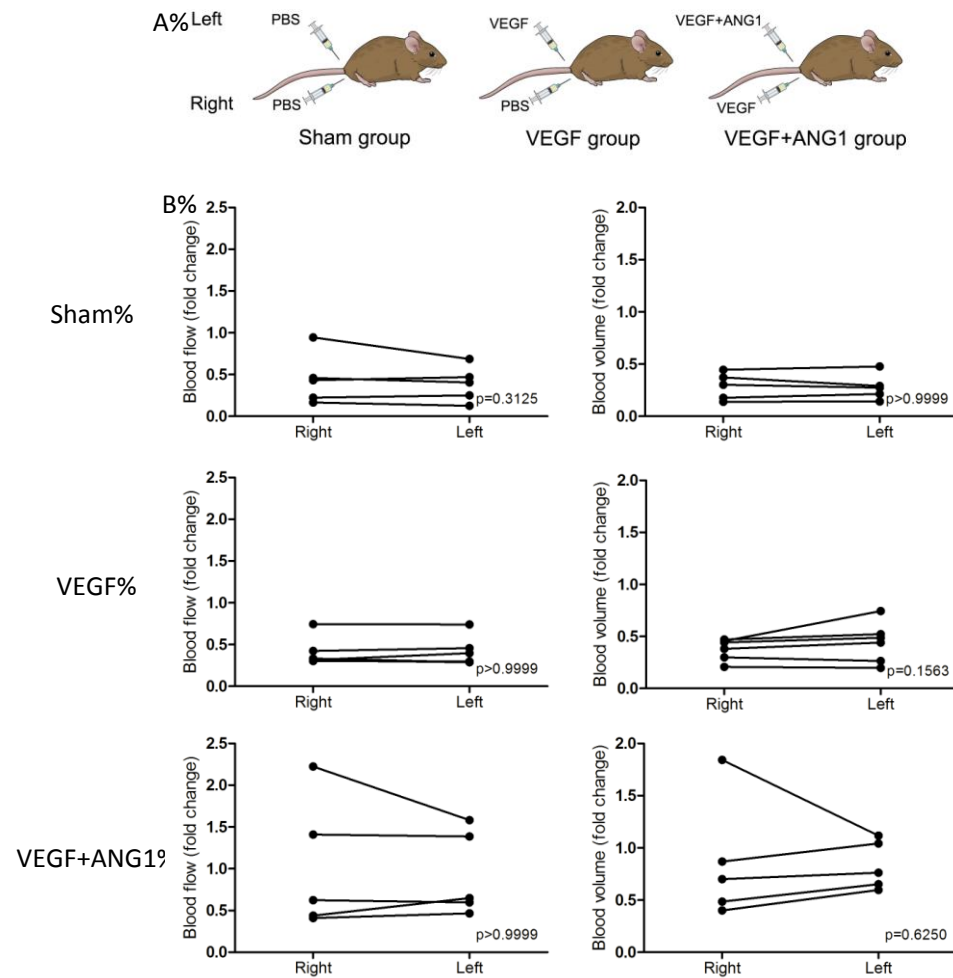
Figure 4.2: Perfusion measured at endpoint is not significantly different between hind limbs, regardless of treatment.

(A) Schematic representation of treatment groups. "Sham" group mice received PBS-soaked beads in both hind limbs. "VEGF" mice received PBS-soaked beads in the right hind limb and VEGF-coated beads in the contralateral limb. VEGF+ANG1 mice received VEGF-coated beads in the right hind limb and VEGF+ANG1-coated beads in the contralateral limb. (B) Blood flow and blood volume did not differ between hind limbs, allowing for perfusion measurements to be assessed based on the averaged BF and BV following treatment. n=5 for sham, n=6 for VEGF, n=5 for VEGF+ANG1, $P < 0.05$, by Wilcoxon signed-rank test.

Table 4.1: Mean absolute values (mean ± SD) of blood flow (BF) and blood volume (BV) for each experimental group at baseline.

P-values to the right of each mean column indicate that no significant difference existed between treatment groups at baseline. n=5 for sham, n=6 for VEGF, n=5 for VEGF+ANG1, $P < 0.05$, by one-way ANOVA.

Treatment	Absolute BF ±SD	BF p-value	Absolute BV ±SD	BV p-value
Sham	59.8 ± 25.1		7.1 ± 3.1	
VEGF	51.6 ± 8.3	0.1008	4.7 ± 2.2	0.1007
VEGF+ANG1	36.8 ± 9.8		3.8 ± 1.6	
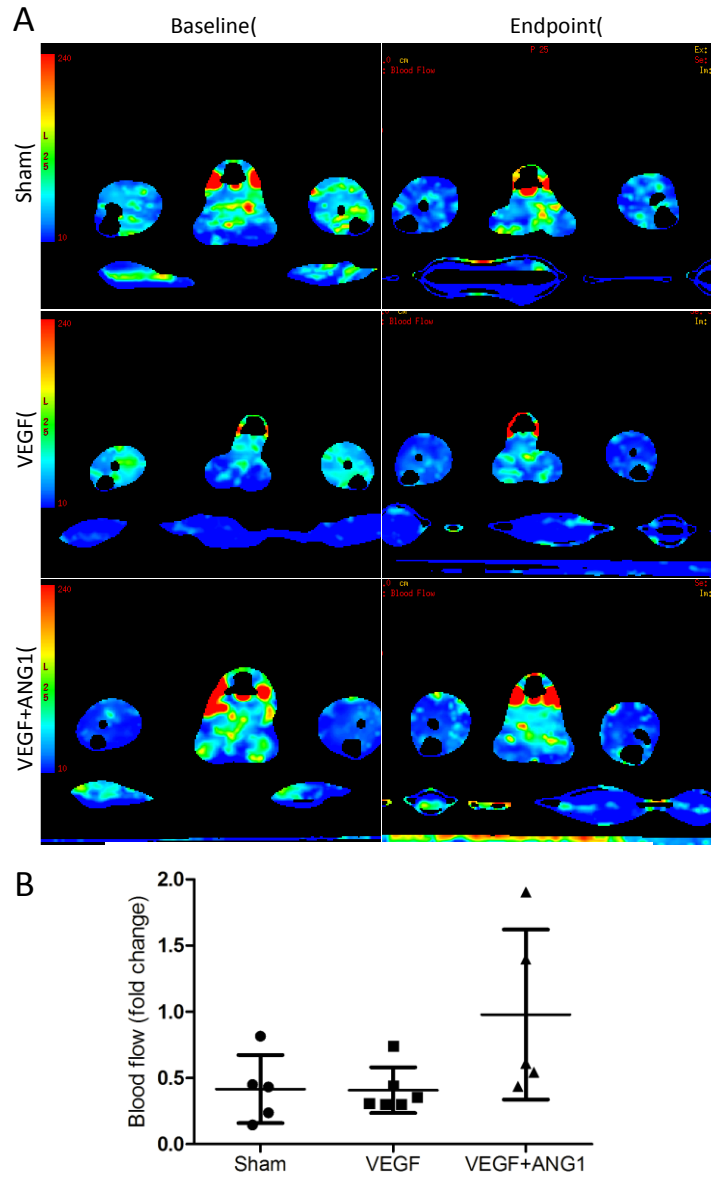
Figure 4.3: Low dose delivery of pro-angiogenic growth factors does not affect blood flow 18 days post-treatment in *mdx/utrn*+/- hind limb skeletal muscle.

A. Representative blood flow maps of sham-injected, VEGF- and VEGF+ANG1-treated hind limbs attained from dynamic contrast-enhanced computed tomography. Display field of view = 5cm. B. Blood flow decreased in all but two mice over the course of the study. Blood flow was not affected by either treatment groups compared to the sham controls. n=5 for sham, n=6 for VEGF, n=5 for VEGF+ANG1, by one-way ANOVA. Error bars represent SD.

Figure 4.4: Ischemia-related reduction in blood volume is circumvented by VEGF+ANG1 treatment in *mdx/utrn*+/- hind limb skeletal muscle.

A. Representative blood volume maps of sham-injected, VEGF- and VEGF+ANG1-treated hind limbs attained from dynamic contrast-enhanced computed tomography. Display field of view = 5cm. B. Blood volume decreased in all but two mice over the course of the study. Blood volume was not significantly different in sham-injected and VEGF-treated hind limbs. VEGF+ANG1 treatment resulted in significantly higher fold-change in blood volume compared to the VEGF and sham group. n=5 for sham, n=6 for VEGF, n=5 for VEGF+ANG1, *P < 0.05, by one-way ANOVA. Error bars represent SD.

Figure 4.5: VEGF+ANG1 increases vessel maturation following treatment in
***mdx/utrn+/-* GM muscle.**

A. Western blot analysis of total alpha smooth muscle actin (αSMA) expression in GM tissue homogenates following treatment. B. Immunohistochemical analysis of αSMA-positive vessels, represented as percent image area. n=6 for all groups **P < 0.01, ***P < 0.001, by one-way ANOVA. Error bars represent SD. C. Representative immunofluorescence images of αSMA expression in sham-injected, VEGF- and VEGF+ANG1-treated GM muscles. D. Growth factor-coated beads are visible at the injection site. More αSMA-positive vessels are detected at the injection site of VEGF+ANG1-treated hind limbs compared to VEGF-treated hind limbs. Scale bar=100 μm.

4.4.4 VEGF and ANG1 reduce leukocyte infiltration and inflammation in gastrocnemius muscle of *mdx*/*utrn*+/- mice

To assess the effect of VEGF alone, or in combination with ANG1, on vascular permeability, we measured the level of CD45 expression, indicative of leukocyte infiltration (Gordon et al. 2013). Expression was assessed via Western blot and IHC analyses (Figure 4.6). While muscle treated with VEGF alone (0.35 ±0.03%) did not exhibit significantly different levels of CD45 compared to the sham-injected controls (0.29 ±0.04%), co-administration of VEGF and ANG1 did significantly reduce leukocyte infiltration (0.15 ±0.04%, p= 0.0084). Since CD45 only identifies infiltrating leukocytes and not resident macrophages already present in the skeletal muscle, H&E staining was employed to qualitatively assess the general degree of inflammation following treatment. Both the sham-injected and VEGF-treated muscles were observed to have diffuse clusters of inflammatory cells throughout the muscle. In contrast, muscle treated with VEGF+ANG1 exhibited little inflammation, with the majority of tissue devoid of inflammation.

4.4.5 VEGF and ANG1 decrease collagen deposition compared to VEGF alone in gastrocnemius muscle of *mdx*/*utrn*+/- mice

To assess the effect of VEGF alone or a combination of VEGF and ANG1 on muscle fibrosis, we measured collagen deposition using Masson's Trichrome stain (Figure 4.7). There was no significant difference in collagen deposition between either the sham-injected (9.82 ± 3.1%) or VEGF-treated (12.61 ± 3.1%) hind limb muscles. In contrast, hind limb muscle treated with the combination of VEGF and ANG1 exhibited only 7.6±2.2% collagen deposition, and this difference was determined to be significantly lower than the amount of collagen deposition measured in VEGF-treated muscle (p=0.0247).
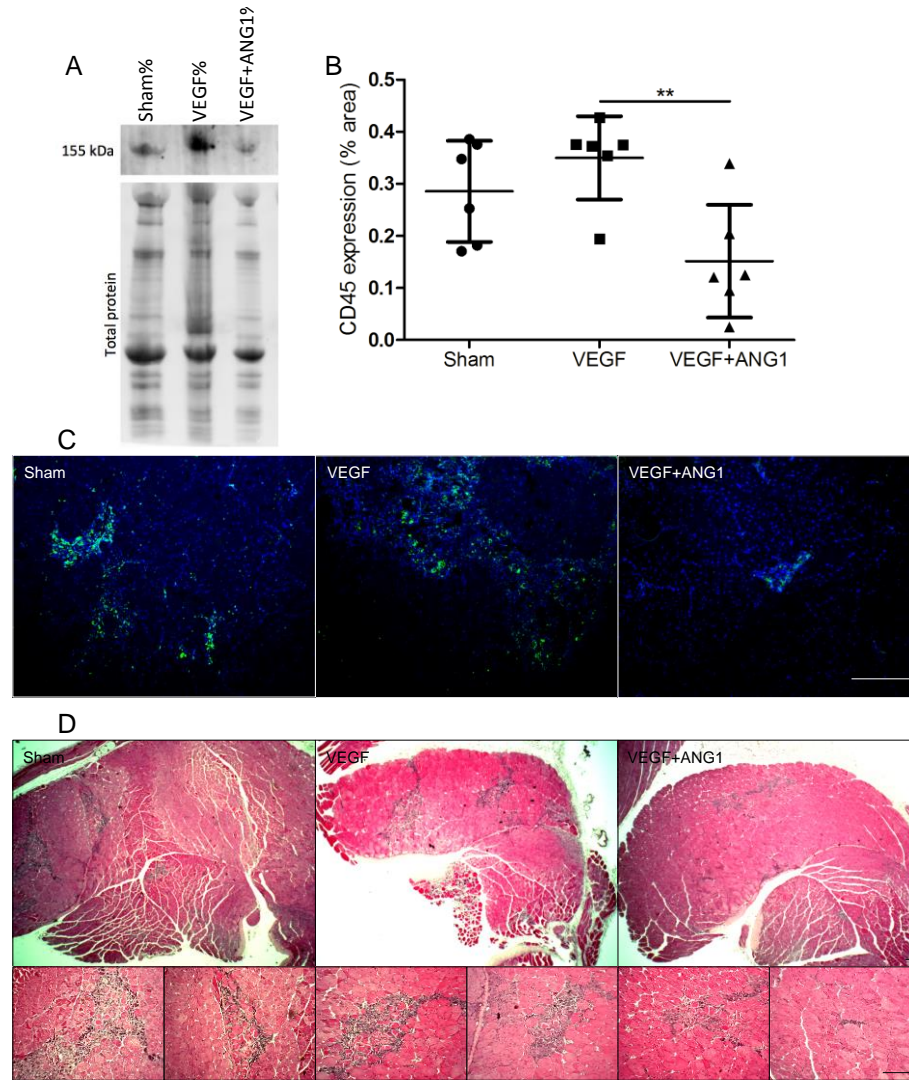
Figure 4.6: VEGF+ANG1 decreases leukocyte infiltration following treatment in
mdx/utrn+/- GM muscle.

A. Western blot analysis of CD45 expression in GM tissue homogenates following treatment. B. Immunohistochemical analysis of CD45, represented as percent image area. n=6 for all groups **P < 0.01 by one-way ANOVA. Error bars represent SD. C. Representative immunofluorescence images of a-CD45 expression in sham-injected, VEGF- and VEGF+ANG1-treated GM muscles D. H&E staining was used to qualitatively assess the extent of inflammation following treatment. Inflammatory foci are present in all groups, but only small, sparse clusters are present in muscle that received the VEGF+ANG1 treatment. Scale bar=100 μm
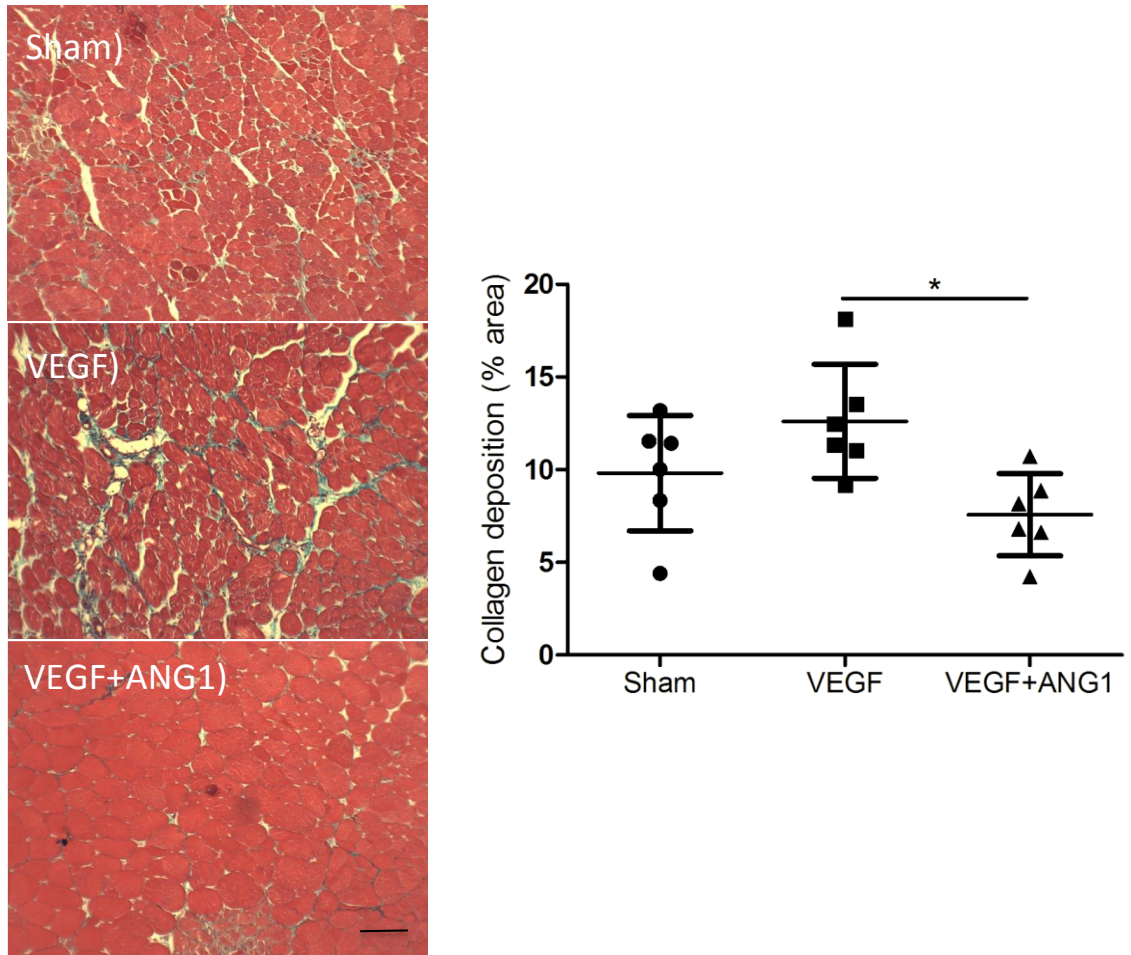
Figure 4.7: VEGF+ANG1 decreases collagen deposition following treatment in
mdx/utrn+/- **GM muscle.**

A. Representative Masson's Trichrome-stained tissue sections of sham-injected, VEGF-
and VEGF+ANG1-treated GM muscles. Scale bar=100 μm B. Quantification of collagen
deposition (blue), represented as percent image area. n=6 for all groups *P < 0.05 by one-
way ANOVA. Error bars represent SD.

4.5 Discussion

Vascular endothelial growth factor (VEGF) and angiopoietin-1 (ANG1) are increasingly being considered for their potential role in reducing or attenuating the muscle ischemia observed in patients with Duchenne muscular dystrophy (DMD) (McClung et al 2015). While prior studies suggest a potential role for these factors in enhancing endogenous repair and cell therapy, studies remain to directly investigate the effects of either factor on functional perfusion in a non-invasive manner. Therefore, in the present study, we utilized the *mdx*/*utrn+/-* mouse, a murine DMD model more prone to fibrosis than the commonly used *mdx* mouse, to measure functional perfusion via dynamic contrast-enhanced computed tomography (DCE-CT). The short-term effect of VEGF alone or in combination with ANG1 was assessed following a low dose, localized delivery for 16 days. Given the high degree of variability between animals with respect to baseline perfusion parameters, the ability to monitor vascular-targeted therapy over time in the same animal is particularly valuable. DCE-CT is a safe and effective means to monitor both disease progression and therapeutic efficacy and shows promise for scaling preclinical studies directly to patients (Stewart et al 2006, Sahani et al 2007). Importantly, we provide the first evidence that VEGF alone is not sufficient to affect functional perfusion parameters in the hind limb skeletal muscle at the dose and duration investigated. In comparison, co-administration of VEGF and ANG1 reduced muscle ischemia over the course of the treatment period, as evidenced by a less marked reduction in blood volume relative to control groups. This finding also highlights the importance of investigating perfusion parameters other than blood flow alone, since the physiological variability of this measurement can overshadow key observations. Blood flow is subject to a number of environmental cues that vastly change flow measurements, such as temperature, fasting, exercise, and stress. While blood volume may also be affected by these factors, it is a more stable function that has the ability to represent changes in the intravascular compartment, or the space that can be perfused during the flow of blood. In addition to the functional measurements observed in this study, we further report that VEGF+ANG1 significantly reduced muscle inflammation related to either sham-injection or VEGF treatment alone, as well as fibrosis, relative to VEGF treatment alone.

The findings from this study highlight the importance of considering the stage of disease progression in assessing vascular therapy. During the first weeks of life, murine models of DMD display classic signs of rapid degeneration and regeneration, accompanied by a robust inflammatory response. This phase is accompanied by a transient increase in perfusion as assessed by DCE-CT (Ahmad et al 2011). By nine-ten weeks of age, the disease evolves to a more degenerative state and fibrosis begins to predominate, coinciding with a progressive decrease in perfusion. Having critically identified a window of opportunity to intervene with therapeutics, the present study aimed to assess the ability of a combination of VEGF and ANG1 to slow or attenuate chronic inflammation, ischemia and fibrosis in DMD mice. Our data on endogenous expression of the two growth factors further points to differences in the vasculature at different phases of disease progression. Although we did not measure differences in either growth factor in the hind limb (gastrocnemius) muscle, there was a significant reduction in both VEGF+ANG1 in the diaphragm. Since the diaphragm develops overt fibrosis and muscle degeneration much earlier than hind limb muscles, these differences may point to possible differences in expression of VEGF+ANG1 in the hind limb at later time points. Overall, having well-defined margins between the different disease states could reveal valuable information regarding the effects of VEGF+ANG1 on perfusion, vascular permeability, and fibrosis.

Given that we did not measure any beneficial functional effects from a low dose of VEGF under the conditions used here, it would be worth investigating whether exogenous VEGF treatment is even necessary or if ANG1 alone may be sufficient to affect change, particularly at earlier stages of disease pathogenesis prior to the onset of overt fibrosis. Since both growth factors were decreased in the more severely affected diaphragm muscle, exogenous administration of these factors at a later disease stage may have an even greater impact on ischemia than what we observed here. In addition to its role in promoting vascular maturity, previous work by others has shown that ANG1 promotes satellite cell self-renewal and inhibits apoptosis (Abou-Khalil et al 2013). Research in other vascular-related diseases such as cardiac ischemia and sepsis have uncovered the deleterious effect that low circulating levels of ANG1 may play in these states (Novotny et al 2008, Lee et al 2011). In human microvascular endothelial cells

(HMVECs), serum from sepsis patients induced intercellular gap formation, and this effect was reversed by supplementation with ANG1 (Parikh et al 2006).

Prior studies have suggested that VEGF treatment decreases fibrosis (Deasy et al 2009; Beckman et al 2013), whereas we reported an increase in collagen deposition 18 days post-treatment compared to VEGF+ANG1 treated hind limbs. This finding is in line with our previous work showing that VEGF induces stress fiber formation in fibroblasts derived from the GM and diaphragm muscles of *mdx/utrn*+/- mice. We have also demonstrated an increase in expression of alpha-smooth muscle actin mRNA in diaphragm fibroblasts following VEGF treatment. Importantly, studies in other fibrotic diseases including idiopathic pulmonary fibrosis and scleroderma have shown that VEGF exacerbates disease pathology (Maurer et al. 2014 & Hostettler et al. 2014). Still, previous work in the DMD field has pointed to an anti-fibrotic role of VEGF. A few variables could account for this discrepancy. The use of the *mdx/utrn*+/- mouse rather than the *mdx* mouse, which our group has validated as a more suitable model due to its increased development of fibrosis, may be more responsive to VEGF than its *mdx* counterpart. This hypothesis speaks to the seed and soil theory whereby the *mdx/utrn*+/- tissue may be "primed" to respond to VEGF and develop fibrosis, relative to the *mdx* mouse. Another important consideration that may account for the differences between our findings and those of others with respect to fibrosis is the disease stage assessed in the current study. A number of studies use either young (5 to 7 week-old) or aged (6 month old) *mdx* mice (Messina et al 2007). It is therefore possible that VEGF plays a reduced pro-fibrotic role in both the early phase of the disease when acute inflammation predominates and in later phases of the disease when overt fibrosis has occurred in the muscle. Lastly, the dose used in this study is much lower than some doses cited in previous studies and may account for differential effects on collagen deposition following treatment. Regardless, a study in rabbit skeletal muscle has also indicated that long-term delivery of VEGF increases collagen deposition. Cumulatively, these findings suggest that the effect of VEGF on fibrosis may significantly impede its use as a therapeutic factor in DMD. Based on the results presented here, the pro-fibrotic effect of VEGF is circumvented when co-administered with ANG1.

There is a critical need to detect disease changes such as ischemia in early stages so that therapies can be developed before damage, i.e., fibrosis, is extensive and irreversible. Advanced non-invasive imaging technologies have immense potential to achieve this; we have used dynamic contrast-enhanced computed tomography (DCE-CT) and positron emission tomography (PET) to identify transient "spikes" in perfusion and ^{18}F-fluorodeoxyglucose (^{18}F-FDG) uptake, respectively, in the hind limb muscles of preclinical mouse models of DMD (Ahmad et al 2011). Intensity of these spikes correlates with disease severity, degree of inflammation, and development of muscle fibrosis. Importantly, these studies identified a window of opportunity to intervene with therapeutics aimed at slowing/attenuating the inflammatory/ischemic/fibrotic process, as demonstrated in the present study. Further use of these technologies to delineate how vascular therapies augment either endogenous muscle repair or cell replacement therapy represent an innovative and critical approach to the treatment of muscle degenerative disorders.

Future directions will aim to develop methods to better control the delivery of angiogenic factors. Although it is well accepted that cell-based delivery systems effectively deliver high payloads, there remains concerns regarding their potential pro-tumorigenic side effects, particularly with regards to VEGF administration (Lee et al). Additionally, although we focused on the hind limb muscles in the current study, vascular therapy will need to be effective in other muscles involved in disease progression, particularly the diaphragm and cardiac muscles. Indeed, fibrosis and degeneration in these tissues account for a majority of fatalities in DMD, and therefore any promising treatment will need to affect these muscles as well. The fact that the combination treatment of VEGF+ANG1 resulted in a significant effect that was detected not only histologically but also functionally supports further investigation for the use of these factors in long term management of DMD-related ischemia, inflammation, and fibrosis.

4.6 References

Abdel-Salam E, Abdel-Meguid I, Korraa S. Markers of degeneration and regeneration in Duchenne muscular dystrophy. *Acta Myol*. 2009;28(3):94–100.

Abdel-Salam E, Abdel-Meguid IE, Shatla R, Korraa SS. Stromal cell-derived factors in Duchenne muscular dystrophy. *Acta Myol*. 2010;29(3):398–403.

Abou-Khalil R, et al. Autocrine and paracrine angiopoietin 1/Tie-2 signaling promotes muscle satellite cell self-renewal. *Cell Stem Cell*. 2009;5:298–309.

Ahmad N, et al. Use of imaging biomarkers to assess perfusion and glucose metabolism in the skeletal muscle of dystrophic mice. *BMC Musculoskelet Disord*. 2011;12: 127.

Beckman SA, et al. Beneficial effect of mechanical stimulation on the regenerative potential of muscle-derived stem cells is lost by inhibiting vascular endothelial growth factor. *Arterioscler Thromb Vasc Biol*. 2013;33(8):2004-12.

Brudno Y, Ennett-Shepard AB, Chen RR, Aizenberg M, Mooney DJ. Enhancing microvascular formation and vessel maturation through temporal control over multiple pro-angiogenic and pro-maturation factors. *Biomaterials.* 2013;34(36):9201-9.

Cenic A, Nabavi DG, Craen RA, Gelb AW, Lee TY. Dynamic CT measurement of cerebral blood flow: a validation study. *AJNR Am J Neuroradiol.* 1999;20(1):63-73.

Chae JK, et al. Coadministration of angiopoietin-1 and vascular endothelial growth factor enhances collateral vascularization. *Arterioscler Thromb Vasc Biol*. 2000; 20(12):2573-8.

Chen F, Tan Z, Dong CY, Chen X, Guo SF. Adeno-associated virus vectors simultaneously encoding VEGF and angiopoietin-1 enhances neovascularization in ischemic rabbit hind-limbs. *Acta Pharmacol Sin*. 2007;28(4):493-502.

Daly, C et al. (2004). Angiopoietin-1 modulates endothelial cell function and gene expression via the transcription factor FKHR (FOXO1). *Genes Dev*. 2004;18(9), 1060–1071.

Deasy BM, Feduska JM, Payne TR, Li Y, Ambrosio F, Huard J. (2009). Effect of VEGF on the Regenerative Capacity of Muscle Stem Cells in Dystrophic Skeletal Muscle. *Mol Ther*. 2009;17(10):1788–1798.

Fukuhara S, Sako K, Noda K, Nagao K, Miura K, Mochizuki N. Tie2 is tied at the cell-cell contacts and to extracellular matrix by Angiopoietin-1. *Exp Mol Med*. 2009;41(3):133–139.

Fukuhara S, Sako K, Noda K, Zhang J, Minami M, Mochizuki N. Angiopoietin-1/Tie2 receptor signaling in vascular quiescence and angiogenesis. *Histol Histopathol*. 2010;25(3):387-96.

Gamble JR, et al. Angiopoietin-1 is an antipermeability and anti-inflammatory agent in vitro and targets cell junctions. *Circ Res*. 2000;87:603–607.

Gavard J, Patel V, Gutkind JS. Angiopoietin-1 prevents VEGF-induced endothelial permeability by sequestering Src through mDia. *Dev Cell*. 2008;14(1):25-36.

Gordon BS, Delgado Díaz DC, Kostek MC. Resveratrol decreases inflammation and increases utrophin gene expression in the *mdx* mouse model of Duchenne muscular dystrophy. *Clin Nutr*. 2013;32(1):104-11.

Grady RM, Teng H, Nichol MC, Cunningham JC, Wilkinson RS, Sanes JR. Skeletal and cardiac myopathies in mice lacking utrophin and dystrophin: a model for Duchenne muscular dystrophy. *Cell*. 1997; 90(4):729-38

Gregorevic P, et al. Systemic delivery of genes to striated muscles using adeno-associated viral vectors. *Nat Med*. 2004;10(8):828-34.

Gutpell KM, Hrinivich WT, Hoffman LM. Skeletal Muscle Fibrosis in the *mdx*/*utrn*+/- Mouse Validates Its Suitability as a Murine Model of Duchenne Muscular Dystrophy. PLoS ONE. 2015;10(1): e0117306.

Hostettler KE, et al. Anti-fibrotic effects of nintedanib in lung fibroblasts derived from patients with idiopathic pulmonary fibrosis. *Respir Res.* 2014;15:157-66

Iivanainen E, et al. Angiopoietin-regulated recruitment of vascular smooth muscle cells by endothelial-derived heparin binding EGF-like growth factor. *FASEB J.* 2003;17(12):1609-21.

Karvinen H, et al. Long-term VEGF-A expression promotes aberrant angiogenesis and fibrosis in skeletal muscle. *Gene Ther.* 2011;18(12):1166-72.

Kobayashi H, DeBusk LM, Babichev YO, Dumont DJ, Lin PC. Hepatocyte growth factor mediates angiopoietin-induced smooth muscle cell recruitment. *Blood.* 2006;108(4):1260–1266.

Lee RJ, Springer ML, Blanco-Bose WE, Shaw R, Ursell PC, Blau HM. VEGF gene delivery to myocardium: deleterious effects of unregulated expression. *Circulation.* 2002;102(8):898-901.

Lee SW, et al. Angiopoietin-1 protects heart against ischemia/reperfusion injury through VE-cadherin dephosphorylation and myocardiac integrin-β1/ERK/caspase-9 phosphorylation cascade. *Mol Med.* 2011;17(9-10):1095-106.

Loufrani L, et al. Absence of dystrophin in mice reduces NO-dependent vascular function and vascular density: total recovery after a treatment with the aminoglycoside gentamicin. *Arterioscler Thromb Vasc Biol.* 2004;24(4):671-6.

Maurer B, et al. Vascular endothelial growth factor aggravates fibrosis and vasculopathy in experimental models of systemic sclerosis. *Ann Rheum Dis.* 2014;73(10):1880-7

Messina S, et al. VEGF overexpression via adeno-associated virus gene transfer promotes skeletal muscle regeneration and enhances muscle function in *mdx* mice. *Faseb J*. 2007;21(13):3737-46.

McClung JM, et al. Muscle cell derived angiopoietin-1 contributes to both myogenesis and angiogenesis in the ischemic environment. *Front Physiol*. 2015;6:161 doi: 10.3389/fphys.2015.00161

Mofarrahi M, et al. Angiopoietin-1 enhances skeletal muscle regeneration in mice. *Am J Physiol Regul Integr Comp Physiol.* 2015;308(7):R576-89.

Nico B et al. HIF activation and VEGF overexpression are coupled with ZO-1 up-phosphorylation in the brain of dystrophic *mdx* mouse. *Brain Pathol*. 2007;17(4):399-406.

Novotny NM, et al. Angiopoietin-1 in the treatment of ischemia and sepsis. *Shock*. 2009;31(4):335-41.

Nguyen F, Guigand L, Goubault-Leroux I, Wyers M, Cherel Y. Microvessel density in muscles of dogs with golden retriever muscular dystrophy. *Neuromuscul Disord*. 2005;15(2):154-63.

Palladino M, et al. Angiogenic impairment of the vascular endothelium: A novel mechanism and potential therapeutic target in muscular dystrophy. *Arterioscler Thromb Vasc Biol*. 2013;33(12):2867-76.

Papapetropoulos A, et al. Angiopoietin-1 inhibits endothelial cell apoptosis via the Akt/survivin pathway. *J Biol Chem.* 2000;31;275(13):9102-5.

Parikh SM, et al. Excess Circulating Angiopoietin-2 May Contribute to Pulmonary Vascular Leak in Sepsis in Humans. *PLoS Med.* 2006;3(3):e46.

Sahani DV, Holalkere NS, Mueller PR and Zhu AX. Advanced hepatocellular carcinoma: CT perfusion of liver and tumor tissue-initial experience. *Radiology.* 2007;243(3):736-43.

Shimizu-Motohashi Y, Asakura A. Angiogenesis as a novel therapeutic strategy for Duchenne muscular dystrophy through decreased ischemia and increased satellite cells. *Front Physiol.* 2014;5:50. doi: 10.3389/fphys.2014.00050.

Shyu KG, Chang H, Isner JM. Synergistic effect of angiopoietin-1 and vascular endothelial growth factor on neoangiogenesis in hypercholesterolemic rabbit model with acute hindlimb ischemia. *Life Sci.* 2003;73(5):563-79.

Stewart E E, Chen X, Hadway J and Lee T Y 2006 Correlation between hepatic tumor blood flow and glucose utilization in a rabbit liver tumor model. *Radiology*. 2006 239(3):740-50.

Taylor SC, Berkelman T, Yadav G, Hammond M. A Defined Methodology for Reliable Quantification of Western Blot Data. *Mol Biotechnol*. 2013;55(3): 217–226.

Yamauchi A, et al. Pre-administration of angiopoietin-1 followed by VEGF induces functional and mature vascular formation in a rabbit ischemic model. *J Gene Med* 2003;5(11):994-1004.

Zacchigna S, et al. In vivo imaging shows abnormal function of vascular endothelial growth factor-induced vasculature. *Hum Gene Ther.* 2007;18(6):515-24.

Zhou L, et al. Haploinsufficiency of utrophin gene worsens skeletal muscle inflammation and fibrosis in *mdx* mice. *J Neurol Sci*. 2008;264(1–2):106–11.

Chapter 5

Discussion

5   General Discussion

5.1 Chapter Summary

The research described in this thesis includes studies that advance current knowledge of vascular-targeted therapy for the treatment of Duchenne muscular dystrophy. Importantly, very little has been reported on whether vascular-targeted therapy may confer functional benefits to the muscle and how angiogenic growth factors may affect fibrosis. This research is novel in that it investigates the effect of VEGF, alone or in combination with ANG1, in the *mdx/utrn*+/- mouse, a clinically relevant murine model that mimics the manifestation of DMD in patients. We focused our studies on the phase of disease progression when acute and rapid inflammation transitions into fibrotic deposition and muscle degeneration, which is around 8-10 weeks of age in the *mdx/utrn*+/- mouse. Given this tightly controlled timeline, we have elucidated some key findings that have not been previously reported (Table 5.1). An important consideration is that findings presented in this thesis include work conducted in a murine model of Duchenne muscular dystrophy and therefore conclusions made here may not fully translate to human DMD patients. Additionally, there are specific limitations to each study that are discussed in the following section. Overall, this chapter will summarize the important conclusions drawn from each study, discuss key limitations to the research, and propose future investigative directions that will be crucial prior to moving vascular therapy into patients.

Table 5.1: Summary of findings from studies described in chapters 2, 3, and 4.

DM: Diaphragm muscle; GM: gastrocnemius muscle; dko: double knockout (*mdx*/*utrn*-/-); ⬆: increased; ⬇: decreased

Chapter 2 Comparison of three murine models of DMD	Chapter 3 Effect of VEGF on DMD fibroblasts *in vitro*	Chapter 4 Effect of VEGF & ANG1 *in vivo*
Young & aged mdx/utrn+/- mice exhibit more GM fibrosis than mdx mice	VEGF does not affect collagen or Ctgf/ccn2 gene expression in DM or GM fibroblasts	Endogenous [VEGF] and [ANG1]: mdx/utrn+/- < wild-type
Fibrosis: GM << diaphragm (for all 3 models)	VEGF ⬆ αSMA gene expression DM fibroblasts	VEGF+ANG1 ⬇ hind limb ischemia
Extent of fibrosis is not different among hind limb muscle groups	VEGF ⬆ fibronectin in DM and GM fibroblasts	VEGF+ANG1, but not VEGF alone, ⬆ vessel maturation
Disease severity: mdx < mdx/utrn+/- << dko	VEGF ⬆ differentiation of GM and DM fibroblasts into myofibroblasts	VEGF+ANG1 ⬇ leukocyte infiltration, inflammation
mdx/utrn+/- is the most suitable model for assessing longitudinal effects of vascular therapy	DM fibroblasts are more responsive to pro-fibrotic cues than GM fibroblasts	VEGF+ANG1 ⬇ fibrosis

5.2   Conclusions by chapter

5.2.1   Chapter 2- Selection of the *mdx*/*utrn*+/- mouse for DMD research

The aim of Chapter 2 was to determine which murine model would be best suited to our research goals for investigating vascular-targeted therapy for DMD. Disease progression in *mdx*, *mdx*/*utrn*+/-, and dko mice was compared to that of healthy wild type controls. We demonstrate that, by as early as seven to eight weeks of age, the heterozygous *mdx*/*utrn*+/- mouse exhibits more collagen deposition (indicative of fibrosis) than age-matched *mdx* littermates. Another important finding from this study was that collagen deposition in the *mdx* mouse was not determined to be significantly higher than that observed in healthy hind limb muscle. Other groups have shown that *mdx* skeletal muscle is fibrotic compared to healthy muscle, so the discrepancy between the literature and our findings may lie in that fact that fibrosis was compared on a spectrum along with *mdx*/*utrn*+/- and dko muscle tissue and the effect size in our study is larger than that comparing only *mdx* and wild-type.

Since our research focuses heavily on the effects on fibrosis of angiogenic growth factors, particularly VEGF, this study allowed us to make intelligent decisions regarding the age and model best suited to assess these effects. As a result, we incorporated 9-10 week-old male *mdx*/*utrn*+/- mice in all subsequent studies as these mice are in the "post' fibrotic phase where significant collagen deposition has occured. This is a key consideration for all DMD research. There are a number of studies that utilize young *mdx* mice and subsequently report decreases in fibrosis (Deasy et al., 2009; Beckman et al*.,* 2013). Using an animal that is pre-fibrotic and drawing such conclusions may lead to misinterpretation of the results and could explain some differences in our results compared to those found in the literature.

Although use of the *mdx*/*utrn*+/- mouse allows us to offer conclusions regarding the effect of angiogenic growth factors on fibrosis, it is clear from the findings of our study that the dko mouse remains, by far, the most severely affected and perhaps most accurate model of DMD. Since *mdx*/*utrn*+/- mice, like their *mdx* counterparts, may live up to 1-2

years of age in a laboratory setting, the disease severity is not considered fatal as it is in the dko mouse. As such, future studies assessing functional efficacy of treatment should also seek to assess effects in the dko mouse prior to scaling studies to large animals or, especially, to patients.

Overall, the findings from this study have a profound impact in the field of DMD research, but some limitations did exist. Disease severity in *mdx*, *mdx/utrn+/-* and dko gastrocnemius (GM) and diaphragm muscles was compared to healthy wild type gastrocnemius and diaphragm muscles of C57BL/6 mice. Although C57BL/6 mice are the most commonly used inbred strain, C57BL/10 mice should have been used in this study since the *mdx* mouse was generated on this background and not the Bl6 background. A few studies have investigated whether behavioural and immunological differences exist between these two strains (Deacon et al. 2007, McClive et al. 1994, Slingsby 1995). While the differences appear to be minor, the results from these studies highlight the need to properly select control strains. Although we would not anticipate this discrepancy to affect conclusions drawn from the study, for the purpose of scientific soundness, C57BL/10s were included for wild type controls in all subsequent studies.

Although collagen deposition occurs earlier in this model compared to the *mdx* mouse, whether or not the difference between the two is sufficient to affect function is not known. We used the term "collagen deposition" synonymously with "fibrosis," but there may in fact be a certain degree of collagen deposition that does not exert a negative impact on muscle function. Therefore, our finding that increased collagen deposition by 7-8 weeks of age classifies the *mdx/utrn+/-* mouse as "more fibrotic" is an important assumption and should be kept in mind when referring to both models in terms of fibrogenesis.

Our use of C57Bl6 mice as the healthy control model and use of a limited definition of fibrosis still revealed importance differences between the *mdx* and *mdx/utrn+/-* murine models. The limitations discussed here, if addressed, would only bolster the key findings observed in Chapter 2. Since there is increasing focus on the importance of fibrosis in DMD, many groups are looking for superior murine models to the *mdx* mouse, and the

work in this study is the first to show that phenotypic differences in collagen deposition arise at a young age between *mdx* and *mdx/utrn+/-* mice. One of the most important initial steps in designing a study is selection of a suitable animal model in which to challenge hypotheses. This study rigorously tested the murine models available to us and allowed us to definitively decide to incorporate the *mdx/utrn+/-* mouse in all subsequent studies described in this thesis. This decision thus allows us to tie a number of findings that contrast previously reported findings to the use of a model that is not commonly cited in the literature, opening the door for a new understanding of the effects of vascular therapy in DMD.

5.2.2   Chapter 3- Role of VEGF in eliciting a fibrotic response

The aim of the studies described in Chapter 3 was to investigate whether exogenous levels of VEGF may exacerbate the fibrotic response in fibroblasts derived from the *mdx*/*utrn*+/- mouse. In other fibrotic diseases, particularly idiopathic pulmonary fibrosis, elevated VEGF levels correlate with more rapid disease progression. Whether this relationship is causative or correlated is not fully understood. Studies in rodents indicate that blocking VEGF signaling can reduce fibrosis in mice and administering VEGF exogenously can exacerbate fibrosis in rats (Hamada et al. 2005; Farkas et al. 2009). Given these observations in other pathologies, we sought to determine whether VEGF might play a role in increasing fibrosis in DMD fibroblasts. Although we did not observe robust induction of a fibrotic response following VEGF treatment, as we did following TGFβ treatment, there were multiple findings that may point to a possible role of the growth factor in exacerbating fibrosis. *Collagen* and *Ccn2/ctgf* gene expression were unaffected by VEGF treatment. Interestingly, we did not measure an increase in fibronectin (*Fn1)* gene expression following treatment with either VEGF or TGFβ. When we assessed protein expression, FN levels increased following VEGF but not TGFβ treatment. This is a particularly interesting finding since TGFβ is well known to induce FN production in fibroblasts derived from lung and other fibrotic tissues, and we did not observe such a response here (Torr et al. 2015; Serini et al. 1998). VEGF binding domains have been identified on FN, and it has been shown that VEGF binding to FN

increases the biological activity of VEGF by promoting a physical interaction between the type 2 VEGF receptor (VEGFR-2) and its integrin $\alpha_5\beta_1$ receptor (Wijelath et al. 2002). Given the role of this interaction, it is plausible that VEGF treatment resulted in increased protein levels, but not as part of a fibrotic response. VEGF expression has been shown to increase following FN administration, but not the other way around, as we observed in this study. This is a finding that warrants further exploration.

One of the most intriguing findings from this study is that VEGF increased gene expression of alpha smooth muscle actin (*Acta2*) in diaphragm fibroblasts. Gene expression increased to a level similar to that following TGFβ treatment. Although VEGF led to a 1.4-fold increase in *Acta2* expression in GM fibroblasts, this change was not considered significant given the high variability in this data set. As such, it should not be fully accepted that VEGF does not induce αSMA gene expression in fibroblasts derived from the GM muscle. In both GM and diaphragm fibroblasts, we observed formation of αSMA-positive stress fibers, a hallmark feature of myofibroblasts, following VEGF treatment. Myofibroblasts are a major cellular contributor to fibrotic tissue and differentiation of fibroblasts into this more contractile phenotype is suggestive of induction of the fibrotic response. These findings point to a potential role of VEGF in exacerbating fibrosis in DMD, which is a finding that contradicts previous studies showing a decrease in fibrosis following VEGF treatment in *mdx* mice.

There are some areas for improvement that could be addressed in future studies. Previous research in the past decade has highlighted the importance of an appropriate substrate for culturing and investigating fibroblasts *in vitro* (Hinz et al. 2015). Mimicking physiological substrate stiffness relevant to the tissue of interest is key in reproducing cellular responses that accurately reflect the *in vivo* scenario. Although the differences in our findings between diaphragm and GM-derived fibroblasts indicate their fibrotic phenotypes were maintained in culture, some changes might have resulted due to our culturing on a collagen skim coat rather than a three-dimensional matrix. *In vivo*, tissues range from very soft, such as bone marrow, to very hard, such as bone. Muscle tissue is mid-range, but moderately stiff compared to many other tissues. The culture conditions should attempt to mimic the stiffness of skeletal muscle ECM since others have shown

that matrix stiffness determines the biological activity of TGFβ available to cells. Thus, if our culture conditions were "too stiff," there may have been an abundance of TGFβ available to produce a basal fibrotic response in all treatment groups. This explanation may account for the relatively low fold increase in gene expression observed in the TGFβ treatment group. Although this is a possibility in our study, we do not believe it played a major role in affecting our data since our immunocytochemistry results reveal little differentiation in the untreated control fibroblasts compared to either TGFβ- or VEGF-treated cells. If our culture conditions were severely affecting TGFβ levels, we would have expected to see a high degree of differentiation in the fibroblasts, indicated by αSMA-positive stress fibers.

Although resident fibroblasts are the most studied cell type involved in fibrogenesis, recent work by others has revealed a possible role for others cells in the process as well. Pericytes, which are located around the endothelium and are surrounded by basal lamina, have been shown to differentiate into myofibroblasts and contribute to ECM production (Schrimpf et al. 2011). The exact role of pericytes in healthy and diseased skeletal muscle has not been well defined, and this is in part due to the fact that different sub-populations of pericytes may have different roles in skeletal muscle repair, angiogenesis, innervation, adipogenesis, and fibrosis (Dellavalle et al. 2007, Birbrair et al. 2013a,b,c). Thus, without proper isolation of specific subtypes, information gleaned from pericyte studies could under- or overestimate their role in fibrosis. For example, only a specific subpopulation of Nestin-NG2+ pericytes has been shown to have myogenic properties capable of regenerating muscle. Another sub-population of nestin+NG2+ pericytes, termed type 1 pericytes, participates in fibrogenesis in aged skeletal muscle. These type 1 pericytes, when stimulated with TGFβ, produce collagen and are positive for fibroblast-specific protein 1. It should be noted, though, this fibrogenic capacity of type 1 pericytes is more pronounced in aged mice, and it has not be fully determined whether these cells play a role in non-age related fibrotic disease such as DMD (Birbrair et al. 2013d). Fibro/adipogenic progenitor cells (FAPs) have also been identified recently as a cell type contributing to fibrogenesis (Joe et al. 2010, Uezumi et al. 2010, 2011, Judson et al. 2013, Contreras et al. 2016). Like pericytes, these cells can undergo myogenesis and repair injured muscle or during the aging process. These integrin-α7−Sca1+PDGFR-α+ cells

have been identified as a major source of extracellular matrix production in repair mechanisms of healthy skeletal muscle. In normal repair processes, these FAPS proliferate upon injury, heal the damaged muscle, and then become quickly quiescent until once again needed. In the *mdx* mouse, this normal process appears to be affected and FAP numbers do not sufficiently reduce during the repair process and therefore contribute to the fibrogenic pool of cells (Lemos et al. 2015).

It is well accepted that myofibroblasts are the major source of fibrosis in DMD and other diseases (Klingler et al., 2012). The knowledge gap that currently exists lies in not fully understanding the origin of these myofibroblasts. Work by others has demonstrated a role for pericytes and FAPs in the fibrogenic response. The study described in chapter 3 assessed the effect of vascular therapy on resident fibroblasts. Whether VEGF elicits a fibrotic response in these other cell types is not currently known and we cannot extrapolate our conclusions to apply to FAPS and pericytes. Thus, given the potency of these cells in promoting fibrogenesis, future studies should address the possibility of off-target effects of VEGF on these cell populations as well.

Though these other cell populations remain to be explored, VEGF elicited some components of a fibrotic response in resident DMD fibroblasts, which is a novel finding that has not been previously reported. Additionally, we show that fibroblasts derived from environments that differ in disease severity (i.e. diaphragm and GM muscles), are phenotypically distinct and respond differently to pro-fibrotic cues. Taken together, these results reveal unexplored territory for future work and could drastically alter our understanding of the interplay between fibrosis and angiogenesis in DMD.

5.2.3   Chapter 4- Effect of VEGF and ANG1 on Functional Perfusion

The aim of chapter 4 was to determine what effect, if any, pro-angiogenic factors exert on functional perfusion *in vivo* in the *mdx/utrn+/-* mouse. Specifically, we sought to determine whether VEGF alone, when delivered locally, was sufficient to affect functional perfusion or if another factor is required. In this study, we tested VEGF alone

or in combination with angiopoietin-1 (ANG1). Dynamic contrast-enhanced computed tomography (DCE-CT) was employed to assess the efficacy of vascular-targeted therapy in dystrophic murine skeletal muscle in affecting blood flow and blood volume. DCE-CT is a novel way to examine muscle perfusion because it can assess global blood flow throughout the hind limb, a benefit not afforded by other modalities such as laser Doppler imaging. Although perfusion decreased over the duration of the study, consistent with progression of ischemia, the degree to which blood volume decreased was less marked in mice that received VEGF+ANG1 in combination. We did not measure a significant effect using VEGF alone when compared to the sham-injected group. Assessment of vessel maturation, indicated by αSMA-positive vessels, validated the imaging findings. In addition to vessel maturation, the combination VEGF+ANG1 treatment resulted in reduced collagen deposition and leukocyte infiltration compared to either the sham or VEGF group, suggesting a potential anti-fibrotic and anti-inflammatory role of VEGF+ANG1 in DMD.

Because the previous study, described in chapter 3, suggested VEGF may enhance the fibrotic response in DMD, we investigated the effect of VEGF with and without ANG1 on fibrosis *in vivo*. Our statistical analysis determined that collagen deposition was not significantly different between sham-injected and VEGF-treated hind limbs, but the 3% difference in collagen deposition should not be overlooked, as this may be sufficient to have a biological effect in muscle function. Lastly, the only measure of fibrosis we assessed in this study was collagen deposition via Masson's Trichrome stain. Even though VEGF did not exacerbate collagen deposition compared to the sham control, further analysis of other fibrotic markers such as FN and CCN2/CTGF could reveal different findings.

Since we showed that vessel maturation was increased following VEGF+ANG1 treatment and leukocyte infiltration was decreased, we concluded this reduction in inflammatory cells at the site of muscle injury could play a role in reducing fibrosis. Since inflammatory cells are the major source of TGFβ (which then acts on fibroblasts to induce extracellular matrix production) reducing the number of these cells in muscle tissue may be an effective way to reduce chronic inflammation that lays the foundation

for the eventual fibrosis. Although we quantitatively assessed infiltration of CD45-positive leukocytes, we only performed a qualitative analysis of total inflammation using the hematoxylin and eosin stain. Infiltrating leukocytes are not the only cellular player involved in skeletal muscle inflammation, so analysis of resident macrophages may reveal an even further role of ANG1 in reducing inflammation.

The delivery system used to administer growth factor treatment to *mdx/utrn*+/- hind limb muscle in chapter 4 represents one of the most important limitations to this study. Alginate beads were coated with VEGF or a combination of VEGF and ANG1. Beads prepared for sham injection were soaked in PBS. Although we performed proof-of-principle studies to confirm presence of growth factor up to a minimum of 14 days post-implant (Appendix C), we were unable to calibrate the actual dose of growth factor delivered. Insulin syringes were used for injections and some beads always remained in the hub of the needle following implant. Further, we did not determine the variability in coating efficiency for either growth factor. Given these considerations, we cannot ascertain that a consistent dose of either VEGF or ANG1 was administered each time. Further, although the alginate beads are relatively small, ranging in size from 50 to 100um, the bolus of beads (approximately 100 per injection) remained at the injection site for as little as 4 weeks post-implant. Given this observation, the beads themselves may have induced a minor chronic inflammatory response, which may have contributed to overall disease progression. Although we attempted to deliver just a localized dose, our analyses reveal that the GFs likely exerted systemic effects, as evidenced by a lack of difference in perfusion between control and treated contralateral hind limbs. Localized drug delivery can often be beneficial, particularly in cases where potent or toxic drugs are administered, but systemic delivery may be the ideal outcome here given the systemic effects of disease progression. Overall, the limitations involved with this bead delivery system highlight the need to deliver a targeted dose of growth factor, ideally systemically, to account for these sources of variability in this study.

Use of DCE-CT has drastically improved patient care for other ischemic diseases such as stroke (d'Esterre et al. 2012). Whether it is the optimal non-invasive imaging modality for assessing vascular targeted therapy deserves further consideration. The reduction in

perfusion observed in this study correlates to the time when fibrosis begins to contribute to a significant portion of the skeletal muscle. Thus, an assumption made here is the ischemia observed functionally is, at least in part, due to the progression of fibrosis. Since fibrotic and non-fibrotic muscle tissue does not differ sufficiently in density, these tissues cannot be well delineated on an anatomical CT scan. It would therefore be valuable to use another imaging modality capable of measuring fibrotic tissue to validate this decline in perfusion and corresponding increase in fibrosis. Since MRI can distinguish tissues composed of differing water content, fibrotic tissue appears as a lower signal area than surrounding skeletal muscle (McIntosh et al., 1998; Chen et al. 2006). Combining MRI perfusion with anatomical imaging of fibrotic areas could strengthen the findings we attained from CT perfusion. Other groups have used MRI to assess vasomodulation in humans following exercise with and without taking vasoregulating compounds. Assessing vasodilation and blood oxygenation could be another useful tool in further clarifying assumptions made in our study (Bulte et al. 2006; Towse et al. 2005).

While taking into account these limitations, this study described a novel way to assess the functional effects of vascular therapy for DMD using a non-invasive, clinically relevant approach. In addition, in contrast to other reports, we do not observe an anti-fibrotic effect of VEGF following treatment, a finding that could be partially explained by our unique use of the *mdx/utrn+/-* murine model. Building on the findings from Chapter 3, we demonstrate potential deleterious effects of VEGF alone as a treatment for DMD and show these effects can be avoided when combined with ANG1.

5.3   Future directions

The conclusions drawn from this thesis examining vascular therapy in the *mdx/utrn+/-* mouse have resulted in a number of questions that remain to be answered. Some of our unanticipated findings have generated new avenues to explore and may eventually expedite the use of vascular therapy in DMD patients. There are also a number of findings from our *in vivo* work that may be extended to other fibrotic and vascular-related diseases.

Given the increasing attention that fibrosis is receiving for its devastating effects in DMD, future research that explores this aspect of the disease could reveal new insights to this process. Our *in vitro* work assessing the effect of VEGF on the fibrogenic response in resident fibroblasts pointed to altered fibrotic phenotypes based on the muscle from which these cells were derived. Since we demonstrate that diaphragm fibroblasts are more responsive to TGFβ and VEGF while GM fibroblasts appear to be more resistant to these cues, we hypothesize altered signaling occurring in these different populations. Future work in our lab will focus on performing microarray gene analysis to determine if there is a novel gene or combination of genes that is/are up- or down-regulated in fibrotic cells. Work in Dupuytren's disease, a fibrotic disease of the palmar fascia, reveals differential gene expression in fibroblasts isolated from the lesion versus fibroblasts parallel to the lesion (Satish et al. 2008). These findings suggest that similar profile differences could exist in diaphragm versus GM fibroblasts to reveal potentially novel molecular targets for future treatments.

One of the most encouraging findings attained from this research was that VEGF+ANG1 treatment prevents overt ischemia, as was observed with VEGF treatment alone. Future studies should aim to determine whether VEGF is even necessary to achieve the desired effects from vascular therapy or if ANG1 treatment alone is sufficient. Given that VEGF produces leaky vasculature and it is implicated in hemangioma formation when administered at a sufficiently high dose, avoiding exogenous use of this growth factor might be ideal in DMD (Lee et al. 2000). Use of ANG1 in other disease models such as acute lung injury and sepsis suggest that protecting against vascular leakage is a powerful approach for attenuating undesired downstream consequences (Huang et al. 2008; Fang et al. 2015). Future studies in our lab should also seek to use cartilage oligomeric matrix protein (COMP)-ANG1, a soluble ANG1 derivative that has more potent effects on the Tie2 receptor than does ANG1 (Cho et al. 2004, 2005, Ryu et al. 2015).

Although work in other fields point to the possibility of using ANG1 alone as a treatment, further work is required to assess whether the effect of VEGF on endogenous repair and cell therapy is ultimately a justified use of the growth factor as a treatment. Since prior studies have shown that VEGF enhances efficacy of cell therapy by optimizing paracrine

effects, VEGF may still play an important therapeutic role that is independent of its effect on perfusion (Beckman et al. 2013). Having now identified a disease time point whereby intervention might be optimal, future studies in our lab will investigate whether vascular-targeted therapy will enhance survival of satellite cell transplants. Since it is well accepted that transplanted cells exert their effects by way of paracrine signaling, increasing their survival post-transplant may be an effective way of enhancing their function. Future studies in our lab will use other non-invasive imaging modalities to target satellite cells post-implant (Appendices G-I). Satellite cells expressing luciferase and/or a mutant herpes simplex virus type 1 sr39 thymidine kinase can be non-invasively targeted using bioluminescence or positron emission tomography imaging, respectively (Ray et al., 2007. Thus, we can directly assess the effect of VEGF on cell transplant survival in longitudinal manner that circumvents the need for repeated *ex vivo* analysis.

A promising new avenue for vascular therapy is development of a targeted delivery system. Targeted drug delivery is a rapidly emerging in the field of cancer research for delivering chemotherapy drugs and radioligands for tumour treatment and imaging, respectively (Khaw et al., 2014). Use of a targeted drug delivery system could have a number of benefits for vascular therapy in DMD. A targeted system would circumvent the use of viral delivery as well as allow for systemic delivery to all damaged muscle, especially ones that are difficult to reach via intramuscular injection such as the diaphragm. This ability to target the diaphragm may be the most important factor since disease progression in the respiratory muscles is the major contributing factor to DMD mortality (Khirani et al., 2014). In all three murine models of DMD discussed in this thesis, fibrosis and muscle degeneration in the diaphragm far exceeds that observed in the hind limb muscles. Thus, regardless of the animal model used, any study that reports efficacy in the diaphragm represents more potential than efficacy reported elsewhere in the body. Systemic delivery would also allow for administration of low doses with little off target effects, addressing the issues related to hemangioma formation following VEGF treatment. In order to develop a targeted drug delivery system, a marker specific to damaged muscle will need to be identified. Markers that would be up regulated in the inflammatory response, such as CCR2 and E-selection, or markers up regulated in the fibrotic response, such as CCN2/CTGF or ADAM12, are attractive candidates

(Mojumder et al. 2014, Farini et al. 2007). A key consideration here is targeting a biomarker without affecting function, if function is still desired. On the other hand, neutralizing the activity of some of these markers with the use of an antibody might have synergistic effects that add to the benefits of vascular therapy.

Overall, the research described in this thesis links two-dimensional histological effects of vascular therapy to non-invasive, global changes following treatment. Future work should answer questions relating to vascular therapy that we did not investigate within the body of this work. Three-dimensional histopathology reconstruction and intravital video microscopy may describe parameters of angiogenic therapy not answered by DCE-CT. Such parameters include vessel enlargement, tortuosity, blood oxygenation, and degree of branching/bifurcation following treatment (Xu et al., 2015; Frontini et al., 2011; Novielli & Jackson, 2014). Combining our findings with these techniques may have profound impacts on the way we utilize vascular-targeted therapy in the context of DMD.

Despite tremendous advances in care for patients living with DMD, the disease remains invariably fatal. Vascular-targeted therapy is just one therapeutic approach currently under investigation. While the findings described in this thesis support the use of pro-angiogenic growth factors for DMD, it is the prevalent opinion in the field that any eventual cure will involve a multifaceted approach. Thus, our long-term goal is to work in concert with groups investigating ways to reintroduce dystrophin to DMD patients, a combinatorial approach that may truly extend life expectancy and, importantly, improve quality of life.

5.4 References

Beckman SA, et al. Beneficial effect of mechanical stimulation on the regenerative potential of muscle-derived stem cells is lost by inhibiting vascular endothelial growth factor. *Arterioscler Thromb Vasc Biol*. 2013;33(8):2004-12.

Birbrair A, et al. Role of pericytes in skeletal muscle regeneration and fat accumulation. *Stem Cells Dev*. 2013a;22:2298–2314

Birbrair A, et al. Skeletal muscle neural progenitor cells exhibit properties of NG2-glia. *Exp Cell Res*. 2013b;319:45–63

Birbrair A, et al. (2013c). Skeletal muscle pericyte subtypes differ in their differentiation potential. *Stem Cell Res*. 2013c;10:67–84

Birbrair A, Zhang T, Wang ZM, Messi ML, Mintz A, Delbono O. Type-1 pericytes participate in fibrous tissue deposition in aged skeletal muscle. *Am J Physiol Cell Physiol.* 2013d;305:C1098–C1113

Birbrair A, Zhang T, Wang ZM, Messi ML, Mintz A, Delbono O. Pericytes: multitasking cells in the regeneration of injured, diseased, and aged skeletal muscle. *Front Aging Neurosci*. 2014;6:245.

Birbrair A, Zhang T, Wang ZM, Messi ML, Mintz A, Delbono O. Pericytes at the intersection between tissue regeneration and pathology. *Clin Sci.* 2015;128:81–93

Bulte DP, Alfonsi J, Bells S, Noseworthy MD. Vasomodulation of skeletal muscle BOLD signal. *J Magn Reson Imaging*. 2006;24:886–890.

Chen CK, Yeh L, Chang W, Pan HB, Yang CF. MRI diagnosis of contracture of the gluteus maximus muscle. *AJR Am J Roentgenol*. 2006;187(2):W169–74.

Cho CH. et al. COMP-ANG1: A designed angiopoietin-1 variant with nonleaky angiogenic activity. *Proc Natl Acad Sci USA*. 2004;101:5547–5552.

Cho CH, et al. Long-term and sustained COMP-ANG1 induces long-lasting vascular enlargement and enhanced blood flow. *Circ Res.* 2005;97:86–94.

Contreras O, Rebolledo DL, Oyarzún JE, Olguín HC, Brandan E. Connective tissue cells expressing fibro/adipogenic progenitor markers increase under chronic damage: relevance in fibroblast-myofibroblast differentiation and skeletal muscle fibrosis. *Cell Tissue Res*. 2016 [Epub ahead of print].

d'Esterre CD, Aviv RI, Lee TY. The evolution of the cerebral blood volume abnormality in patients with ischemic stroke: A ct perfusion study. *Acta radiologica*. 2012;53:461-467

Deacon RM, Thomas CL, Rawlins JN, Morley BJ. A comparison of the behavior of C57BL/6 and C57BL/10 mice. *Behav Brain Res*. 2007;179:239–247.

Deasy BM, Feduska JM, Payne TR, Li Y, Ambrosio F, Huard J. Effect of VEGF on the regenerative capacity of muscle stem cells in dystrophic skeletal muscle. *Mol Ther.* 2009;17(10):1788-98.

Dellavalle A. et al. Pericytes of human skeletal muscle are myogenic precursors distinct from satellite cells. *Nat Cell Biol.* 2007;9:255–267.

Duffield JS, Lupher M, Thannickal VJ, Wynn TA. Host responses in tissue repair and fibrosis. *Annu Rev Pathol* 8: 241–276, 2013

Dulauroy S, Di Carlo SE, Langa F, Eberl G, Peduto L. Lineage tracing and genetic ablation of ADAM12(+) perivascular cells identify a major source of profibrotic cells during acute tissue injury. *Nat Med* 18: 1262–1270

Fang Y, Li C, Shao R, Yu H, Zhang Q, Zhao L. Prognostic significance of the angiopoietin-2/angiopoietin-1 and angiopoietin-1/Tie-2 ratios for early sepsis in an emergency department. *Critical Care.* 2015;19:367.

Farini A, et al. T and B lymphocyte depletion has a marked effect on the fibrosis of dystrophic skeletal muscles in the scid/*mdx* mouse. *J Pathol.* 2007;213: 229–238.

Farkas L, Farkas D, Ask K, et al. VEGF ameliorates pulmonary hypertension through inhibition of endothelial apoptosis in experimental lung fibrosis in rats. *J Clin Invest* 2009;119: 1298–1311.

Frontini MJ, et al. Fibroblast growth factor 9 delivery during angiogenesis produces durable, vasoresponsive microvessels wrapped by smooth muscle cells. *Nat Biotechnol.* 2011;29(5):421-7.

Hamada N, et al. Anti-vascular endothelial growth factor gene therapy attenuates lung injury and fibrosis in mice. *J Immunol.* 2005;175:1224–1231.

Hinz B. The extracellular matrix and transforming growth factor-β1: Tale of a strained relationship. *Matrix Biol.* 2015;47:54-65,

Huang YQ, et al. Angiopoietin-1 increases survival and reduces the development of lung edema induced by endotoxin administration in a murine model of acute lung injury. *Crit Care Med.* 2008;36:262–7.

Joe AWB, Yi L, Natarajan A, Le Grand F, So L, Wang J, Rossi FMV. Muscle injury activates resident fibro/adipogenic progenitors that facilitate myogenesis. *Nat Cell Biol*. 2010;12(2):153–163.

Judson RN, Zhang RH, Rossi FM. Tissue-resident mesenchymal stem/progenitor cells in skeletal muscle: collaborators or saboteurs? *FEBS J*. 2013;280(17):4100–4108.

Khaw BA, et al. Bispecific antibody complex pre-targeting and targeted delivery of polymer drug conjugates for imaging and therapy in dual human mammary cancer xenografts: targeted polymer drug conjugates for cancer diagnosis and therapy. *Eur J Nucl Med Mol Imaging.* 2014;41(8):1603-16.

Khirani S, et al. Respiratory muscle decline in Duchenne muscular dystrophy. *Pediatr Pulmonol.* 2014;49(5):473-81.

Kim I, Moon SO, Park SK, Chae SW, Koh GY. Angiopoietin-1 reduces VEGF-
stimulated leukocyte adhesion to endothelial cells by reducing ICAM-1, VCAM-1,
and E-selectin expression. *Circ Res.* 2001;89:477–479.

Klingler W, Jurkat-Rott K, Lehmann-Horn F, Schleip R. The role of fibrosis in Duchenne
muscular dystrophy. *Acta Myol.* 2012;31(3):184-95.

Lee RJ, Springer ML, Blanco-Bose WE, Shaw R, Ursell PC, Blau HM. VEGF gene
delivery to myocardium: deleterious effects of unregulated expression. *Circulation.*
2002;102(8):898-901.

Lemos DR, et al. Nilotinib reduces muscle fibrosis in chronic muscle injury by promoting
TNF-mediated apoptosis of fibro/adipogenic progenitors. *Nat Med.* 2015;21:786–94

McClive PJ, Huang D, Morahan G. C57BL/6 and C57BL/10 inbred mouse strains differ
at multiple loci on Chromosome 4. *Immunogenetics.* 1994;39(4):286-8.

McIntosh LM, Baker RE, Anderson JE. Magnetic resonance imaging of regenerating and
dystrophic mouse muscle. *Biochem Cell Biol.* 1998;76532-41.

Mojumdar K, et al. Inflammatory monocytes promote progression of Duchenne muscular
dystrophy and can be therapeutically targeted via CCR2. *EMBO Mol Med.*
2014;6(11):1476–1492.

Novielli NM, Jackson DN. Contraction-evoked vasodilation and functional hyperaemia
are compromised in branching skeletal muscle arterioles of young pre-diabetic mice.
Acta Physiol (Oxf). 2014;211(2):371-84.

Ray P, Tsien R, Gambhir SS. Construction and validation of improved triple fusion
reporter gene vectors for molecular imaging of living subjects. *Cancer Res.*
2007;67(7):3085.

Ryu JK, Kim WJ, Koh YJ, Piao S, Jin HR, Lee SW, Suh JK (2015). Designed
angiopoietin-1 variant, COMP-angiopoietin-1, rescues erectile function through

healthy cavernous angiogenesis in a hypercholesterolemic mouse. *Scientific Reports*, 5, 9222.

Satish L, et al. Identification of differentially expressed genes in fibroblasts derived from patients with Dupuytren's Contracture. *BMC Med Genomics*. 2008;23:10.

Schrimpf C, Duffield JS. Mechanisms of fibrosis: the role of the pericyte. *Curr Opin Nephrol Hypertens*. 2011;20:297–305.

Serini G, et al. The fibronectin domain ED-A is crucial for myofibroblastic phenotype induction by transforming growth factor-beta1. *J Cell Biol.* 1998;142:873-881.

Simler NR, Brenchley PE, Horrocks AW, et al. Angiogenic cytokines in patients with idiopathic interstitial pneumonia. Thorax 2004; 59: 581–585.

Slingsby JH, Hogarth MB, Simpson E, Walport MJ, Morley BJ. New microsatellite polymorphisms identified between C57BL/6, C57BL/10, and C57BL/KsJ inbred mouse strains. *Immunogenetics*. 1995;43:72–75.

Thurston G. et al. Angiopoietin-1 protects the adult vasculature against plasma leakage. *Nat Med.* 2000;6:460–463.

Torr EE, Ngam CR, Bernau K, Tomasini-Johansson BR, Acton B, Sandbo N. Myofibroblasts exhibit enhanced fibronectin assembly that is intrinsic to their contractile phenotype. *J Biol Chem.* 2015;Epub ahead of print.

Towse TF, Slade JM, Meyer RA. Effect of physical activity on MRI-measured blood oxygen level-dependent transients in skeletal muscle after brief contractions. *J Appl Physiol.* 2005;99:715–722.

Uezumi A, et al. Fibrosis and adipogenesis originate from a common mesenchymal progenitor in skeletal muscle. *J Cell Science*. 2011;124(Pt 21):3654–3664.

Uezumi, A. et al. Mesenchymal progenitors distinct from satellite cells contribute to ectopic fat cell formation in skeletal muscle. *Nat Cell Biol*. 2010;12:143–152.

Vavken P, Saad FA Fleming BC Murray MM. VEGF Receptor mRNA expression by ACL fibroblasts is associated with functional healing of the ACL. *Knee Surg Sports Traumatol Arthrosc.* 2011;19(10):1675-82

Wijelath ES, et al. Novel vascular endothelial growth factor binding domains of fibronectin enhance vascular endothelial growth factor biological activity. *Circ Res.* 2002;91:25–31.

Xu Y, Pickering JG, Nong Z, Gibson E, Arpino J-M, Yin H, et al. (2015) A Method for 3D Histopathology Reconstruction Supporting Mouse Microvasculature Analysis. PLoS ONE 10(5): e0126817. doi:10.1371/journal.pone.0126817

Appendices

Appendix A: Colour thresholding to analyze collagen content in histological sections stained with Masson's Trichrome.
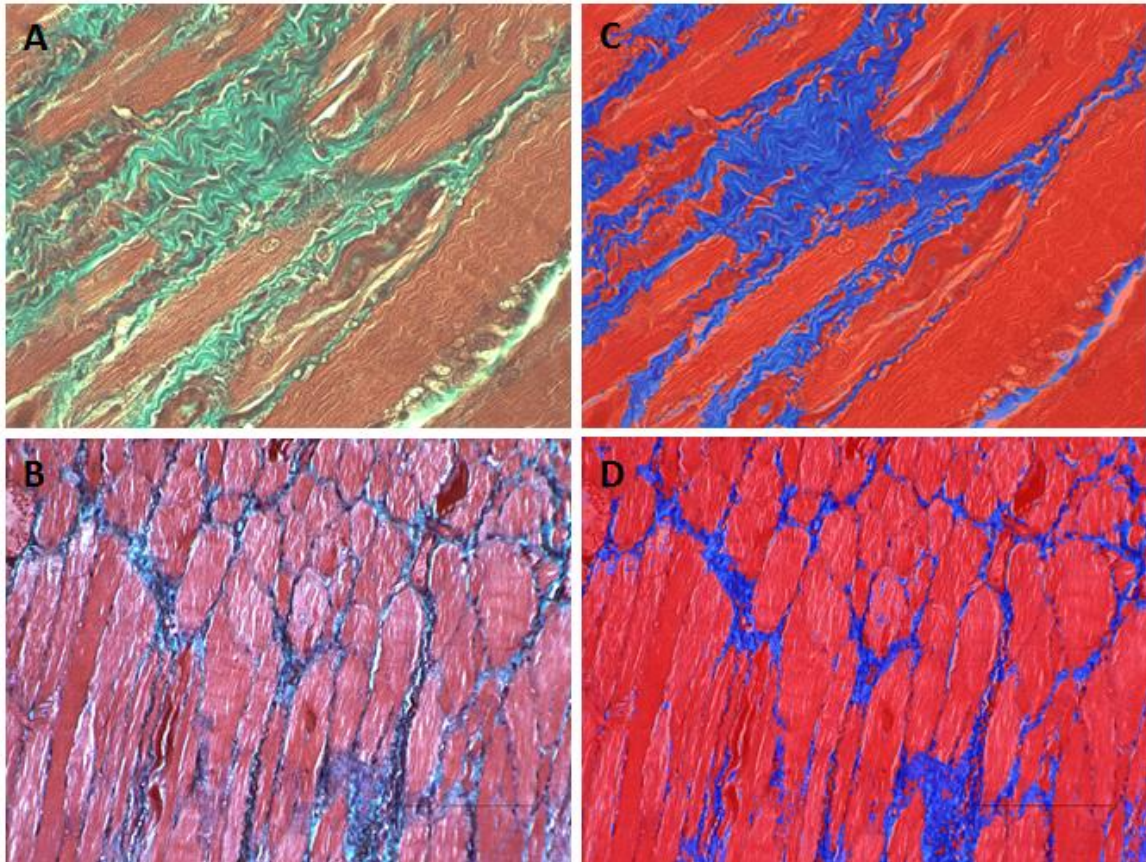

Quantifying collagen deposition in Masson's Trichrome stained tissue sections. 5um sections of gastrocnemius tissue were stained with Masson's Trichrome (A,B) on separate days and imaged on a Zeiss Microscope using different exposure windows, producing different hues of blue (collagen) and orange (muscle). Images were transformed into Lab colour space allowing the isolation of the colour and lightness components of each pixel. A k-means clustering algorithm was then applied to the colour components of each individual image to partition the pixels into groups of relatively 'red' or 'blue' colour values (C,D).

Appendix B: Fibroblasts isolated from dystrophic *mdx/utrn+/-* mice.
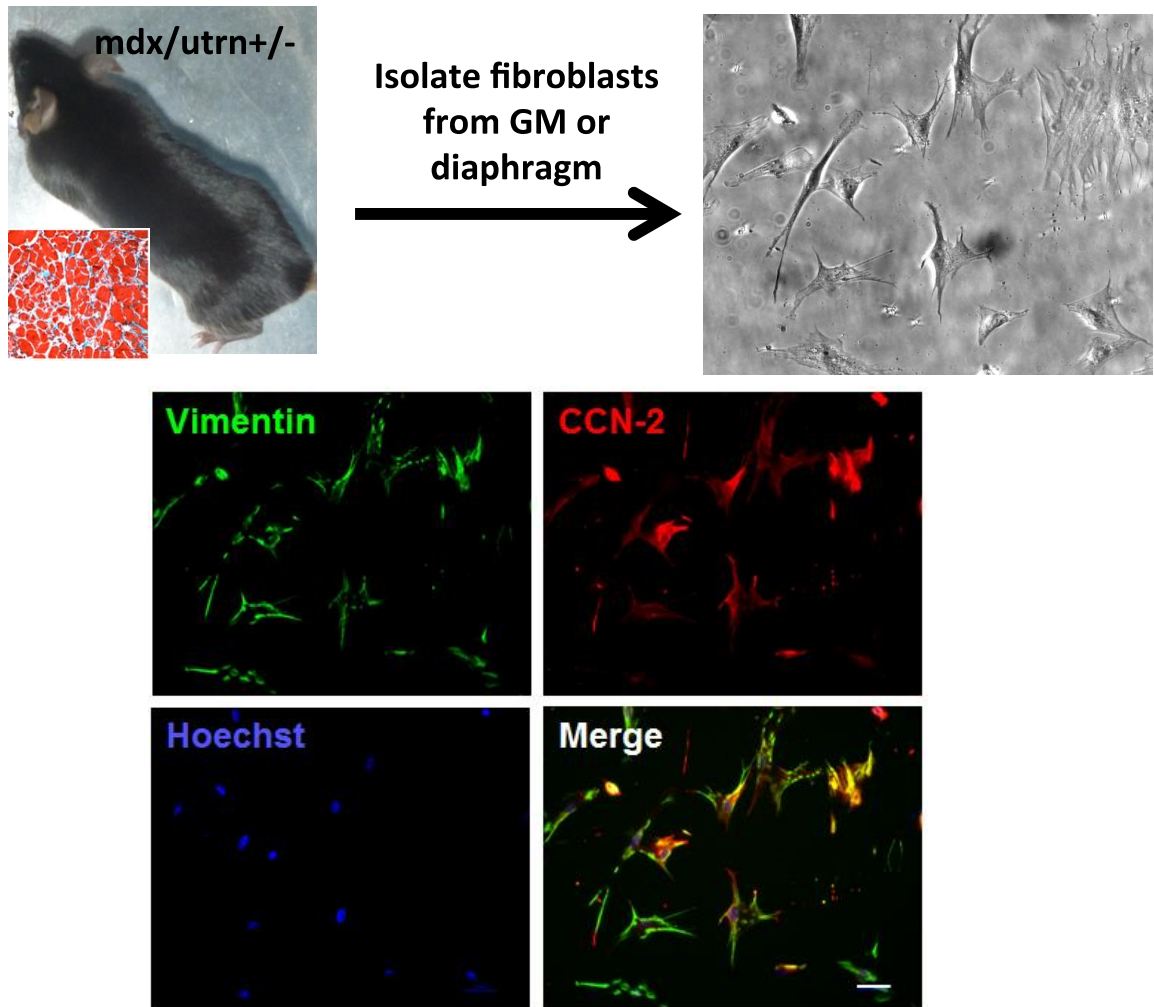
Primary fibroblasts isolated from mdx/utrn+/- muscle. Fibroblasts migrate away from tissue explants (shown above: diaphragm fibroblasts). Immunocytochemistry confirms presence of fibroblasts by assessing vimentin and CCN2 expression. Scale bar=50μm.

**Appendix C: ELISA analysis demonstrates that localized delivery of vascular endothelial growth factor (VEGF$_{165}$) results in slow release of the growth factor for up to two weeks post-injection.**
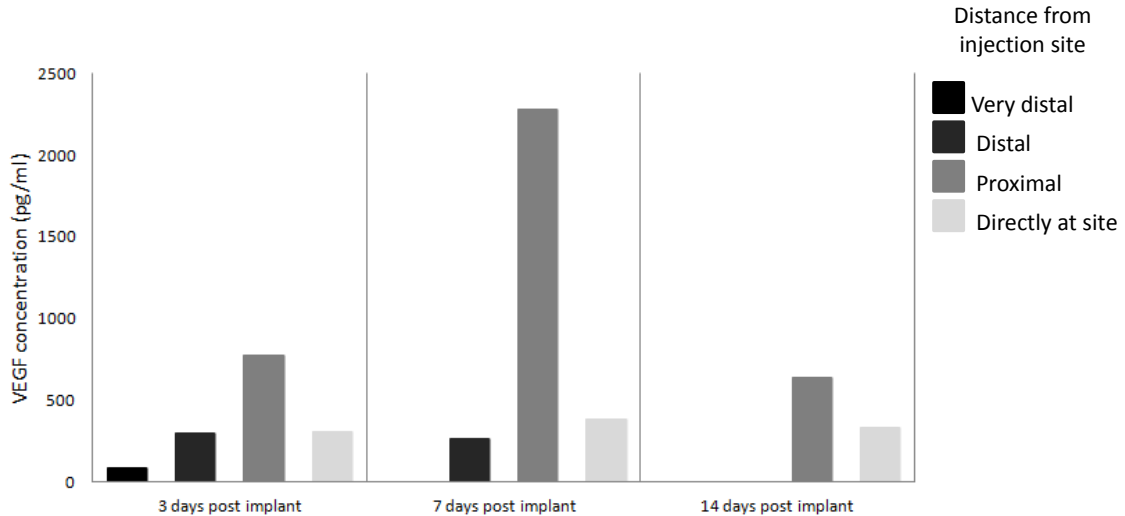
VEGF$_{164}$ levels following intramuscular implantation of VEGF$_{164}$-coated beads. Alginate beads were coated with 0.5ug of recombinant human VEGF$_{165}$ and injected into the lateral head of the gastrocnemius muscle of *mdx* mice. At 3, 7, and 14 days post-injection, mice were sacrificed and tissue was collected for ELISA analysis (n=2 per time point). Tissue was collected from four different regions to indicate how far VEGF treatment diffused (tissue directly surrounding and including the injection site [black], tissue less than 5mm from the injection site [dark grey], tissue more than 1cm from the injection site [medium grey], and tissue from the contralateral limb [light grey]). VEGF was still measured 14 days post-implant. Note: No cross-reactivity with mouse VEGF$_{164}$ was detected using this assay.

Appendix D: Results from initial perfusion study using 5-7 week-old *mdx* mice
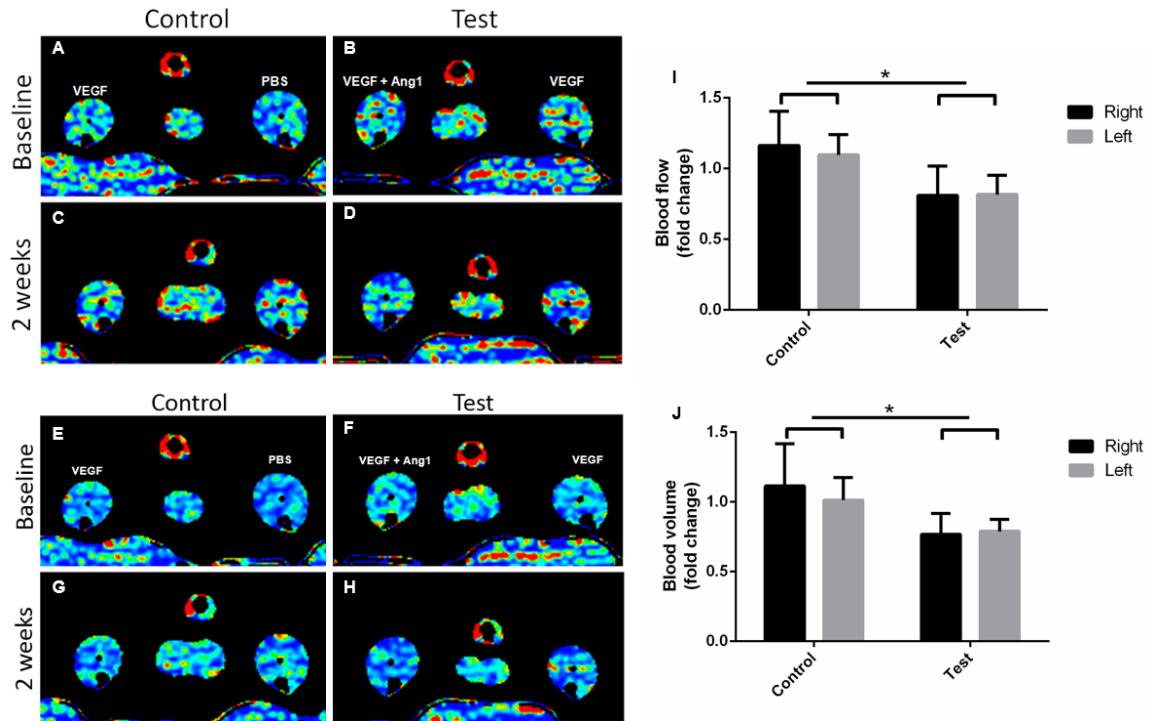
Blood flow and blood volume perfusion maps acquired from DCE-CT scans at baseline and two weeks following treatment with pro-angiogenic growth factors. *Mdx* mice were injected with either PBS and VEGF-coated beads (A,C,E,G) or VEGF and VEGF+ANG1-coated beads (B,D,F,H) . Mice were scanned at baseline (A,B,E,F) and two weeks post-implant (C,D,G,H). Blood flow (A,B,C,D,I) and blood volume (E,F,G,H,J) were measured using CT Perfusion 5 software (n=5, p<0.05).

Appendix E: Dynamic contrast-enhanced CT scans acquire data that can be used to attain functional perfusion maps.
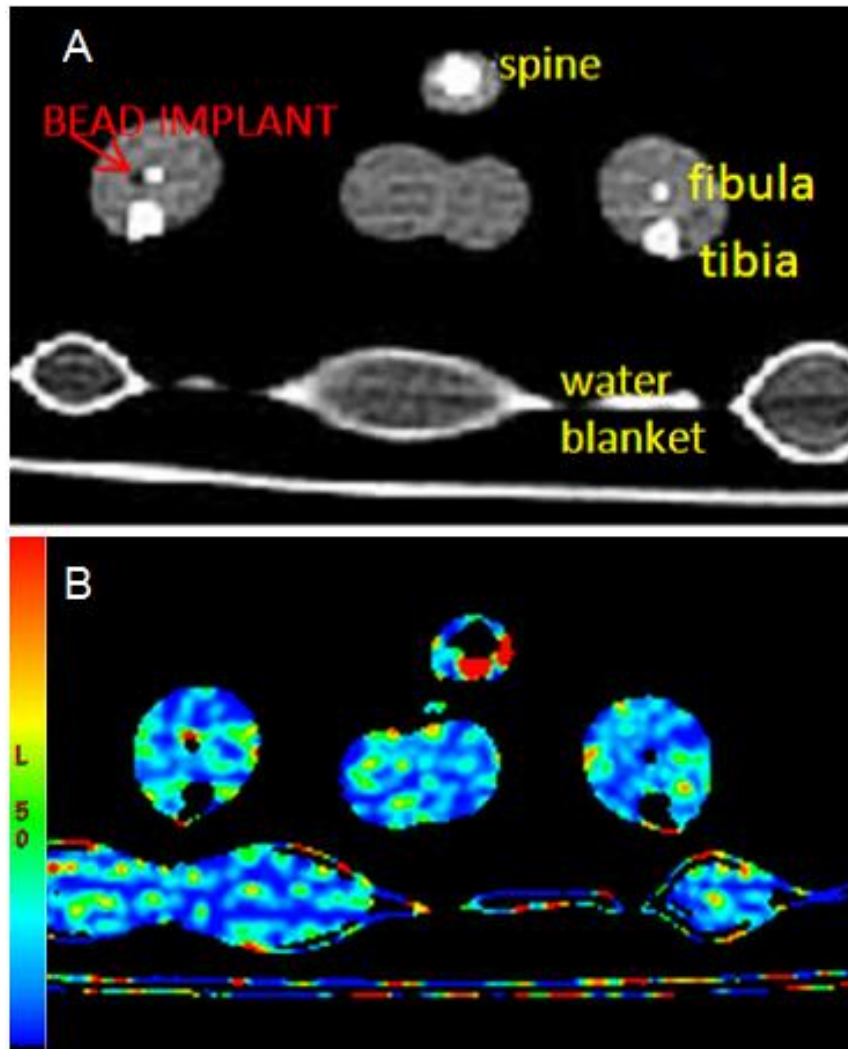
An anatomical and functional map acquired from DCE-CT scans. An axial anatomical scan (A) yields cross-sectional images. Bony landmarks such as the tail, fibula and tibia are easily identified. A black void is visible after injection of Affi-Gel Blue Gel beads (either soaked in PBS or coated with growth factor). Following a bolus of iodinated contrast agent, a series of one-second scans are taken to acquire functional data. CT Perfusion 5 software is used to generate perfusion maps (B).

Appendix F: Quantifying fluorescence images to include αSMA+ blood vessels and exclude αSMA+ myofibroblasts

Green arrows identify vessels

Pink brackets identify myofibroblasts

Raw immunofluorescence image   Segmented image
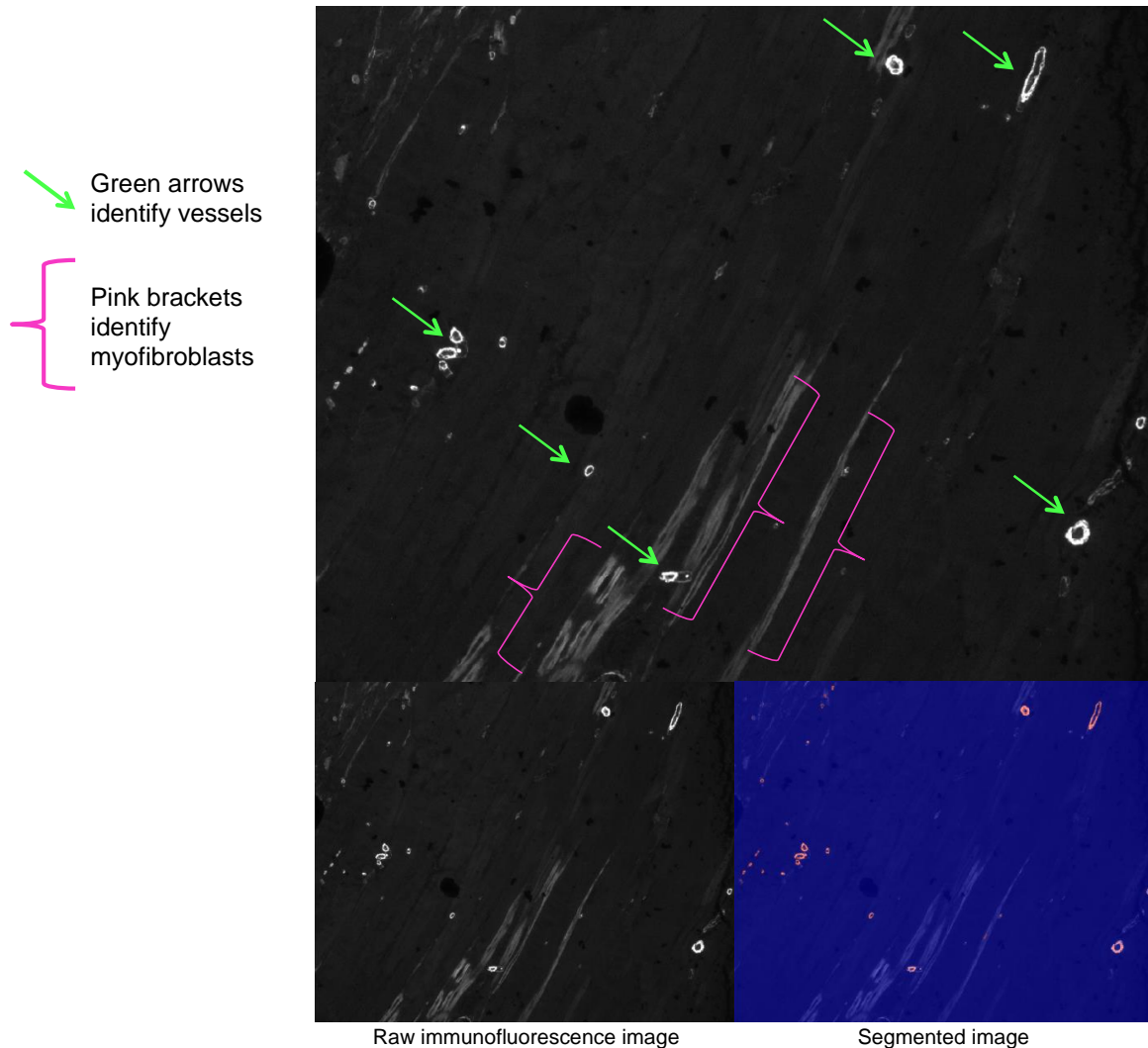
An anti-αSMA primary antibody marks both mature vasculature and myofibroblasts in dystrophic muscle. To accurately quantify mature blood vessels (green arrows) on histological sections, extreme care must be taken to exclude αSMA+ myofibroblasts (pink brackets). Implementation of a semi-automatic grey scale thresholding algorithm detects presence of vessels only (pink signal in segmented image).

Appendix G: Molecular Imaging to Target Transplanted Muscle Progenitor Cells[4]

<u>Introduction</u>

Duchenne muscular dystrophy (DMD) is a severe genetic neuromuscular disorder that affects 1 in 3,500 boys, and is characterized by progressive muscle degeneration (Emery 2002; Blake et al. 2002). In patients, the ability of resident muscle satellite cells (SCs) to regenerate damaged myofibers becomes increasingly inefficient4. Therefore, transplantation of muscle progenitor cells (MPCs)/myoblasts from healthy subjects is a promising therapeutic approach to DMD. A major limitation to the use of stem cell therapy, however, is a lack of reliable imaging technologies for long-term monitoring of implanted cells, and for evaluating its effectiveness. Here, we describe a non-invasive, real-time approach to evaluate the success of myoblast transplantation. This method takes advantage of a unified fusion reporter gene composed of genes (firefly luciferase [fluc], monomeric red fluorescent protein [mrfp] and sr39 thymidine kinase [sr39tk]) whose expression can be imaged with different imaging modalities (Ray et al. 2004, 2007). A variety of imaging modalities, including positron emission tomography (PET), single-photon emission computed tomography (SPECT), magnetic resonance imaging (MRI), optical imaging, and high frequency 3D-ultrasound are now available, each with unique advantages and limitations (Massoud & Gambhir 2003). Bioluminescence imaging (BLI) studies, for example, have the advantage of being relatively low cost and high-throughput. It is for this reason that, in this study, we make use of the firefly luciferase (fluc) reporter gene sequence contained within the fusion gene and bioluminescence imaging (BLI) for the short-term localization of viable C2C12 myoblasts following implantation into a mouse model of DMD (Sicinski 1989; Mattson 2001; Anderson et al.

---

[4] This appendix includes content reproduced with permission from

Gutpell K, McGirr R, Hoffman L (2013). Molecular Imaging to Target Transplanted Muscle Progenitor Cells. J Vis Exp (73), e50119, doi:10.3791/50119.

1988). Importantly, BLI provides us with a means to examine the kinetics of labeled MPCs post-implantation, and will be useful to track cells repeatedly over time and following migration. Our reporter gene approach further allows us to merge multiple imaging modalities in a single living subject; given the tomographic nature, fine spatial resolution and ability to scale up to larger animals and humans (Massoud & Gambhir 2003), PET will form the basis of future work that we suggest may facilitate rapid translation of methods developed in cells to preclinical models and to clinical applications.

Keywords: Molecular Biology, Issue 73, Medicine, Biophysics, Biomedical Engineering, Cellular Biology, Anatomy, Physiology, Genetics, Surgery, Diseases, Musculoskeletal Diseases, Analytical, Diagnostic and Therapeutic Techniques and Equipment, Therapeutics, Bioluminescence imaging (BLI), Reporter Gene Expression, Non-invasive Targeting, Muscle Progenitor Cells, Myoblasts, transplantation, cell implantation, MRI, PET, SPECT, BLI, imaging, clinical techniques, animal model

Protocol

Maintenance and Propagation of C2C12 Myoblasts

1. Plate C2C12 myoblasts in a 75 cm2 flask and maintain cells in high glucose Dulbecco's Modified Eagle's Serum (HG-DMEM) supplemented with fetal bovine serum (FBS) to a final concentration of 10%. Do not allow cells to become confluent at any time, as this will deplete the myoblast population. Medium should be changed every other day. Note: always warm medium to 37 °C in a water bath prior to use.

2. When myoblasts become approximately 80% confluent, passage cells to a new flask. Aspirate culture medium. Wash cells with 4-5 ml Hanks Balanced Salt Solution (HBSS) to remove all traces of culture medium, which contains trypsin-inhibiting serum. Briefly rinse the cell layer with 2-3 ml 0.25% (w/v) trypsin-EDTA solution to dissociate the adherent myoblasts from the flask. Aspirate trypsin and place flask in incubator at 37 °C for 5 min.

3. During this incubation, prepare a new flask with 9 ml of HG-DMEM/10% FBS medium. After trypsinization, add 10 ml of complete medium to cells and pipette 4-5 times to ensure collection of all cells in the medium. Add 1 ml of cell suspension to the new flask and incubate in 5% CO2 at 37 °C.

C2C12 Cell Transfection

1. Once cells have reached 50% confluency, transfect according to manufacturer's instructions from Invitrogen. Briefly, combine 90 μl Lipofectamine 2000 reagent with 4.5 ml OPTI-MEM medium. In another tube, combine 36 μg CMV-trifusion reporter gene DNA with 4.5 ml OPTI-MEM. Flick each tube to combine and wait 5 min. Combine contents of both tubes, mix gently and incubate at room temperature for exactly thirty minutes. Note: A second flask should also be set up for untransfected cells that only receive Lipofectamine and OPTI-MEM to serve as a negative control.

2. Remove medium from C2C12 cells and add 15.5 ml of fresh HG-DMEM/10%FBS medium. Add transfection medium to bring total volume to 20 ml.

3. Allow cells to transfect overnight for at least 20 hr at 37 °C.

4. Next day, aspirate transfection medium and add 10 ml HG-DMEM/10%FBS.

5. View cells under an inverted fluorescent microscope. Capture both bright field and red fluorescence images (using a TRITC filter cube; mrfp ex/em: 584/607 nm). Count the number of RFP-expressing cells viewed under fluorescence divided by total number of cells viewed under bright field for multiple fields of view to generate transfection efficiency.

Assessment of Cell Survivability/MTT Assay

1. One day prior to transfection, plate 1x105 C2C12 cells into each well in a 24-well plate. Cells should be plated in 500 μl volumes in HG-DMEM/10%FBS .

2. Next day, transfect myoblasts overnight as previously described. Follow manufacturer's suggestions for transfection reagent volumes for a 24-well plate.

Incubate a set of wells with Lipofectamine only (no DNA) as a control. View cells under fluorescence to ensure that proper transfection has occurred.

3. Remove transfection medium and incubate myoblasts with 5 mg/ml thiazolyl blue tetrazolium bromide (MTT) in HG-DMEM/10% FBS. Add D-luciferin to eight of the transfected wells, and incubate at 37 °C for four hours.

4. Remove medium from wells. Solubilize blue formazan crystals by adding 180 µl isopropanol to each well. Shake at 37 °C for 15 min.

5. Avoiding any precipitate, pipette solution into a 96-well plate and read absorbance at 575 nm.

Preparation of Myoblasts for Transplant

1. Remove medium, wash myoblasts with HBSS, and trypsinize cells as outlined in 1.1.

2. Re-suspend cells in 4 ml of complete medium.

3. Using a hemocytometer, count cells to generate volumes containing 106 myoblasts. Pipette volume into sterile 1.5 ml microtubes. With a transfection efficiency of ~10%, these values indicate that 100,000 luciferase-expressing cells are detectable on the GE ExploreOptix scanner after transplant.

4. Attain a final injection volume of 15 µl, containing 106 C2C12 cells. If necessary, centrifuge microtubes at 2,000 rpm for one minute. Carefully aspirate supernatant with a pipette. Re-suspend cells in 15 µl of HG-DMEM lacking FBS.

Cell Implantation

1. Anesthetize mouse with 2% isoflurane/2%O2. Pluck hair from the dorsal hind limb area. Maintain anesthesia at 1.5%isoflurane/2%O2.

2. Ensure C2C12 myoblasts are well suspended. With the mouse in a prone position, extend the hind limb and use an insulin syringe to inject cells directly into the lateral

head of the gastrocnemius muscle at a 30 ° angle. Inject transfected myoblasts into the right hind limb and untransfected myoblasts into the contralateral (left) hind limb.

3. Perform a baseline bioluminescence scan: Quickly transfer mouse to stage in the optical scanner, laying the mouse in a prone position. Hook up the anesthetic line. To ensure the mouse remains anesthetized, a second person should be present to hook up the anesthetic line while the other places the animal in the scanner.

4. Gently extend the hind limb so the area of injection is visible. Tape hind limbs in place with a gentle adhesive such as medical tape.

5. Close the chamber and ensure that no light can access the interior of the scanner, as this will increase the background signal detected. The scanner should be set to parameters included in your manufacturer's instructions for bioluminescence imaging. Specifically, ensure "no laser" is selected.

6. Draw a region of interest (ROI) around the plucked area and start scan.

Injection of Fluc Substrate, D-luciferin, into Mdx Mouse

1. While the mouse is anesthetised intraperitoneally inject 150 mg/kg of firefly luciferase substrate, D-luciferin (from a 40 mg/ml stock solution, made up according to manufacturer's instructions).

2. Recover mouse and allow a 15 min uptake period before preparing mouse for the next scan.

BLI to Target Luc-expressing MPCs Following Implant into Mouse Models of DMD

1. After the uptake period, anesthetise mouse again, as described in 5.1.

2. Transfer the mouse back to the optical scanner and perform another bioluminescence scan in the same manner as the background scan.

3. Although a 20 min uptake period should provide maximal signal intensity, a subsequent scan may be performed.

4. Upon completion of image acquisition, sacrifice the mouse according to guidelines set by your Institutional Animal Ethics Committee and the Canadian Council on Animal Care (CCAC). Isolate hind limb muscle and place immediately in 10% formalin to fix for paraffin embedment. Perform immunohistochemistry staining for luciferase to confirm intramuscular injection of myoblasts.

Representative Results

Upon 50-60% confluency, C2C12 myoblasts were transiently transfected with the above-mentioned fusion reporter gene construct composed of firefly luciferase [fluc], monomeric red fluorescent protein [mrfp] and sr39 thymidine kinase [sr39tk](Figure 1A). Transfection efficiency was calculated via fluorescence microscopy (Figures 1B,C), making use of the mrfp sequence in our reporter construct. Cell survivability was not affected by labeling with the BLI substrate, D-luciferin (Figure 1D). Following transfection, approximately 100,000 mrfp-expressing myoblasts were implanted intramuscularly into the gastrocnemius muscle of *mdx* mice (determined previously); 100,000 untransfected cells were similarly implanted into the contralateral hind limb as a control. Immediately following cell implantation, mice were injected intraperitoneally (IP) with 150 mg/kg D-luciferin. Following an uptake period of ~20 min, mice were imaged on a small animal optical scanner (GE ExplorOptix black box that is equipped for live animal bioluminescence and fluorescence). As previously demonstrated, both *in vitro* and post-implantation (manuscript submitted) uptake of D-luciferin were specific to fluc-expressing myoblasts, with no detectable bioluminescence in untransfected cells (Figure 2). Immunohistochemistry confirmed intramuscular transplantation of myoblasts.
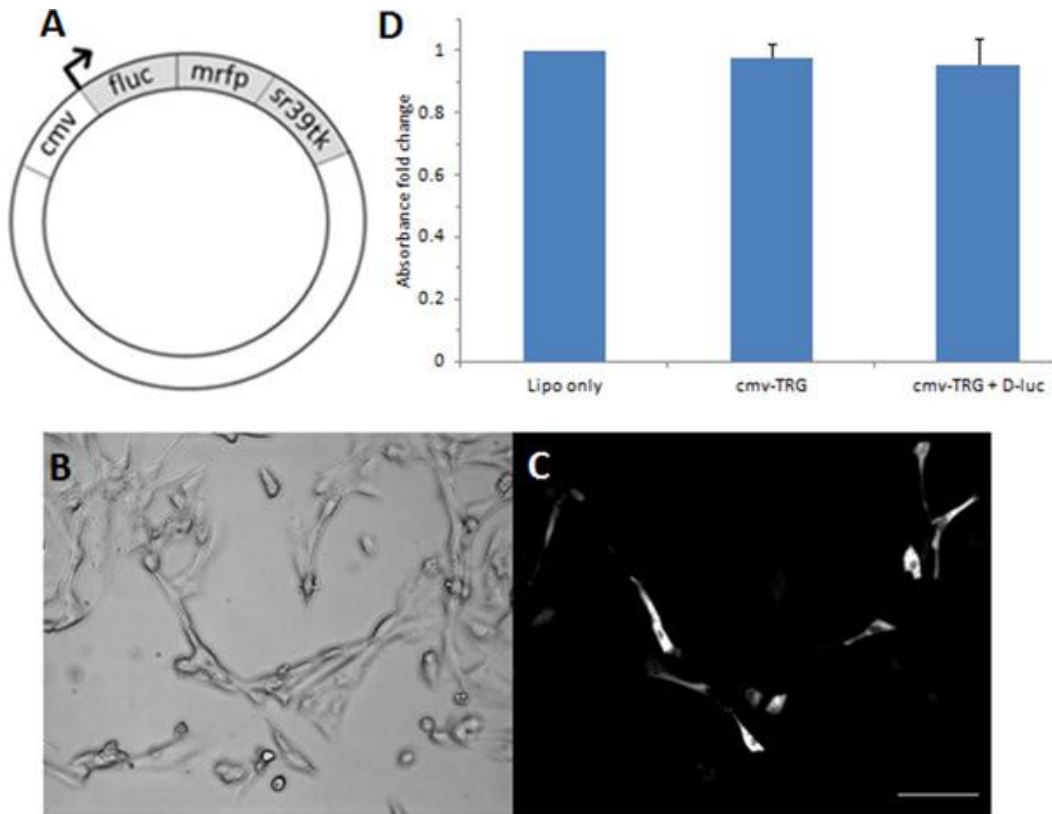
Figure 1. Schematic of CMV-trifusion reporter construct (A); brightfield/fluorescence images of C2C12 myoblasts transfected with the trifusion reporter plasmid (B,C); MTT assay to assess C2C12 cell survivability following labeling with BLI substrate, D-luciferin (D).
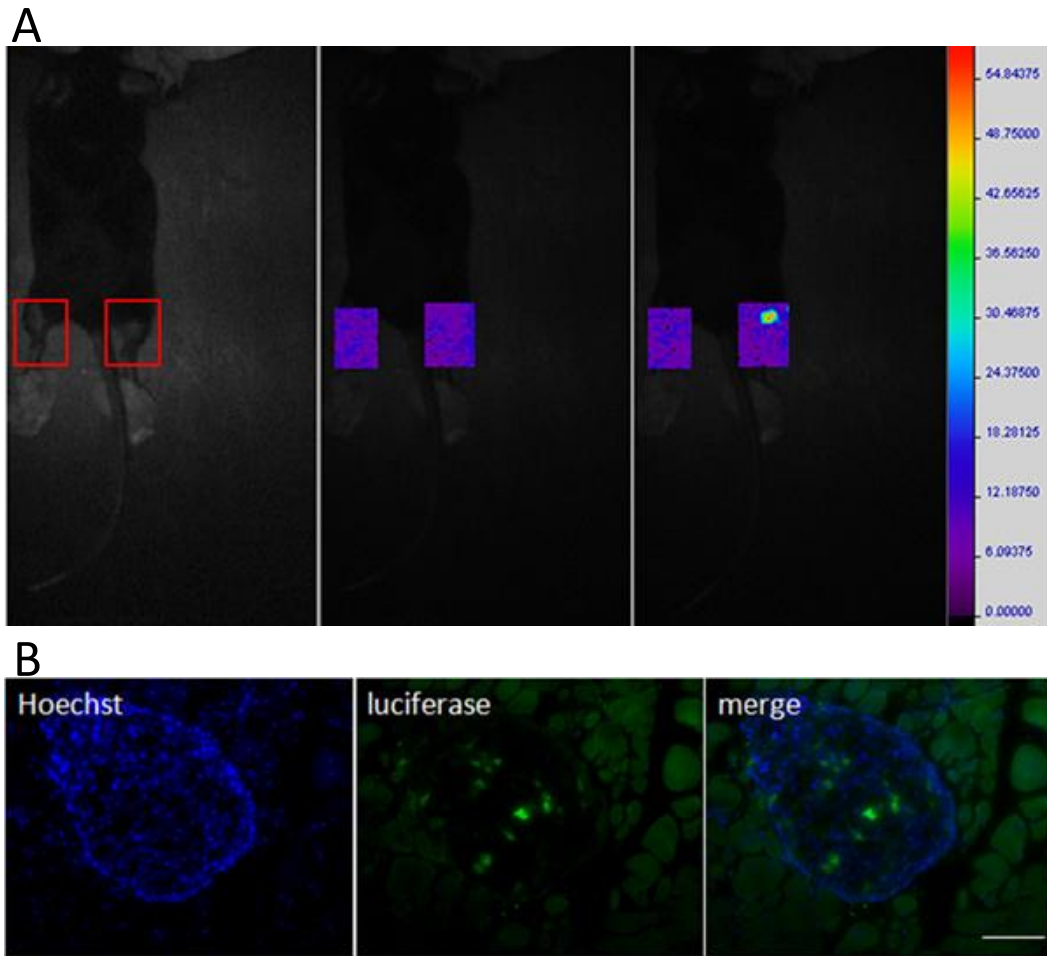
Figure A2. Bioluminescence imaging (BLI). BLI targets luciferase-expressing cells following transplant (A). A region of interest is drawn to enclose the plucked hind limb area where myoblasts are injected. Bioluminescence is not detected during a background scan. At 23 min after injection of D-luciferin, a clear signal is detected from the right hind limb where luciferase-expressing myoblasts are injected. No bioluminescence is detected in the contralateral hind limb injected with untransfected myoblasts. IHC using a firefly luciferase antibody confirms intramuscular implantation of transfected C2C12 cells (B). DAPI was used as a counterstain. Scale bar= 50um.

Discussion

In this study, we have described a fast and reliable molecular imaging, reporter gene approach to non-invasively target myoblasts/MPCs following transplantation. While this study demonstrates the short-term localization of transplanted MPCs via bioluminescence imaging (BLI), the manner in which cells are targeted can, in fact, be easily applied to a longitudinal assessment of cell engraftment, through the implantation of cells that stably express the reporter gene. To this end, our group has generated transgenic mouse lines that harbour the unified reporter gene. Only cells expressing the reporter gene oxidize D-luciferin to produce photons for visualization using BLI. Since oxidation of D-luciferin is dependent on gene expression, this is a powerful technology with which to non-invasively image viable transplanted cells. Muscle tissue harvested from these transgenic mice and satellite cells (SCs) isolated via FACS can indeed be targeted following implantation into *mdx* mice. Additionally, we can track their differentiation status through the use of a muscle-specific promoter, further heightening the usefulness and importance of molecular imaging technologies, such as presented herein, to the field of DMD research. In addition to its rapidity and low-cost, BLI is non-toxic, making it an attractive choice for frequent imaging of small animals. This feature, as well as its high specificity, will be invaluable in refining myoblast replacement therapies in pre-clinical disease models of Duchenne muscular dystrophy before advancing to clinically applicable studies involving technologies such as PET.

References

Andersson JE, Bressler BH, Ovalle WK. Functional regeneration in hind limb skeletal muscle of the *mdx* mouse. J. Muscle Res. *Cell Motil*. 1988;9:499–515.

Blake DJ, et al. Function and genetics of dystrophin and dystrophin-related proteins in muscle. *Physiol Rev*. 2002;82:291–329.

Emery AE. The muscular dystrophies. *Lancet*. 2002;359:687–695.

Goldring K, Partridge T, Watt D. Muscle stem cells. *J Pathol*. 2002;197:457–467.

Hoffman EP, et al. Characterization of dystrophin in muscle-biopsy specimens from patients with Duchenne's or Becker's muscular dystrophy. *N Engl J Med*. 1988;318:1363–1368.

Kuang S, Rudnicki MA. The emerging biology of satellite cells and their therapeutic potential. *Trends Mol Med*. 2008;14(2):82.

Massoud TF, Gambhir SS. Molecular imaging in living subjects: seeing fundamental biological processes in a new lights. *Genes Dev*. 2003;17:545–580.

Mattson MP. Pathogenesis of neurodegenerative disorders. In: Contemporary neuroscience. X. Totowa, NJ: Humana; 2001. p. 294.

Partridge TA. Cells that participate in regeneration of skeletal muscle. *Gene Ther*. 2002;9:752–753.

Ray P, et al. Imaging tri-fusion multimodality reporter gene expression in living subjects. *Cancer Res*. 2004;64:1323–1330.

Ray P, Tsien R, Gambhir SS. Construction and validation of improved triple fusion reporter gene vectors for molecular imaging of living subjects. *Cancer Res*. 2007;67(7):3085.

Sicinski P, et al. The molecular basis of muscular dystrophy in the *mdx* mouse: a point mutation. *Science*. 1989;244:1578–1580.

Appendix H: C2C12 myoblasts expressing the trifusion reporter under control of the myogenin promoter can be targeted ex vivo following injection
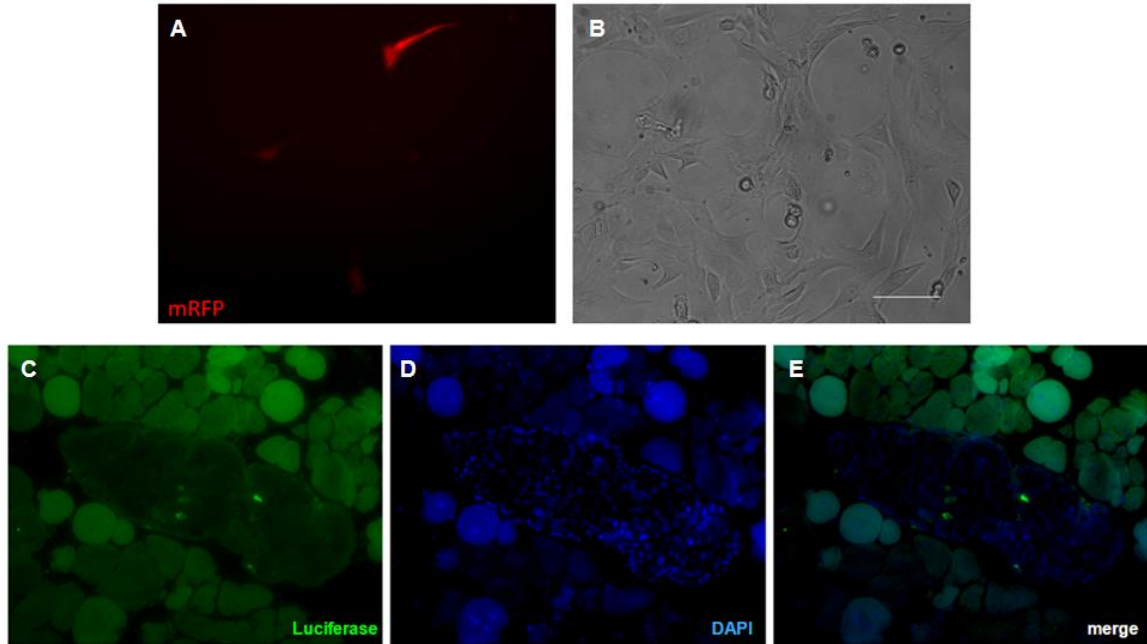
Immunohistochemistry confirms intramuscular implantation of myogenin-FMT-expressing C2C12 myoblasts. Differentiated C2C12 myoblasts transiently transfected with myogenin-FMT DNA express mRFP (A). Bright field and fluorescence images reveal an expression level of less than 1% (A, B) scale bar=50µm. One million C2C12 cells (10,000 luciferase-expressing) are transplanted into the hind limb muscle of an *mdx* mouse. Immunohistochemistry confirms intramuscular implant (C-E).

Appendix I: Fluorescence activated cell sorting of satellite cells from transgenic mice expressing a trifusion imaging reporter driven by the muscle-specific promoter myogenin
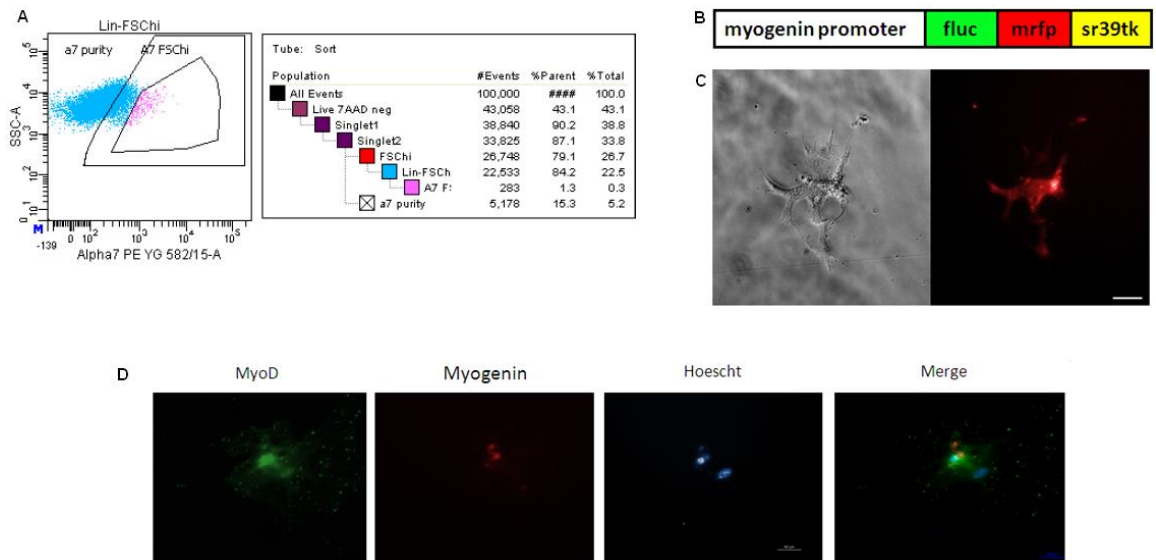
Satellite cells FACS-isolated from a transgenic myogenin-FMT mouse. Satellite cells are sorted based on positive staining of alpha-7 integrin, negative staining of the lineage markers CD31, CD45, CD11b and Ly6A/E, and a forward-scatter high profile (A). After 7 days in culture, satellite cells differentiate into myogenin-expressing myocytes that express the mRFP reporter (B,C). Immunocytochemistry confirms differentiation along the myogenic pathway, as indicated by the expression of MyoD and myogenin. MyoD, an early indicator of myoblast activation, is not expressed in more differentiated cells where myogenin is expressed (scale bar=50μm).

Appendix J: License agreement from Springer allowing use of publication content for thesis purposes only

**SPRINGER LICENSE
TERMS AND CONDITIONS**

Jan 26, 2016

This is a License Agreement between Kelly Gutpell ("You") and Springer ("Springer") provided by Copyright Clearance Center ("CCC"). The license consists of your order details, the terms and conditions provided by Springer, and the payment terms and conditions.

All payments must be made in full to CCC. For payment instructions, please see information listed at the bottom of this form.

License Number	3796550254091
License date	Jan 26, 2016
Licensed content publisher	Springer
Licensed content publication	Journal of Cell Communication and Signaling
Licensed content title	VEGF induces stress fiber formation in fibroblasts isolated from dystrophic muscle
Licensed content author	Kelly M. Gutpell
Licensed content date	Jan 1, 2015
Volume number	9
Issue number	4
Type of Use	Thesis/Dissertation
Portion	Full text
Number of copies	1
Author of this Springer article	Yes and you are the sole author of the new work
Order reference number	None
Title of your thesis / dissertation	Angiogenic therapy in a murine model of DMD
Expected completion date	Apr 2016
Estimated size(pages)	200
Total	0.00 CAD
Terms and Conditions	

Introduction
The publisher for this copyrighted material is Springer. By clicking "accept" in connection with completing this licensing transaction, you agree that the following terms and conditions apply to this transaction (along with the Billing and Payment terms and conditions established by Copyright Clearance Center, Inc. ("CCC"), at the time that you opened your Rightslink account and that are available at any time at http://myaccount.copyright.com).
Limited License
With reference to your request to reuse material on which Springer controls the copyright, permission is granted for the use indicated in your enquiry under the following conditions:

Appendix K: Animal Use Protocol Approval

Western

2008-067::7:

AUP Number: 2008-067
AUP Title: Non-Invasive Imaging of Therapeutics in Mouse Models of DMD

Yearly Renewal Date: 12/01/2015

The YEARLY RENEWAL to Animal Use Protocol (AUP) 2008-067 has been approved, and will be approved for one year following the above review date.

1. This AUP number must be indicated when ordering animals for this project.
2. Animals for other projects may not be ordered under this AUP number.
3. Purchases of animals other than through this system must be cleared through the ACVS office.
   Health certificates will be required.

REQUIREMENTS/COMMENTS
Please ensure that individual(s) performing procedures on live animals, as described in this protocol, are familiar with the contents of this document.

The holder of this Animal Use Protocol is responsible to ensure that all associated safety components (biosafety, radiation safety, general laboratory safety) comply with institutional safety standards and have received all necessary approvals. Please consult directly with your institutional safety officers.

Submitted by: Kinchlea, Will D
on behalf of the Animal Use Subcommittee

Curriculum Vitae

Name: Kelly Gutpell

POST-SECONDARY EDUCATION AND DEGREES

May 2011-
Apr. 2016

Doctor of Philosophy
Department of Anatomy and Cell Biology (Molecular Imaging)
Western University, London, Ontario, Canada
Supervisor: Dr. Lisa Hoffman

Sept. 2006-
Apr. 2010

Bachelor of Medical Science
Honors Specialization in Medical Science
Western University, London, Ontario, Canada
(Conferred June 2010)

HONOURS AND AWARDS

March 2016   **Top 100 Abstract- London Health Research Day**

May 2015   **Queen Elizabeth II Scholarship in Science and Technology-** $15,000

May 2014   **Ontario Graduate Scholarship-** $15,000

Jun. 2013   **Till and McCulloch Top Abstract Travel Award**- $1000

Mar. 2012   **Till and McCulloch Top Abstract Travel Award**- $1000

Apr. 2012   **Molecular Imaging Travel Grant-** $500

Sept. 2011-
Aug. 2013   **Canadian Institute of Health Research Strategic Training Fellowship in Vascular Research**- $12,000 per annum for two years

May 2011-
Present   **Western Graduate Research Scholarship-** $7000 per year of graduate study

Sept. 2008-
Apr. 2010   **Dean's List Student**

Sept. 2006   **Western Scholarship of Distinction-** $1000

RELATED WORK EXPERIENCE

Sept. 2012- Apr. 2016	**Teaching Assistant:** Psychology 2075- Human Sexuality (King's College, Western University)
Sept. 2012- Apr. 2016	**Teaching Assistant:** Psychology 2050- Human Adjustment (King's College, Western University)
Jan. 2013- Apr. 2015	**Laboratory Coordinator:** Anatomy and Cell Biology 3319- Systemic Human Anatomy (Western University)
Sept. 2011- Apr. 2012	**Teaching Assistant**: Anatomy and Cell Biology 3319- Systemic Human Anatomy (Western University)
Sept. 2012- Present	**Teaching Assistant:** Psychology 2075- Human Sexuality (King's College, Western University)

PUBLICATIONS

First Authored Publications

Gutpell KM, Tasevski N, Wong B, Hrinivich WT, Su F, Hadway J, Desjardins L, Lee T-Y, Hoffman L. Vascular therapy reduces ischemia and fibrosis in DMD mice. *(In preparation for submission in May 2016).*

Gutpell KM, Hoffman LM (2015). VEGF induces stress fiber formation in fibroblasts isolated from dystrophic muscle. *J Cell Commun Sig* (4):353-60.

Gutpell KM, Hrinivich WT, Hoffman LM (2015) Skeletal Muscle Fibrosis in the *mdx/utrn*+/- Mouse Validates Its Suitability as a Murine Model of Duchenne Muscular Dystrophy. *PLoS ONE* 10(1): e0117306. doi:10.1371/journal.pone.0117306.

Gutpell K, Hoffman L (2013). Non-invasive assessment of skeletal muscle pathology and treatment for Duchenne muscular dystrophy. *OA Musculoskeletal Medicine* (4):33.

Gutpell K, McGirr R, Hoffman L (2013). Molecular Imaging to Target Transplanted Muscle Progenitor Cells. *J Vis Exp* 73. doi:10.3791/50119.

Co-authored Publications

Bondoc AB, Detombe S, Dunmore-Buyze J, **Gutpell KM**, Liu L, Kaszuba A, Han S, McGirr R, Hadway J, Drangova M, Hoffman L (2014). Application of 3-D Echocardiography and Gated Micro-Computed Tomography to Assess Cardiomyopathy in a Mouse Model of Duchenne Muscular Dystrophy. *Ultrasound Med Biol* 40(12):2857-67.

Published Abstracts

Gutpell K, Hadway J, Desjardins L, Su F, Lee TY, Hoffman L (2015). Alleviating ischemia in a murine model of DMD using VEGF and ANG1. *Wound Repair Regen* 23:A10.

Gutpell K, Faubert S, Hoffman L (2014). Non-invasive assessment of therapeutic approaches in a murine model of Duchenne muscular dystrophy. *J Cell Commun Signal* A:5

Selected Abstracts and Presentations

Gutpell KM, Tasevski N, Wong B, Hrinivich WT, Su F, Hadway J, Desjardins L, Lee T-Y, Hoffman L. Vascular therapy reduces ischemia and fibrosis in DMD mice. *London Health Research Day*. March 29, 2016, London Ontario. **Poster presentation.**

Gutpell K, Hrinivich W, Hadway J, Desjardins L, Su F, Lee TY, Hoffman L. Considerations for the use of angiogenic therapy as an approach to treat DMD. *London Health Research Day*. April 1 2015, London Ontario. **Poster presentation**.

Gutpell K, Hoffman L. An angiogenic approach to enhancing cell therapy for the treatment of Duchenne muscular dystrophy. *Department of Anatomy and Cell Biology Research Day*. October 23 2014, London, Ontario. **Oral presentation.**

Gutpell K, Hoffman L. Non-invasive assessment of therapeutic approaches in a murine model of Duchenne muscular dystrophy. *20th Canadian Connective Tissue Conference*. June 8-10 2014, London, Ontario. **Oral presentation.**

Gutpell K, Hoffman L. Non-invasive assessment of angiogenic therapy in a murine model of Duchenne muscular dystrophy. *London Health Research Day*. March 18 2014, London, Ontario. **Poster presentation.**

Gutpell K, Hoffman L. Non-invasive assessment of the stem cell microvascular "niche" in a murine model of Duchenne muscular dystrophy. Till and McCulloch Meeting 2013, Banff, Alberta. **Poster presentation (abstract #109)**.

Gutpell K, Faubert S, McGirr R, Hoffman L. Enhancing cell therapy for the treatment of Duchenne muscular dystrophy through non-invasive assessment of the cell transplant "niche." *2013 London Health Research Day.* London, Ontario, March 19 2013. **Poster presentation.**

Gutpell, K, Hoffman L. Non-invasive imaging of cell therapy in murine models of Duchenne muscular dystrophy. *Department of Anatomy and Cell Biology Research Day*. October 25 2012, London, Ontario. **Oral presentation.**

Gutpell, K., Burke, P., Chamson-Reig, A., Hoffman., L. Bioluminescence imaging to

track the location and differentiation of myoblasts after transplant into a mouse model of Duchenne Muscular Dystrophy. *Till and McCulloch Meeting.* April 29-May 2 2012, Montreal, Quebec. **Poster Presentation.**

ACADEMIC COMMUNITY INVOLVEMENT

Apr. 2015-present **Peer Reviewer- PLOS ONE**

Sept. 2013-May 2015 **Chair- Schulich Graduate Student's Council**
Western University, London, ON

Jan. 2015-Apr. 2015 **Workshop Founder- Careers in Academia**
Western University, London, ON

May 2013-Jan. 2014 **Committee Member- Non-Academic Careers in Science**
Western University, London, ON

Dec. 2012-May 2015 **Molecular Imaging Program Student Representative**
Western University, London, ON

Jun. 2014 **Session Chair- 20th Annual CCTC Meeting**
Western University, London, ON

Jan. 2014-Jun. 2014 **Organizing Committee Member- Canadian Connective Tissue Conference**
Western University, London, ON